CONTROL SYSTEM DESIGN FOR A HAPTIC DEVICE

A THESIS SUBMITTED TO
THE GRADUATE SCHOOL OF NATURAL AND APPLIED SCIENCES
OF
MIDDLE EAST TECHNICAL UNIVERSITY

BY

SÜLEYMAN BİDECİ

IN PARTIAL FULFILLMENT OF THE REQUIREMENTS
FOR
THE DEGREE OF MASTER OF SCIENCE
IN
MECHANICAL ENGINEERING DEPARTMENT

SEPTEMBER 2007

Approval of the thesis

"CONTROL SYSTEM DESIGN FOR A HAPTIC DEVICE"

Submitted by **SÜLEYMAN BİDECİ** in partial fulfillment of the requirements for the degree of **Master of Science in Mechanical Engineering Department, Middle East Technical University** by,

Prof. Dr. Canan Özgen ______________________
Dean, Graduate School of **Natural and Applied Sciences**

Prof. Dr. Kemal İder ______________________
Head of Department, **Mechanical Engineering**

Assist. Prof. Dr. İlhan Konukseven ______________________
Supervisor, Mechanical Engineering Dept., METU

Examining Committee Members:

Prof. Dr. Reşit Soylu ______________________
Mechanical Engineering Dept., METU

Assist. Prof. Dr. İlhan Konukseven ______________________
Mechanical Engineering Dept., METU

Assoc. Prof. Dr. Veysel Gazi ______________________
Electrical Engineering Dept., TOBB

Assist. Prof. Dr. Buğra Koku ______________________
Mechanical Engineering Dept., METU

Assist. Prof. Dr. Yiğit Yazıcıoğlu ______________________
Mechanical Engineering Dept., METU

Date: 07 / 09 / 2007

I hereby declare that all information in this document has been obtained and presented in accordance with academic rules and ethical conduct. I also declare that, as requires by thesis rules and conduct, I have fully cited and referenced all material and results that are not original to this work.

Name, Last Name : Süleyman Bideci

Signature :

ABSTRACT

CONTROL SYSTEM DESIGN FOR A HAPTIC DEVICE

Bideci, Süleyman

M.S. Department of Mechanical Engineering
Supervisor: Asst. Prof. Dr. E. İlhan Konukseven

September 2007, 108 Pages

In this thesis, development of a control system is aimed for a 1 DOF haptic device, namely Haptic Box. Besides, it is also constructed. Haptic devices are the manipulators that reflect the interaction forces with virtual or remote environments to its users. In order to reflect stiffness, damping and inertial forces on a haptic device position, velocity and acceleration measurements are required. The only motion sensor in the system is an incremental optical encoder attached to the back of the DC motor. The encoder is a good position sensor but velocity and acceleration estimations from discrete position and time data is a challenging work. To estimate velocity and acceleration some methods in the literature are employed on the Haptic Box and it is concluded that Kalman filtering gives the best results. After the velocity and acceleration estimations are acquired haptic control algorithms are tried experimentally. Finally, a virtual environment application is presented.

Keywords: haptic control, velocity estimation, acceleration estimation, Kalman Filter

ÖZ

BİR HAPTİK CİHAZ İÇİN KONTROL SİSTEMİ TASARIMI

Bideci, Süleyman

Yüksek Lisans, Makina Mühendisliği Bölümü
Tez Yöneticisi: Yrd. Doç. Dr. E. İlhan Konukseven

Eylül 2007, 108 Sayfa

Bu tezde, Heptik Kutu isimli, tek serbestlik dereceli bir heptik cihaz için kontrol sistemi geliştirilmesi amaçlanmıştır. Ayrıca, Heptik Kutu bu çalışma kapsamında oluşturulmuştur. Heptik cihazlar sanal yada uzak ortamlardaki etkileşim kuvvetlerini kullanıcıya yansıtan manipülatörlerdir. Sertlik, sönümleme ve atalet kuvvetlerini heptik cihaza yansıtmak için konum, hız ve ivme ölçümüne ihtiyaç vardır. Sistemdeki tek hareket algılayıcısı DC motorun arkasına takılı olan optik bir artırımlı kodlayıcıdır. Artırımlı kodlayıcılar iyi konum algılayıcılarıdır fakat kesikli konum ve zaman bilgisinden hız ve ivme tahmini zor bir iştir. Hız ve ivme tahmini için literatürdeki bazı metotlar Heptik Kutu üzerinde denenmiş ve Kalman filtrelemesinin en iyi sonucu verdiği görülmüştür. Hız ve ivme bilgisi elde edildikten sonra deneysel olarak heptik algoritmaları denenmiştir. Son olarak bir sanal ortam uygulaması yapılmıştır.

Anahtar Kelimeler : heptik kontrol, hız tahmini, ivme tahmini, Kalman Filtresi

To My Family

ACKNOWLEDGMENT

I would like to thank my thesis supervisor Asst. Prof. Dr. E. İlhan Konukseven for providing me this research opportunity, and guiding me through the study.

I owe special thanks to Asst. Prof. Dr. Uluç Saranlı from Department of Computer Engineering, Bilkent University for his invaluable help to construct the Haptic Box, and for his support.

I would like to express my gratitude to Özgür Cavbozar, Arda Özgen, Hüseyin Öztürk and Halit Şahin who are the staff of METU BILTIR – CAD/CAM and Robotics Center.

I thank to my friends Anas Abidi, Emre Sezginalp, Faruk Yazıcıoğlu, Onur Yarkınoğlu, Umut Koçak and Varlık Kılıç who studied in the METU Mechatronics Laboratory for their precious support and presence.

Finally, I am deeply grateful to my very dear family, especially my parents, for supporting me and for showing me love to carry on my work successfully.

TABLE OF CONTENTS

LIST OF FIGURES

LIST OF SYMBOLS

Z	Impedance
Z^{-1}	Admittance
J	Jacobian Matrix
N	Number of lines per encoder channel
T	Sampling period
f	Generalized force
$\dot{x}$	Generalized motion
υ	Velocity
T_{el}	Elapsed time
R_e	Encoder resolution
θ	Angular position
r_j	Relative accuracy
X	State matrix
$\hat{X}$	Estimated state matrix
K	Kalman gain matrix
ϕ	State transition matrix
ψ	State input matrix
Y	Measurement matrix
P	Estimated variance matrix
R	Variance matrix of the measurement noise
Q	Variance matrix of the system noise
H	Measured values matrix
K_t	Transducer torque-voltage constant
K_{av}	Servo amplifier current-voltage constant
K_a	Motor torque constant
k	Stiffness constant
b	Damping constant
i	One dimensional inertia constant
K_p	Proportional controller gain

CHAPTER 1

INTRODUCTION

1.1 Introduction

Haptic devices are the force reflecting manipulators in haptic interfaces. A haptic device is simply a manipulator that is in interaction with its human user. It accepts the user motion/force and makes him/her feel the virtual or remote environment characteristics by applying forces on him/her. In order to provide a force feedback, according to the simulated environment, a manipulator with certain degrees of freedom is required. For general applications a 6 DOF haptic device is suitable but for the development of control algorithms and the studies a 1 DOF device can also be used. Therefore, we have decided to use a 1 DOF haptic device in this study (Figure 1.1).

The Haptic Box has a DC motor as an actuator and an incremental encoder as a sensor. The device control is maintained using these two components. There are many studies on haptic control algorithms. General control schemes are named as *impedance* and *admittance* controls. The control type is named according to the behavior of the virtual/remote environment. If the virtual/remote environment accepts the device motion and produces a reference force to be reflected to the user, the control mode is said to be *impedance display mode*. Contrarily, if the virtual/remote environment accepts the force applied to the device and produces a reference motion to be maintained than the control mode is said to be *admittance display mode* [1].

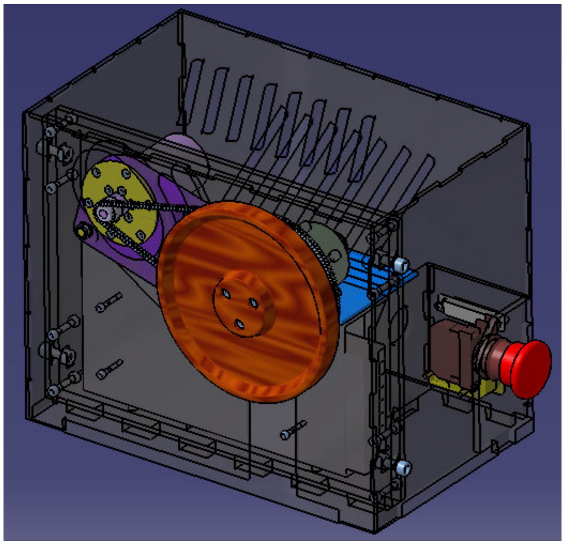

Figure 1.1 Haptic Box

Whatever the type of the controller is, the control system requires the information about the device motion. Position measurement is done via the incremental encoder discretely and precisely but velocity and acceleration estimation from this discrete data is not easy. Gathering accurate measurement/estimation data is another important part of the control work and it determines the effectiveness of the haptic interface. To estimate velocity from discrete position and time data, many methods are proposed in the literature. *Fixed time* and fixed *position velocity* estimations are two commonly used methods. To improve these estimators some other numerical techniques such as use of Taylor series and backward expansions and curve fits are used [2]. To decrease discretization errors counters for position and time are used simultaneously in the CET method [3]. To detect velocities at various speeds adaptive algorithms are proposed that allows the user to choose between relative accuracy and time delay [4]. Some observer based estimators are used in [5]. Finally, Kalman Filters are employed to estimate velocity from incremental encoder data [6,7,8,9,10,11].

1.2 Objectives of the Thesis

The first objective of this thesis is to develop a haptic device for experimental applications. Next objective is to try haptic control algorithms on the developed haptic device. Most of the haptic devices in the market do not have any force feedback capability. The third objective of this thesis is to add force feedback capability to the developed haptic device.

1.3 Thesis Outline

The study is arranged as, in Chapter 2 haptic devices are presented and some haptic applications are described. The Haptic Box is explained in Chapter 3. In Chapter 4 haptic control schemes are described and velocity and acceleration estimation methods are given in Chapter 5. System implementation using the Haptic Box is expressed in Chapter 6 and conclusions are made in Chapter 7.

CHAPTER 2

HAPTIC DEVICES

Manipulators have been used for a long time in industrial applications. They are simply some mechanical devices simulating human motions to replace man handwork with machine precision and speed. For example, robots in automotive production lines are used for welding, drilling, part placement, etc., simulating human arm motions. These manipulators are commanded by a computer which is programmed by an operator. To control the device position and sometimes velocity, encoders on the joints of the manipulators are used. For general industrial robot applications, motion feedback is sufficient. However, for some others, the interaction force between the robot and workpiece becomes very important as this force may damage the workpiece or the manipulator. In these kind of applications force transducers are used to measure the interaction force. Thereby, the force feedback signal may be used to control the interaction force.

The way of using manipulators mentioned above requires a computer that is programmed by an operator. The application is in the control of the computer. On the other hand, in some applications human inspection becomes unavoidable. Hazardous experiments can be given as an example. The operator grasps the objects using the remote robot by visual information. As the user is not given any force information, he/she does not know how hard he/she handles the objects. Another example can be given in the area of Virtual Reality (VR). In VR operations 3D environments are examined by stereo glasses and this gives the user only visual information. However, besides the visual feedback from the virtual or remote environments, touching them would be more impressive and this is possible with haptic devices. Thanks to haptic devices touching those virtual and remote environments becomes possible. Ueberle and Buss made a definition of haptic devices as “Haptic displays are force reflecting human system interfaces that are in physical contact with the operator providing bidirectional interaction by sensing user motion and exerting forces on him/her." [1]. As described in Chapter4 sensing motion for device control is not a single way to render the contact force. Thus, the definition "Haptic displays aim to provide users with a sense of touch, rendering contact forces as if interactions were occurring with real objects." made by Hwang, Williams and Niemeyer gives a more generic and realistic explanation [12].

2.1 Some Commercial Haptic Devices

In recent days, use of haptic devices has become popular. Universities are developing new haptic devices and some companies produce their products. Phantom Premium 1.5/6 DOF Haptic Device [13] from Sensable Technologies, Inc. shown in Figure 2.1 is one of those devices. It can apply force in three translational directions and torque in three rotational directions.

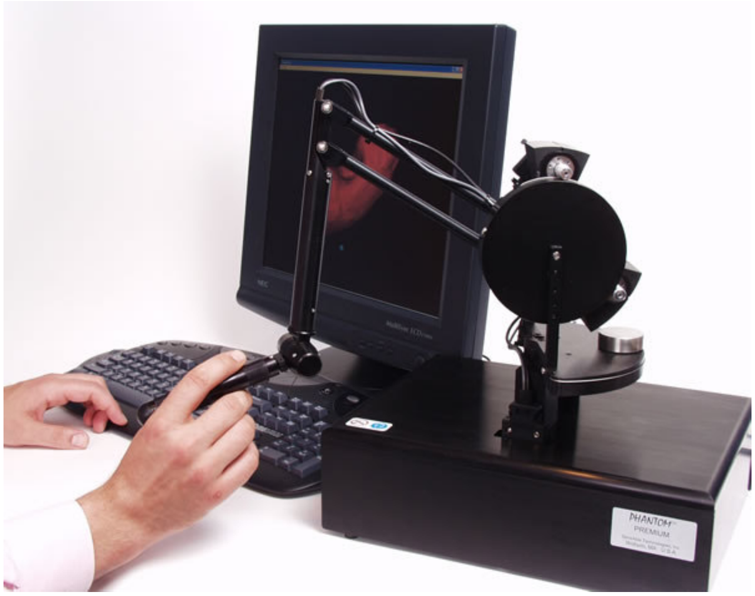

Figure 2.1 PHANTOM Premium 1.5/6 DOF Haptic Device

In Figure 2.2, The CyberGrasp[14] from Immersion Corporation is shown with an application. This device allows the user feel the forces on his/her fingers.

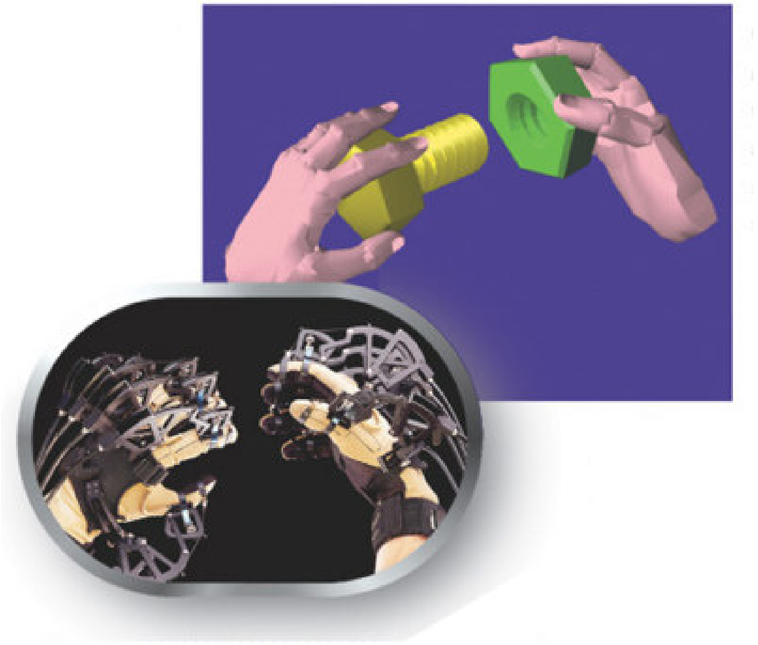

Figure 2.2 The CyberGrasp

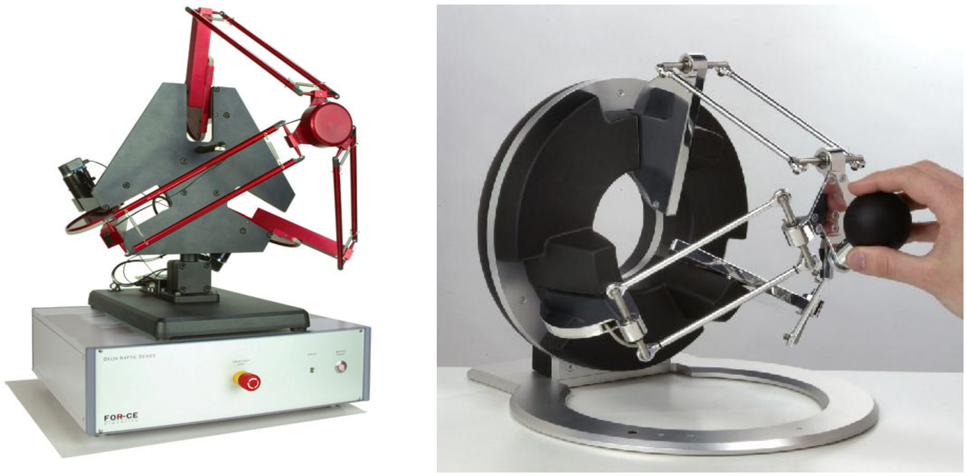

Figure 2.3 Delta 3DOF and Omega.3

In essence haptic devices are some kind of mechanical manipulators with special controlling units, so the manipulator type can vary. Delta 3DOF and Omega.3 [15] shown in Figure 2.3 are haptic devices with parallel manipulators, which are from Force Dimension Company. Parallel structures are preferred for high force applications, thus these devices are used to reflect large forces in three translational dimensions.

2.2 Haptic Applications

As described before, with haptic devices human motion can be simulated. Considering this fact, any human work can be a haptic application; however, general studies are on medicine, military, education and training, entertainment, CAD/CAM, reverse engineering and art fields.

A simple and illustrative example is the CAD application given in Figure 2.2. Using the CyberGrasp, the user assembles the nut and bolt. In this application, by the operator motion the virtual objects are moved and also the user feels the forces on his/her fingers as if he/she assembles a real nut and bolt pair.

Surgical trainings are another great application filed. Haptic interfaces are getting used more at different medical operational simulations. New haptic devices IOMaster7D and IOMaster5D are developed to apply to endoscopic neurosurgery, ENT surgery and laparoscopy simulation [16].

There are some training simulators for some works requiring practice. Military and medical operations can be given as examples. A medical application is examined in [17] in which a tennis simulator is developed to examine human arm characteristics from arm movement.

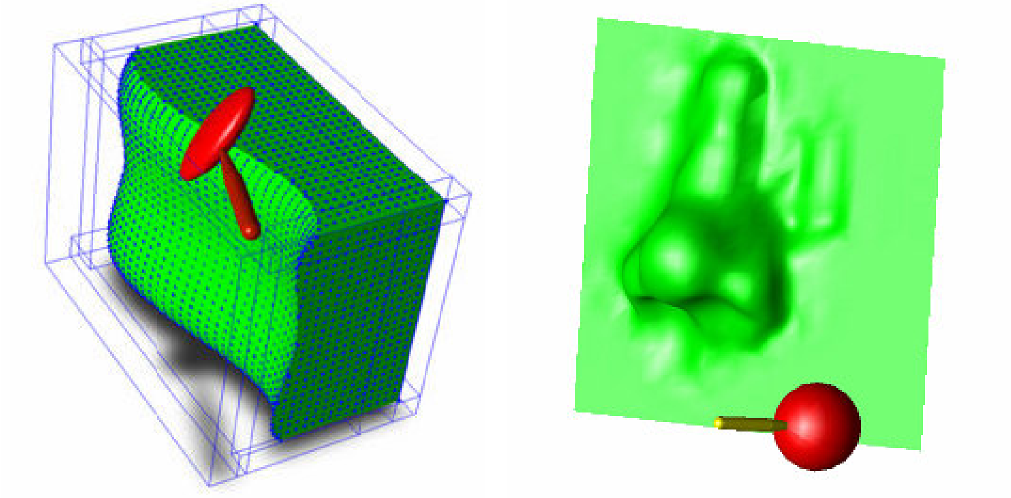

Figure 2.4 a) Virtual Clay b) Virtual Sculpting

An interesting application area is field of art in which a haptic device takes place of an art tool. Virtual sculpting and virtual painting are two good examples. In a virtual sculpting operation virtual clay is used and it is deformed by the virtual tool (Fig.2.4a) [18]. The virtual clay is modeled as a real one, such that, it is deformable, has stiffness and damping properties. Thus, the user shapes it feeling realistic touch. In Figure 2.4b, an application on human nose is shown. In this operation a spherical virtual tool is used. The tools are interchangeable with different shapes so the tool shape is taken into consideration at deformation stage.

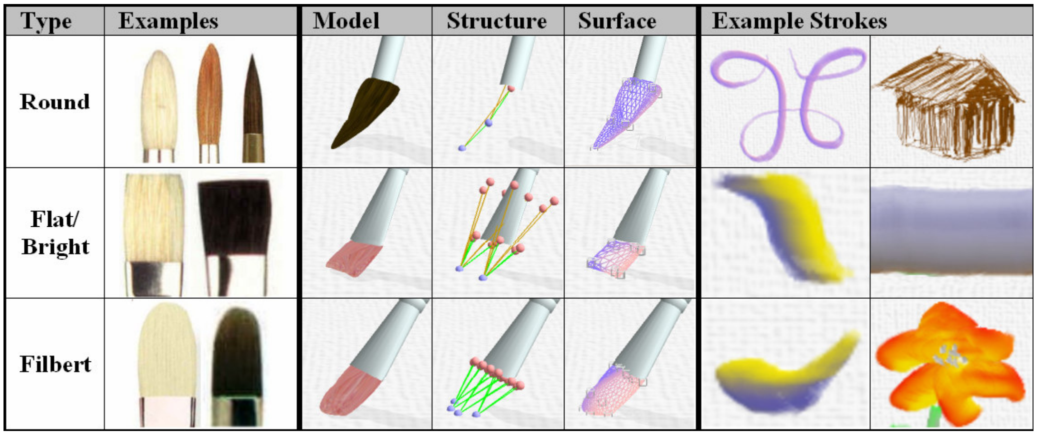

Type	Examples	Model	Structure	Surface	Example Strokes	
Round						
Flat/ Bright						
Filbert						

Figure 2.5 Haptic Painting brush models

Virtual painting is an application similar one to the virtual sculpting. However, the deformation and forces are also calculated at the tool tip, namely that the brush head is deformed at strokes. To reflect these properties to the user, brush models are made as shown in Figure 2.5. In the figure, the column named *structure* is used for force calculation and so the deformation, and visual models are given in the *surface* column. The user uses the haptic device end-effector as the brush as shown in Figure 2.6a. And a sample painting made by a user of the system is shown in Figure 2.6b [19].

Besides these virtual environment applications, there are some real world applications, in which haptic devices are used. These kinds of applications are called teleoperations. Teleoperations are important applications as they mostly serve to the surgical operations. In these operations, the virtual environments are replaced by real remote environments. This is also needed in hazardous experiments and in some variety of applications where contact force is needed to be controlled by a human operator. Such an application is shown in Figure 2.7. The ViSHARD10 is 10DOF haptic device and it is called the master manipulator. And the 7DOF remote robot is the slave one.

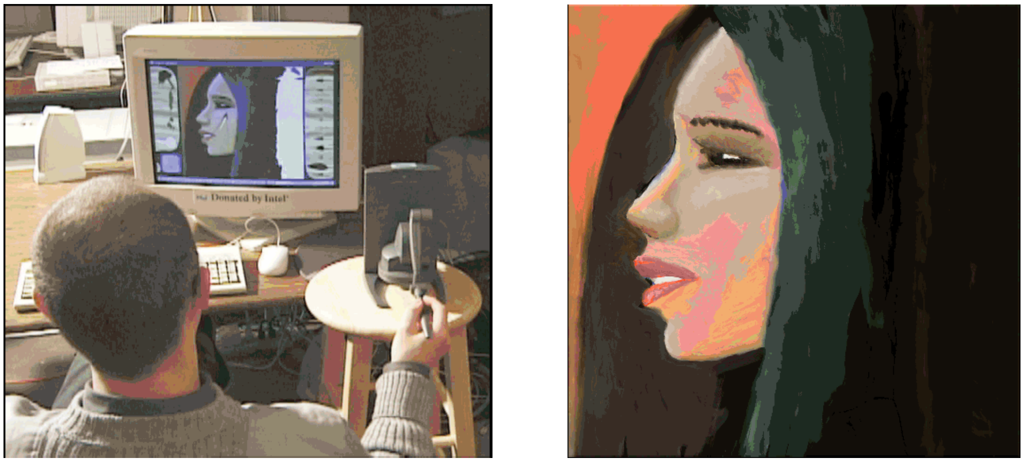

Figure 2.6 a) Virtual Painting Application b) Virtual Painting

The slave robot copies the motion of the master one. The force sensors attached to the slave robot contact forces sense the contact forces and transmit them to the master robot, which is the haptic device. A stereo camera is also employed to gather the visual information [20].

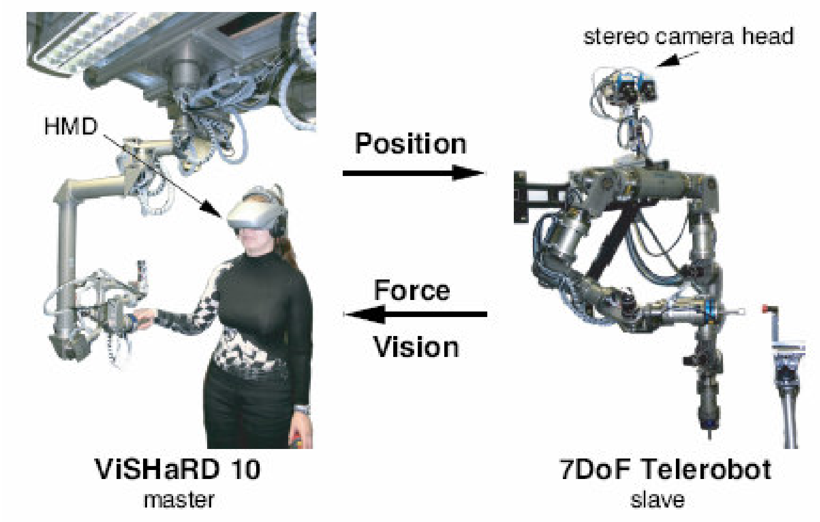

Figure 2.7 Teleoperation employing a haptic device

As is seen, haptic devices are playing important roles in many applications. They take place in virtual environment applications for modeling some lost human parts to manufacture prosthesis. They can be used to train students for surgical practices, art students to gain experience, and in many computer games. In military field, it can be used to reflect realistic forces in simulators. In telemanipulation applications they can be employed to perform surgical operations and hazardous experiments.

The applicability to many simulations make haptic devices important. Thanks to them lots of simulations can be done to gather information from different systems. By this way, repeatability of experiments increases and as the used experimental set up is virtual, experiment costs can be decreased if accurate system models can be done. Effects of products can be estimated using virtual models before producing them and damages of hazardous environments can be avoided with the help of haptic interfaces.

CHAPTER 3

HAPTIC BOX

In this study a 1 DOF haptic device is designed and manufactured [21]. The device is a Haptic Box which is shown in Figure 3.1. The Haptic Box is simply a motor driven wheel with other peripheral units. As the box has only one degree of freedom, 1 DOF virtual or remote environments can be simulated.

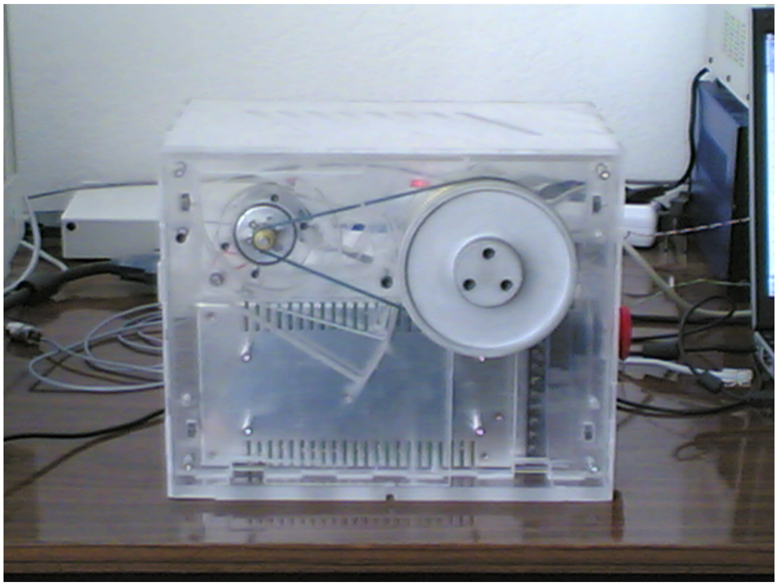

Figure 3.1 Haptic Box

The box is designed using mechanical, electromechanical and electronic components. The frame is formed by plexiglas parts cut out from sheets. The drawings of the manufactured parts are given in Appendix D. The actuating unit is a MaxonRE40 DC brush motor which has a 150W power. It is connected to a Copley413CE DC Brush Servo Amplifier. The diagrams for electrical connections of the box are given in

Appendix C. The motor torque is amplified using sprocket and chain by a 128/18 ratio. User interaction is maintained by the knob attached to the large sprocket, and the motion is sensed by a HP HEDS5540A optical encoder attached to the rear side of the motor. Specifications for off-the-shelf components are given in Appendix B.

3.1 Haptic Box Specifications

The Haptic Box is composed of mechanical, electronic and electromechanical elements. In Figure 3.2 a simple schematic representation of the box is given. For haptic applications on the Haptic Box, the torque/motion on the knob is controlled. When the reference input to the Copley 413CE servo amplifier is given, the amplifier controls the current on the motor. Thus the motor is current controlled.

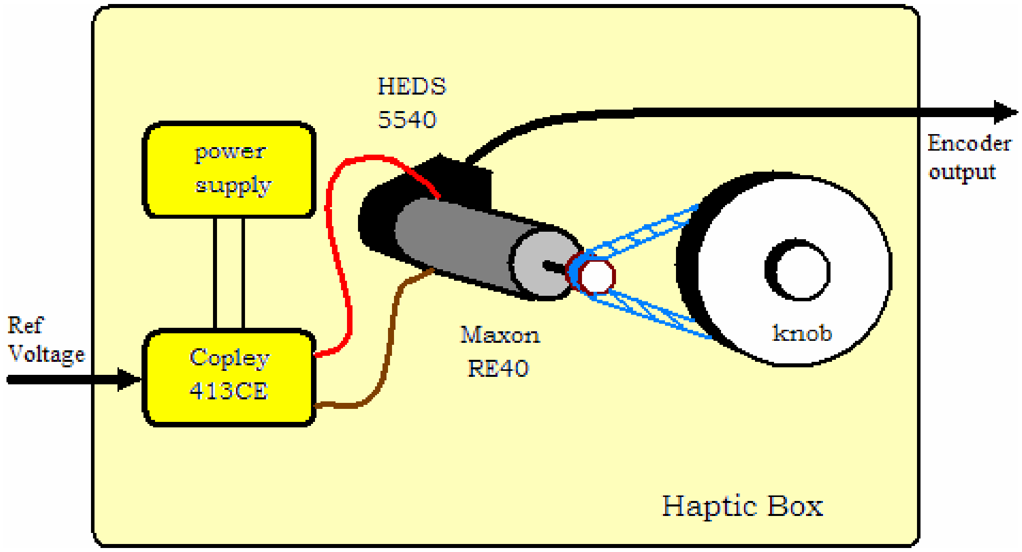

Figure 3.2 Haptic Box Components

Haptic Box components are described in the following sections and their specifications can be found in Appendix B.

3.1.1 Copley 413CE DC Brush Servo Amplifier

Copley 413CE is a servo amplifier for DC brush motors. With its torque and velocity modes, motor torque and velocity can be controlled easily using an analog ±10V reference voltage. The amplifier is excited with 24V voltage from an external power supply (requires a minimum of 2.7W). It can supply a peak power of ±30A@±80V for a peak time of 1 second maximum. Copley 413CE comes with default adjustments however some important values can be set using the 40-pin socket. As the Haptic Box is a torque control device, current limitation becomes conceivable. Using proper resistances on the socket *continuous and peak current* values and *peak time* can be limited.

3.1.2 Maxon RE40 DC Motor and Optical Incremental Encoders

Maxon RE40 is a 150W DC motor with graphite brushes. It has a 48V nominal voltage, but can be used at lower voltages in this study. The motor can generate 2500mNm stall torque, and has a torque constant $K_a = 60.3mNm$.

At the back of the motor, there is a HP HEDS 5540A optical encoder attached. The encoder has 500 lines per revolution for A and B channels and it also has an index channel. We have also used a Scancon encoder for velocity and acceleration monitoring. It has 5000 pulse at A and B channels, and an additional index channel I.

3.1.3 Other Components

There are some other components which are necessary for the proper functioning of the system. Two sprockets and one chain twined on them are first group of them. They transmit the torque from one to the other. The small sized one is attached to the shaft of the motor and it has 18 teeth. The large one is attached to the shaft to which knob is attached and it has 128 teeth. Thus, a 128/18 gear ration is used to amplify the motor torque. Another unit to complete the system is the emergency button. As the Maxon RE40 is a powerful motor, an emergency button is added to the system. For conformation and some control applications a torque transducer is also used.

CHAPTER 4

HAPTIC CONTROL

Haptic devices are the manipulators which can be controlled by some ways similar to robot control methods. However, haptic devices must be taken into account as a whole system, as haptic interfaces, and the haptic interface control should be done keeping this fact in mind. Since the haptic interfaces are force reflecting system, force is the controlled value.

The origin of haptic devices dates back to 1950's. In these years master arms are used in radioactive applications. Later on, force sensing capability is added to those devices that were proportional to the felt force at the slave. With the computational power of computers, more complex master arms are built. After a period of time, researchers realized that these devices could have been used in virtual and real applications for reflecting forces and these Force Reflecting Hand Controllers belonging to a class of robotic mechanisms usually referred to as *haptic devices* [22].

Most of the haptic devices in the market does not have force sensing capability because of the price of the force transducers and the price of the implementation of these sensors to the system. Therefore, these devices are open loop force controlled. However, this method requires a lightweight device structure not to effect dynamics of the application by the device dynamics. When larger workspaces and force capabilities are required device structure becomes more cumbersome. In this case, force feedback becomes vital [23].

In this chapter, first general robot control algorithms will be given, than the haptic control method will be explained. The general structures of the following titles are taken from studies of Ueberle and Buss [23]. In order to make it clear thorough the rest of the chapter, first *impedance* and *admittance* terms will be described firstly.

4.1 Impedance & Admittance

Parts forming any system have some dynamic properties. These properties become apparent when a single part or systems of parts move. Depending on these properties some forces act on the part bodies that can be grouped as inertial, gravitational, frictional, coriolis, centrifugal and external forces. The sum of these forces in vector domain gives the net force that causes the body to move. There is a relationship between the net force on the body and the body motion. This relationship can be modeled mathematically by some differential equations. However, those differential equations are generally complicated and using them in description of system structures (not in details) becomes incomprehensible. Therefore, more understandable terms are used for those relations. These relationships are called *impedance* and *admittance* of a body or a system.

In electrical applications the term impedance is used to define *the total resistance to the current flow of a body*. This can be used to define impedance for mechanical systems as *the total resistance of a body to motion* and this resistance is felt as a force. Thus, impedance is the relation between the body motion and the total force acting on it and it is denoted by the capital letter Z. Impedance can be written mathematically as:

$$f = Z * \dot{x} \tag{4.1}$$

Here f is used to denote both *force* and *torque* and it is called *generalize force*, and $\dot{x}$ is used to represent *motion* (position, velocity, acceleration) and it is called *generalized motion.*

Sometimes, the inverse of impedance is needed in mathematical presentations. Thus, the inverse of impedance is defined as *admittance* that relates force to motion and it is denoted by Z^{-1}. The mathematical representation of admittance can be written as:

$$\dot{x} = Z^{-1} * f \tag{4.2}$$

Again, f and $\dot{x}$ are used to represent generalized force and motion respectively.

4.2 Robot Control

Ueberle and Buss made a classification of robot and haptic control algorithms [23] and they have adopted the following classification scheme for general robot control algorithms from Volpe [24]. The term position is replaced by generalized motion:

- Motion control
- Force control
    - Explicit force control
        - Open loop explicit force control
        - Force-based explicit force control
        - Motion-based explicit force control
    - Impedance control
        - Impedance control without force feedback
        - Impedance control with force control
- Hybrid control

In *motion control* of robots, desired motion trajectory is commanded and internal and external forces (e.g. due to interaction with environment) are rejected. In this control type, if a contact by an object causes any motion error, then the high motion gain tries to compensate for this error. If the object is stiff or immovable then the manipulator or object take damage. On the other hand, there are robot control algorithms not considering internal and external forces as disturbance. This type of control is called *force control*. Force control schemes can be grouped as *explicit force control* and *impedance control*.

In *explicit force control algorithms* the desired interaction force is commanded. Explicit force control algorithms with no force feedback are called *open loop explicit force control.* Other implementations use the force feedback to compare it with the commanded force and control error is obtained. This control error is then used to control the plant directly (*force-based explicit force control*), or it is first transformed into a reference motion through an admittance and then it is given to a motion controller (*motion-based force control*). This type of control is also known as *admittance control.*

In Figure 4.1 *force-based explicit force control* diagram is shown. The measured force is compared by the reference and the control error is given to a force controller. Thus the force robot exerts on the object is controlled. Another explicit force control example is given in Figure 4.2 named *position based explicit force control.* In this control scheme the control error is calculated by comparing measured and reference forces. However, the control error is transformed into a reference motion (it is position in the figure) through a desired admittance. This reference motion is compared by the robot motion and the control error is obtained in units of motion. And the control error is processed by a motion controller.

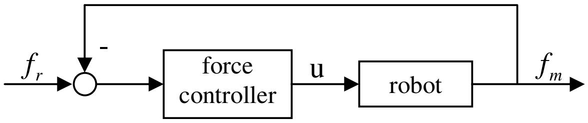

Figure 4.1 Force based explicit force control

An example diagram to *impedance control with force feedback* is shown in Figure 4.3. The device motion information is fed back to the virtual environment (computer or microcontroller), the control error is obtained and a reference force is calculated via desired impedance. If the system has a force transducer then the force is closed-loop controlled as shown in Figure 4.3. If the robot does not have a force sensing capability then the force is open-loop controlled. This control type is also called *open loop impedance control* or *implicit force control*. In this case a light weight device structure is preferred to reduce the effects of device dynamics on the output force.

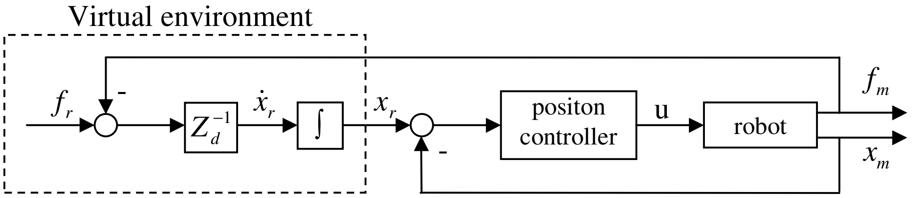

Figure 4.2 Position based explicit force control

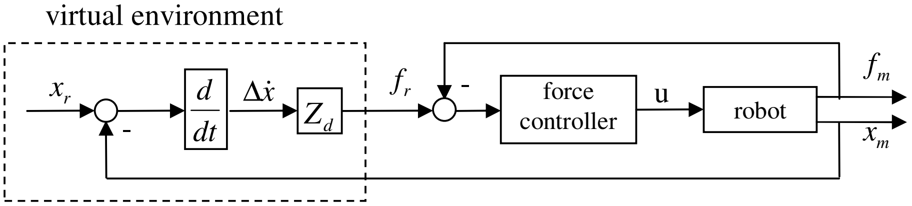

Figure 4.3 Impedance control with force feedback

The hybrid method is a combination of motion and force control used by switching in an application. It is denoted that one does not have to use force control in entire workspace. Thus, it is possible to use motion control in unconstrained subspaces (no contact, free trajectory following) and force control in constrained subspaces (contact with objects).

4.3 Haptic Control

A good description of control strategy of haptic interfaces is made by Ueberle and Buss as: “The haptic simulation of a human’s bilateral interaction with a virtual or remote environment requires the control of the motion-force relation between the operator and the robot.” [13]. A comparison for robot and haptic system controls can be made as follows: Robot control requires a reference data given by a computer or microcontroller in means of motion trajectory or force to maintain and the system tries to follow that reference. However, in haptic interfaces, the motion of haptic user is assumed to be the reference. Accordingly, a force is reflected to the user and his /her motion is affected by the system. That is to say, in haptic systems a user and machine interaction is present.

Most of the simulators built so far are concentrated on modeling virtual environments and used relatively simple control algorithms [22]. There are two main class of haptic control schemes used. The first one is *impedance display mode* and the second one is *admittance display mode*. The classification is made according to the behavior of the virtual environment. As the admittance is conversion of force to motion, force feedback is required. However, in impedance display force feedback is not a requirement.

4.3.1 Impedance Control

In impedance control shown in Figure 4.4, the virtual environment acts as impedance. It accepts motion and produces a respective force. In the figure Z_d is the desired virtual environment impedance, Z_r^{-1} is the robot admittance, Z_{EE} is the impedance of the end-effector which is between force sensor and the user. The parameter with a hat symbol shows that it is the model of that parameter.

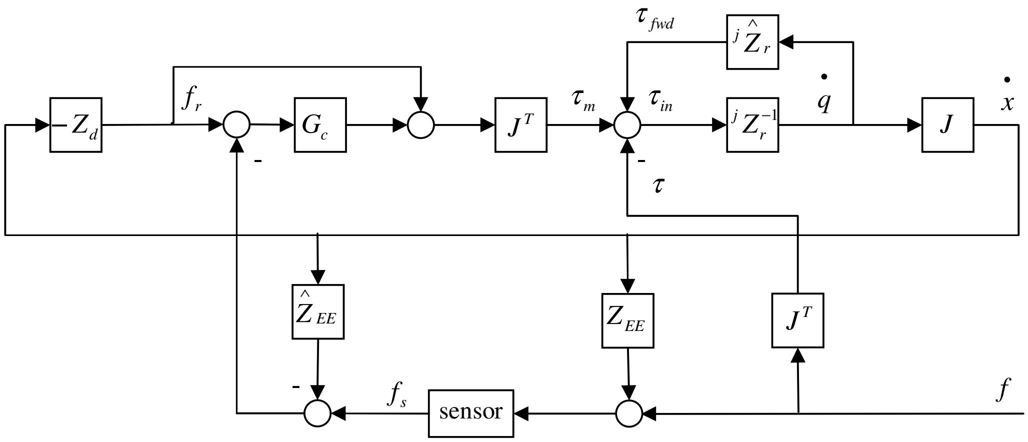

Figure 4.4 Impedance control with force feedback and model feed forward

From the block diagram, the following equation can be derived:

$$\dot{x} = J\,{}^{j}Z_r^{-1}\left[I - {}^{j}\hat{Z}_r\,{}^{j}Z_r^{-1}\right]^{-1} J^T\left[-f - Z_d\dot{x} - G_c\left[Z_d\dot{x} + f + \left[Z_{EE} - \hat{Z}_{EE}\right]\dot{x}\right]\right] \qquad (4.3)$$

Here G_c is the transfer function of the controller. From Eq.4.1 the following equation for closed-loop impedance relating the device motion $\dot{x}$ to the operator force $-f$ can be obtained arithmetically as:

$$Z_{RCL} = Z_d + \left[I + G_c\right]^{-1}\left[\mathbf{Z}_r - \hat{Z}_r + G_c\left[Z_{EE} - \hat{Z}_{EE}\right]\right] \qquad (4.4)$$

Z_{RCL} gives the impedance of the system, that is, it gives the dynamic relation between device motion to the operator force. It can be shown mathematically as:

$$-f = Z_{RCL}\dot{x} \qquad (4.5)$$

The desired haptic system should reflect the virtual/remote environment properties precisely. Thus the closed-loop impedance Z_{RCL} of the system should represent the desired virtual environment impedance Z_d $\left(Z_{RCL} \cong Z_d\right)$. This shows that force feedback plays an important role in haptic systems and it is clear with Eq.4.4. When there is no force feedback the equation takes the following form:

$$Z_{RCL} = Z_d + \left(Z_r - \hat{Z}_r\right) \tag{4.6}$$

Eq.4.6 shows that when there is no force feedback and compensating for device dynamics becomes hard as the only reduction in device dynamic is done on the feed forward line, and this requires a perfect modeling for device dynamics $\left(\hat{Z}_r\right)$. Such a diagram is shown in Figure 4.5 named open loop impedance control. Because the only reduction in robot dynamics can be done by model feed forward, open-loop impedance control is preferred for haptic devices with light structures.

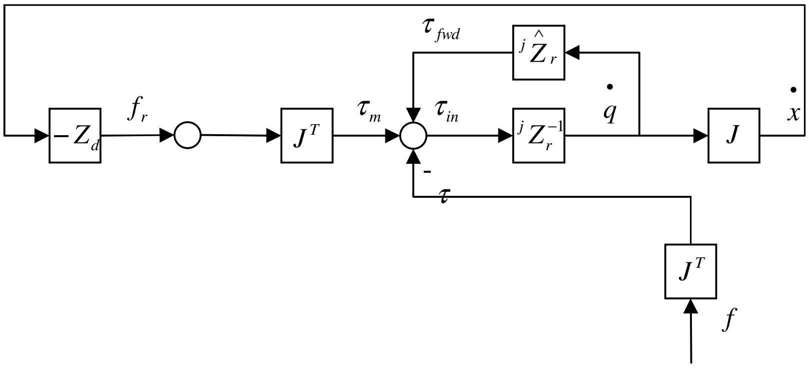

Figure 4.5 Open Loop Impedance Control with model feed forward

4.3.2 Admittance Control

Figure 4.6 shows the block diagram of admittance control. The virtual environment acts as admittance that it accepts force and produces motion. The impedance Z_{d1} converts the reference end-effector velocity $(\dot{x}_r)$ to a reference force f_r and virtual environment admittance Z_{d2} transforms the reference force to reference velocity. Thus, Z_{d1} and Z_{d2} forms the virtual environment and the virtual environment impedance becomes:

$$Z_d = Z_{d1} + Z_{d2} \tag{4.7}$$

If the inner loop position controller gain is sufficiently large then the closed-loop impedance of the system becomes:

$$Z_{RCL} \approx Z_d + Z_{EE} - \hat{Z}_{EE} \tag{4.8}$$

End-effector terms takes place in Eq.4.8 as the force transducer is places just before the end-effector. It is pointed by Ueberle and Buss that by this method providing a more natural feel to the operator is possible compared to impedance control that does not apply model based inertia compensation. However, on the other hand, extracting reference position from force error adds more poles than zeros and this increases the phase lag in the system's open-loop transfer function.

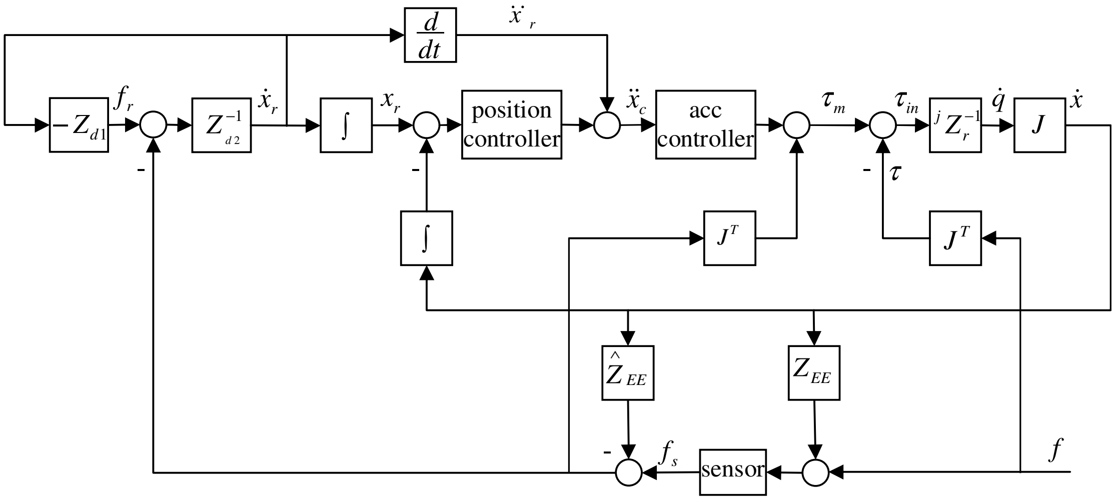

Figure 4.6 Admittance Control

4.3.3 Haptic Control Conclusions

There are many studies in the haptic field and they are generally on developing some interfaces for some application such as virtual simulators for art, medical, military, etc., simulations. These kinds of works generally depend on buying a commercial haptic device and combining it with a computer to form the haptic interface. As they are on the shelf products their software and electronics comes within the package and the user implements the haptic device to his/her interface directly. Thus there is not a choice for choosing the control law for that device. Generally, haptic devices on the market do not have any force transducer attached to the gripper and so they are controlled with *open-loop impedance control* algorithms. Therefore, the virtual environment being simulated is tried to be modeled so as the haptic device can reflect forces in that environment.

On the other hand, some studies compares impedance and admittance display modes with the same hardware. Ueberle and Buss examined the control methods for haptic devices and concluded that there is not a best one between these control algorithms [23]. Carignan and Cleary made a similar study and concluded that one method is not superior to the other. However, it is pointed that the admittance controller gives better results at lower impedance values, and the impedance control is superior for higher impedances values being simulated. [22].

CHAPTER 5

VELOCITY AND ACCELERATION ESTIMATION

Incremental optical encoders are widely used in many robotic and mechatronics applications. An incremental optical encoder is basically a disk with very low inertia and hollow lines on it and some electronic components. As the disk rotates, a phototransistor generates a square wave (0-5 Volts) according to the solid-hollow stages of the disk. A region on the disk with solid and hollow sections is called a channel. The signal is read from the channel of the encoder, and decoded according to its rising and falling edges. If the encoder has two channels in quadrature, it can be read in 1X, 2X and 4X decoding modes which increases the resolution 1, 2 and 4 times respectively.

Velocity and acceleration measurements are required in advanced control applications to improve the effect of the controllers on the system. On the other hand, in haptic applications, for a realistic simulation, velocity and acceleration data is required to reflect the damping and inertial forces of the simulated environment besides position which is used to simulate the stiffness property. Tachometers and accelerometers are direct solutions for velocity and acceleration measurement; however they occupy large spaces, add inertia to the joints, have a noisy output and they are expensive. Additionally, in recent years, micro processors $(\mu Ps)$and Digital Signal Processors $(DSPs)$ are used widely in digital systems. Their widespread usage also makes it easier to implement encoders to digital systems. Thus, encoders, which are very precise position measurement devices, are good value for velocity and acceleration estimations from discrete position data.

Encoders are used for position measurement and they do not measure velocity and acceleration directly. As an encoder produces a square wave signal, position data can not be gathered continuously or at every sample. This signal is a discrete signal and its frequency depends on its resolution for a constant shaft velocity. Obtaining precise velocity information from this discrete signal is a challenging work, especially for low velocities [4]. There are many methods proposed in the literature to estimate velocity from discrete position and time data. General applications are on processing position and time data using arithmetic operations at specified sampling times. This type of applications are easy to implement but have some problems at some velocity regions. Besides, Kalman filters can also be used to estimate velocity from incremental encoder output and they give good results. These methods are described below and to show their performance on the Haptic Box some of them are tried experimentally.

5.1 Velocity Estimation Methods in Literature

Most of the studies on velocity estimation from an incremental encoder data show that there is not a way suitable for every velocity profiles [2,6,26]. In [2,26], some velocity estimators; lines per period (LPP), reciprocal-time, Taylor series expansions, backward difference expansions, and least square curve fits are presented. It is pointed in [2] that the least-squares velocity estimators filtered the measurement noise best, whereas the Taylor series expansions and backward difference equation estimators respond better to velocity transitions. In [26] it is concluded that using fixed-time algorithms for high-speed, fixed-displacement algorithms for low-speed, and least square fit algorithms for general situations proved advantageous. An adaptive sampling rate is used in [3], in which the sampling rate is changed adaptively for different velocities. In [4] a similar way is followed to let the algorithm to estimate the velocity for different velocities better, allowing the user to select the estimation precision and time delay. The reference [27] proposes an adaptive scheme designed in conjunction with a linear observer. In [6] a method called asynchronous sampling method (ASPM) is presented for determining velocity in systems with low-variable speeds and/or with low-resolution encoders. The method uses an auxiliary sampling period to estimate the velocity via an observer. It is shown in [28] that counting lines for a regular time period become degraded as sampling rates increase for velocity and acceleration estimations, and a Kalman filter is proposed. Kalman filters are widely used for filtering or estimating states in systems. Thus, it can be applied to velocity estimation for the discrete position data coming from incremental encoders.

In this study disadvantages of fixed time/position algorithms are explained and shown. For better estimation results adaptive velocity estimation is employed and results are evaluated. Finally, Kalman filters are used for velocity and acceleration estimation. Constant velocity and constant acceleration Kalman filter algorithms are used and both have given very good results. As acceleration estimation for reflecting inertia and mass properties is required, constant acceleration model of Kalman filter is used for the rest of the implementation work. Details of used methods are given in the following sections and applications are explained in Chapter 6.

5.2 Velocity Estimation Algorithms

Once the position and time information is stored for every sampling time, the first method one will think of is generally discrete differentiation. However, discrete-time derivative filters known are not satisfactory and as known derivative operators tend to magnify errors [26]. It is stated in [3] that arithmetic differentiation introduces significant error and does not give accurate results at low rotational velocities. Thus, some techniques are proposed in the literature for estimating velocity from discrete position data. To estimate the velocity from a discrete position signal, there are two general ways used. The first one is counting the number of encoder pulses in a specified constant time period, so time is fixed between two successive position measurements and this is called fixed-time estimator. The second way is measuring the time duration to travel a fixed distance, which is called fixed-position estimator [2].

5.2.1 Fixed-time Velocity Estimation

Obtaining good estimation values at low velocities are important in haptic applications to reflect small forces to the user. However, this type of velocity estimation does not give satisfactory results at low velocities. As the time is fixed, the number of pulses in this time interval will be less at low velocities resulting in greater errors in the velocity estimation. On the other hand, for high velocities, the sampling rate can be increased to decrease delay.

The simplest way of estimating velocity is counting lines per period (LPP) [2]. If at a sampling instance t_k, the measured position is x_k the velocity can be estimated as $\hat{\upsilon}_k = \Delta x_k / T$ where $\Delta x_k = x_k - x_{k-1}$ the traveled distance and $T = t_k - t_{k-1}$ the sampling interval. Some other methods are also reviewed in the reference. They are Taylor Series Expansion (TSE) Velocity Estimator, Backward Difference Expansion (BDE) Velocity Estimator and Least Squares Fit (LSF) Velocity Estimator.

In TSE velocity estimator, the velocity $\hat{\upsilon}_k$ at t_k is estimated from the velocity $\hat{\upsilon}_\beta$ at time t_β by a Taylor Series Expansion around time instance t_β:

$$\hat{\upsilon}_k = \hat{\upsilon}_\beta + \frac{1}{1!}\frac{d\hat{\upsilon}_\beta}{dt}\left(t_k - t_\beta\right) + \frac{1}{2!}\frac{d^2\hat{\upsilon}_\beta}{dt^2}\left(t_k - t_\beta\right)^2 + \frac{1}{3!}\frac{d^3\hat{\upsilon}_\beta}{dt^3}\left(t_k - t_\beta\right)^3 + \ldots \tag{5.1}$$

As $\hat{\upsilon}_k$ is sad to be the average velocity during sampling period t_k and it occurs at the middle of that period then Eq.5.1 becomes

$$\hat{\upsilon}_k = \sum_{j=0}^{N} \frac{1}{j!}\hat{\upsilon}_\beta^{(j)}\left(\frac{T_k}{2}\right)^j \tag{5.2}$$

where N is the order of the derivative.

In BDE velocity estimator, the function $x(t_k)$ formed by measured values is replaced by an interpolating polynomial that exactly fits the data points. For fixed time data the backward difference equation is obtained by expanding x_{k-i} in a Taylor series around x_k and than solving for dx_k / dt,

$$x_{k-i} = x_k + (-i)\frac{dx_k}{dt} + \frac{(-i)^2}{2!}\frac{d^2x_k}{dt^2} + \frac{(-1)^3}{3!}\frac{d^3x_k}{dt^3} + \dots \tag{5.3}$$

the first-order BDE for dx_k / dt is obtained from (5.3) as,

$$\frac{dx_k}{dt} = (x_k - x_{k-1}) + \frac{(-1)^2}{2!}\frac{d^2x_k}{dt^2} + \frac{(-1)^3}{3!}\frac{d^3x_k}{dt^3} + \dots \tag{5.4}$$

LSF velocity estimator is another method for estimating velocity. This method is explained in Section 5.2.2.

5.2.2 Fixed-position Velocity Estimation

Fixed position estimation gives very accurate velocity values at low velocities. In this approach, the time duration between two encoder pulses is measures. The accuracy is dependent on the sampling rate in the calculation as Δx_k is exactly equals to one (or an integer) and $\Delta t_k = NT$ where N is the number of timer ticks. Therefore, time resolution depends on T (sampling period) and so does the velocity as $\hat{v} = 1/(NT)$ with one fixed position step.

For fixed-position estimation the TSE and BDE, explained in fixed-time section, are directly applicable by an replacement of x_k and t_k. The function $t(x_k)$ is used in stead of $x(t_k)$ in Eq.5.4.

LSF velocity estimator is another method using exact data fit. An approximating polynomial of the form

$$t_k = c_0 + c_1 x_k + c_2 x_k^2 + c_3 x_k^3 + \ldots + c_N x_k^N \tag{5.5}$$

and the velocity at t_k is obtained by

$$\frac{d\hat{t}_k}{dx} = c_1 + c_2 x_k + \ldots + N c_n x_k^{N-1} \tag{5.6}$$

The coefficients $c_0 \ldots c_N$ are chosen to minimize total squared error. By this method an N^{th} order polynomial can be fit to M most recent data points provided that $N > M + 1$ in Eq.5.5.

5.2.3 Combined and Adaptive Velocity Estimation Algorithms

General applications are on measuring encoder pulses or time duration between encoder pulses, which are described as fixed-time and fixed-position estimation methods. However, there are some other techniques measuring both time and position, and some using variable intervals. There are some general velocity measurement techniques given in [29],

1) Direct pulse counting,
2) Single pulse time measurement
3) Constant elapsed time (CET)
4) Pulse time measurement using a variable number of counted pulses

The methods 1 and 2 are fixed-time and fixed-position estimations using only time or position measurement. 3 and 4 are a combination of time and encoder pulse counting. It is pointed in the reference that the CET method gives better results than 4. Two counters for time and position are used in the CET method. These counters are started at a rising edge of the encoder signal. For duration of a constant elapsed time

T_{el} waited and at the next rising edge, the encoder pulse after T_{el}, the counters are stopped. The contents of position counter C_p and time counter C_t are used to calculate the average velocity for the period T_{el}.

A later study using CET method with a variable time step (variable elapsed time T_{el}) is proposed in [3]. The method uses the CET technique; however, the desired elapsed time T_{el} is not fixed. According to the previously estimated velocity data, next desired sampling interval T_{el} is selected. By this way, an improvement on system accuracy at low velocities achieved while the response time is decreased at high velocities.

A simple and efficient method is proposed in [4]. This method allows the user to select the estimation precision and to tune the time delay, and it requires less calculation time. It is mentioned that the Euler estimation is the simplest way of obtaining velocity, if the position is precisely sampled. This is not possible using an incremental encoder pulse train as it contains stochastic error. An improvement is to tracking some backward steps, which gives a smoother velocity profile but it introduces some time delay. R is the encoder resolution and $q(t)$ is the real angular position of the shaft. If it is sampled with T, the discrete position can be denoted as $\theta(k)$ where $k = 1,2,...$. Assuming the encoder pulse train is uniform, the position error can be written as,

$$\left|\theta(k) - q(k)\right| < R \tag{5.7}$$

When a position segment $q(kT) - q((k-j)T)$, where $j = 1,2,...$ is selected than the estimated velocity can be written as,

$$\frac{\theta(k) - \theta(k-j)}{jT} = \hat{v}_j \tag{5.8}$$

If the velocity resolution is defined as $v_R = \dfrac{R}{T}$ than the error in velocity becomes,

$$\left|\hat{v}_j - v_j\right| < \frac{2}{j} v_R \tag{5.9}$$

From the Eq.5.9 it is seen that the absolute accuracy is increased by more backward steps j. However, the relative error r_j is more concerned than absolute error and it is written as,

$$r_j = \left|\frac{\hat{v}_j - v_j}{v_j}\right| \tag{5.10}$$

If $\hat{v}_j$ and v_j are written in Eq.5.10 the following expression can be obtained as

$$r_j = \left|\frac{\theta(k) - \theta(k-j) - q(kT) + q((k-j)T)}{\theta(k) - \theta(k-j)}\right| < \left|\frac{1}{\theta(k) - \theta(k-j)}\right|.2R$$

Using this expression and considering a number of encoder pulses traced back that is denoted by s_j, Eq.5.10 can be simplified to

$$\left|\theta(k) - \theta(k-j)\right| = s_j R \tag{5.11}$$

where for a given relative accuracy r_j, s_j can be calculated as,

$$s_j = \frac{2}{r_j} \tag{5.12}$$

Using these parameters, an algorithm is proposed in [4]. To satisfy the desired relative accuracy r_j is defined previously. However, especially in low velocities, satisfying the desired relative accuracy can take too long. To deal with this problem, a maximum number of backward steps is defined as m. Figure 5.1 shows the algorithm to estimate the velocity.

The method output is compared with the velocity measurement device outputs experimentally in the reference. It is seen that the method gives good results. When the relative accuracy is decreased the method response returns with a greater delay.

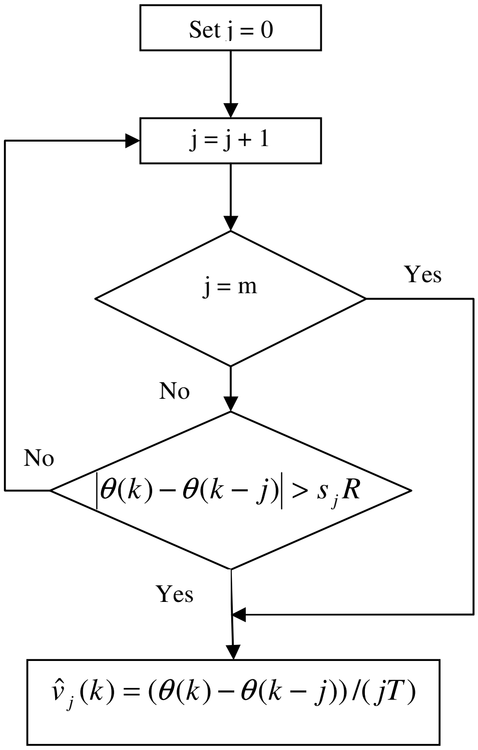
Set j = 0
j = j + 1
j = m
Yes
No
No
$|\theta(k)-\theta(k-j)| > s_j R$
Yes
$\hat{v}_j(k) = (\theta(k)-\theta(k-j))/(jT)$

Figure.5.1 The velocity estimation algorithm proposed in [4]

5.2.4 Velocity and Acceleration Estimation with Kalman Filters

Kalman filters are widely used to filter or estimate states of dynamic systems from measurements contaminated by random noise. A Kalman filter is an algorithm proposed by Rudolf E. Kalman in 1960 [7]. It can be applied to the systems with zero-mean white Gaussian noises [11]. The algorithm predicts the value of a state according to system parameters and the input to the system and it corrects that value according to measurement. Thus, it is a prediction/correction algorithm for states of dynamic systems.

The methods described up to here are about processing position and time data by arithmetic operations to get the velocity information. At high speeds many of these methods may work well, but they can not measure velocity correctly at low speeds. There are also some model based estimators, in which the model parameters and disturbances must be know accurately and this is not possible for most cases. Therefore, some models called constant velocity and constant acceleration models can be employed in Kalman filters, which do not require system information. These methods, which use kinematic models, are also called kinematic Kalman filters (KKF) in some references [11]. Kalman filters also provide important advantage to the stability of the control systems. In the methods requiring a period of time to estimate the velocity, there is not any information about velocity given to the controller or the previous velocity is held. However, Kalman filters can provide an estimate of velocity at every sample time.

By the widespread use of microcontrollers and computers, discrete time implementations of algorithms became popular and Kalman filters are one of them. Simply a Kalman filter estimates a value of a state according to previous value and recent measurement of that state. To do that, the algorithm uses a gain K called Kalman gain. The simplest form of a Kalman filter with constant K can be given as [8]:

$$\hat{x}_{i+1} = (1 - K)\hat{x}_i + Ky_{i+1} \tag{5.13}$$

Supposing that $\hat{x}_i$ is the best estimate of the state at time i, the state at time $(i+1)$ can be estimated from the previous value $\hat{x}_i$ and the recent measurement y_{i+1} using a weight between them by the constant K. Here, K determines how much the measurement is reliable. If measurement is fully reliable than K goes to one ($K \to 1$), and if it is fully faulty than K goes to zero ($K \to 0$).

To get familiar with Kalman filter notifications, some matrix presentations are explained below. G. C. Dean [8] uses i, and $(i+1)$ in the subscript of matrices to show prediction/correction and time instances. For a constant velocity model of a system the matrices can be written as:

$$\begin{bmatrix} \hat{x} \\ \hat{\dot{x}} \end{bmatrix}_{i+1} = \begin{bmatrix} 1 & T \\ 0 & 1 \end{bmatrix} \begin{bmatrix} \hat{x} \\ \hat{\dot{x}} \end{bmatrix}_i \tag{5.14}$$

where T is sampling period. In a general form Eq.5.14 can be written as

$$\hat{X}_{i+1/i} = \phi_i \hat{X}_{i/i} \tag{5.15}$$

X is the state vector defining the system and ϕ is the state transition vector. Some of the states are measured in the system to control it. The measurement values are shown by

$$\begin{bmatrix} y \\ \dot{y} \end{bmatrix}_{i+1} \tag{5.16}$$

and it is represented by Y_{i+1}. Similar to the system defined by a single state in Eq.5.13, a weighted mean can be written as

$$\hat{X}_{i+1/i+1} = (I-K)\hat{X}_{i+1/i} + KY_{i+1} \tag{5.17}$$

where I is the identity matrix and K is 2x2 matrix. The term $(i+1/i)$ in the subscript in Eq.5.15 show time instance/prediction and the term $(i+1/i+1)$ in the subscript in Eq.5.17 shows time instance/correction. Eq.5.13 and Eq.5.17 form the filter to estimate states with constant Kalman gain K. However, for general applications K is not constant. In Kalman filtering, system and measurement noises are taken into account. The system noise is denoted by the capital letter Q. The capital letters P and R used to represent variances of estimate and measurement noises respectively. The variance of the new estimate is given by

$$\hat{P}_{i+1} = E\left[\left(\hat{x}_{i+1} - E\left(\hat{x}_{i+1}\right)\right)^2\right] \tag{5.18}$$

$E\left(\hat{x}_{i+1}\right)$ is the expected value of the new estimate $\hat{x}_{i+1}$, Eq.5.18 is the formula for variance. As is known, the Kalman gain K is tried to be found (for example in Eq.5.17). And now, it can be calculated by

$$K_{i+1/i+1} = \hat{P}_{i+1/i} H_{i+1}^T x \left(H_{i+1} \hat{P}_{i+1/i} H_{i+1}^T + R_{i+1}\right)^{-1} \tag{5.19}$$

where, H is the matrix identifying the measured states. To find K, $\hat{P}_{i+1/i}$ should be calculated first.

$$\hat{P}_{i+1/i} = \phi_i \hat{P}_{i/i} \phi_i^T + Q_i \tag{5.20}$$

where, Q is the system noise matrix, and it estimates the modeling errors. Here, the subscript $(i+1/i)$ of $\hat{P}_{i+1/i}$ means that the matrix $\hat{P}$ is calculated at time $(i+1)$ and it is the predicted one pointed by (i). Thus, a correction of it should be calculated as

$$\hat{P}_{i+1/i+1} = \left(I - K_{i+1} H_{i+1}\right) \hat{P}_{i+1/i} \tag{5.21}$$

to be used in the next calculation time $(i+2)$. Thus, all the Kalman equations are obtained to estimate the states. The Kalman loop can be explained by a diagram as shown in Figure 5.2 [10]. For compatibility with the previous notation subscripts are left as they were but superscripts are changed as it is simpler to understand using the (-) symbol in the superscript to denote the prediction.

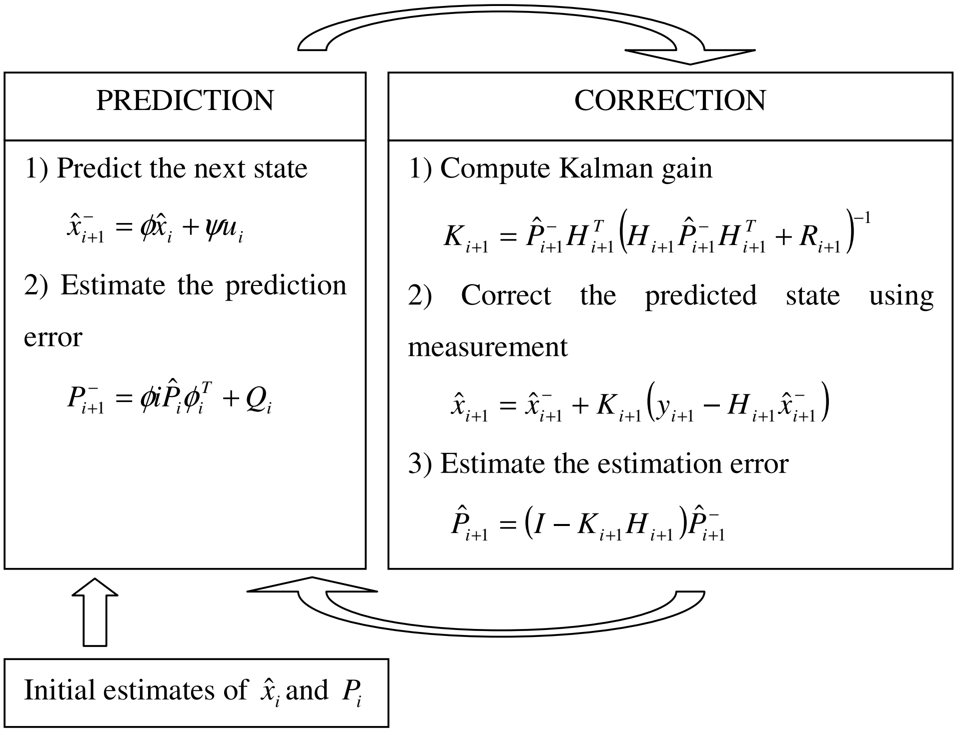
PREDICTION
1) Predict the next state
$\hat{x}^-_{i+1} = \phi\hat{x}_i + \psi u_i$
2) Estimate the prediction error
$P^-_{i+1} = \phi i\hat{P}_i\phi_i^T + Q_i$
CORRECTION
1) Compute Kalman gain
$K_{i+1} = \hat{P}^-_{i+1}H^T_{i+1}\left(H_{i+1}\hat{P}^-_{i+1}H^T_{i+1} + R_{i+1}\right)^{-1}$
2) Correct the predicted state using measurement
$\hat{x}_{i+1} = \hat{x}^-_{i+1} + K_{i+1}\left(y_{i+1} - H_{i+1}\hat{x}^-_{i+1}\right)$
3) Estimate the estimation error
$\hat{P}_{i+1} = \left(I - K_{i+1}H_{i+1}\right)\hat{P}^-_{i+1}$
Initial estimates of $\hat{x}_i$ and P_i

Figure 5.2 Recursive Prediction-Correction Structure of the Kalman Filter

CHAPTER 6

SYSTEM IMPLEMENTATION

The system implementation of velocity estimation and haptic control methods are given in this chapter. First, the velocity and acceleration estimation from the incremental encoder is implemented and the results are presented. Next, using the velocity and acceleration estimation virtual environment characteristics in the system haptic control is developed. Finally, employing the Virtual Reality Toolbox® of MATLAB® in the interface the system demonstration is done.

6.1 Experiment Setup

The experimental setup consists of the *Haptic Box, target computer and the host computer* as shown in Figure 6.1. The Haptic Box is used as an input and output device for the user interaction with the system. The target computer is the control unit of the system. It receives the encoder and transducer signals from the user, processes them to extract motion and torque information, and trough the control law it generates a reference voltage to be sent to the servo amplifier of the Haptic Box. The input-output operations to the target computer are done via the data acquisition (DAQ) cards. There are two main roles of the host computer. The first is to compile, download and manage the applications that will run on the target computer via the LAN connection. And the second is to collect the motion data processed by the target computer and use it to manipulate the virtual environment on the screen. The applications running on the target computer are modeled using the Simulink® and the xPC Target® libraries. Virtual environments are modeled using the VRML language and they are simulated using the Virtual Reality Toolbox® of MATLAB® on the host pc.

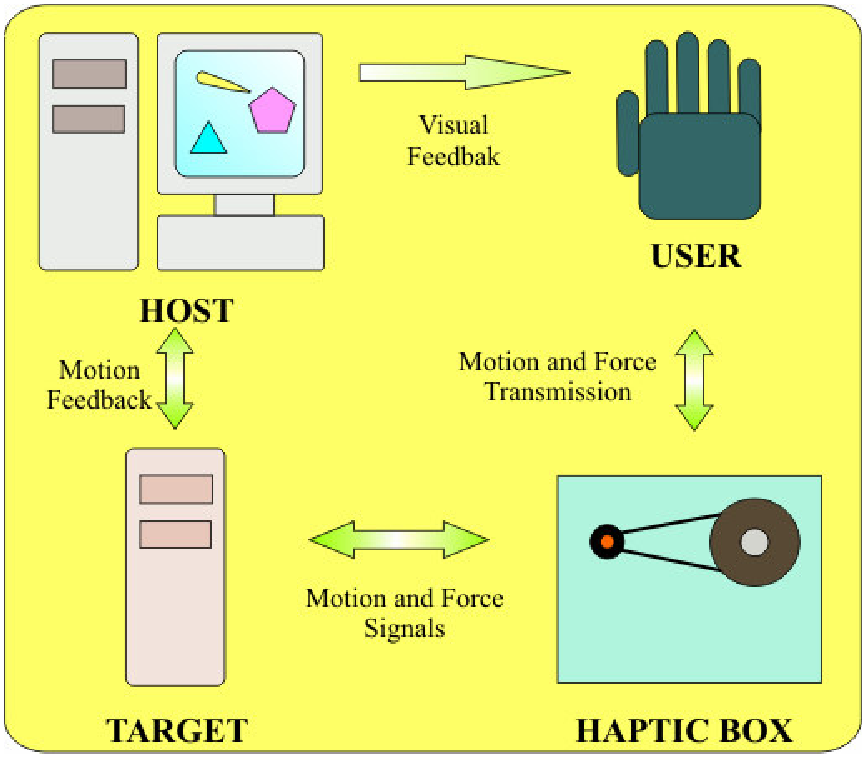

Figure 6.1 Haptic Interface

The Haptic Box is explained in Chapter 3. It has a DC Maxon RE40 DC motor and a HEDS5540A encoder attached to the back of it. The position is read from this optical incremental encoder discretely. The encoder has 500 lines at A, B channels and it also has an Index channel. The position is read in 4X counting mode so that the resolution increases to 2000 counts/rev on the motor side. There is a gear ratio of 18/128 between the motor and the knob of the box. Thus the resolution at the knob side is (128/18)*2000 counts/rev. There is an encoder with 5000 pulse/rev at A and B channels. This encoder is attached to the front side of the motor and it is used for velocity and acceleration monitoring. A torque transducer is also introduced in to the box that is capable of measuring 10Nm torque load.

The target computer has a Pentium 1.80 GHz processor and 512 MB of RAM. There are two DAQ cards to collect data from the system. National Instruments Company NI PCI-6602 and NI PCI-6052E DAQ cards are used for encoder input and analog I/O respectively.

The host computer is a HP XW8200 workstation with a Xeon 3.60 GHz processor, 3GB of ram and a NVIDIA Quadro FX 4500 512MB ram graphics card. This powerful computer is needed for making the real time applications more realistic as a refresh rate of 30Hz is required for a good perception for human eye and the simulation sapling period is set to $T = 0.001s$ as the refresh rate for force should be at last 1kHz [22].

6.2 Velocity and Acceleration Estimations

Velocity estimation methods are described in Chapter5. The first and simplest way is numerical differentiation, a *fixed time* method, in which the number of counts in a period of fixed time is divided by the time period. This method is simple and gives good results at high speeds. However, when the angular speed is low or the encoder resolution is decreased the method becomes degraded. As an encoder converts the motion into a discrete signal, discretization error increases and so the error in velocity increases as shown in Figure 6.2, at low speeds. Another problem is that if the period of the encoder output becomes larger than the sampling period than the same level of the encoder signal (a high level for example) is sampled two times or more and they get the same value as the position does not change in that time interval. This results in a zero velocity due to constant position and this situation will be a problem for stability. To avoid this problem *constant position* method can be employed. This method will prevent system from detecting an unwanted zero velocity but introduce a considerable time delay in to the system. Thus, to avoid these problems improvements of those methods are developed in the literature. Constant Elapsed Time (Figure 6.3) can be treated as an improvement to the fixed-time velocity estimation algorithms, which reduces the discretization errors. In this method a constant elapsed time is selected and for this period the system waits. When this time is reached the next position pulse is waited and time is measured at this encoder pulse. By this way more accurate velocity estimation is done than a fixed-time velocity estimation (estimating velocity at elapsed time).

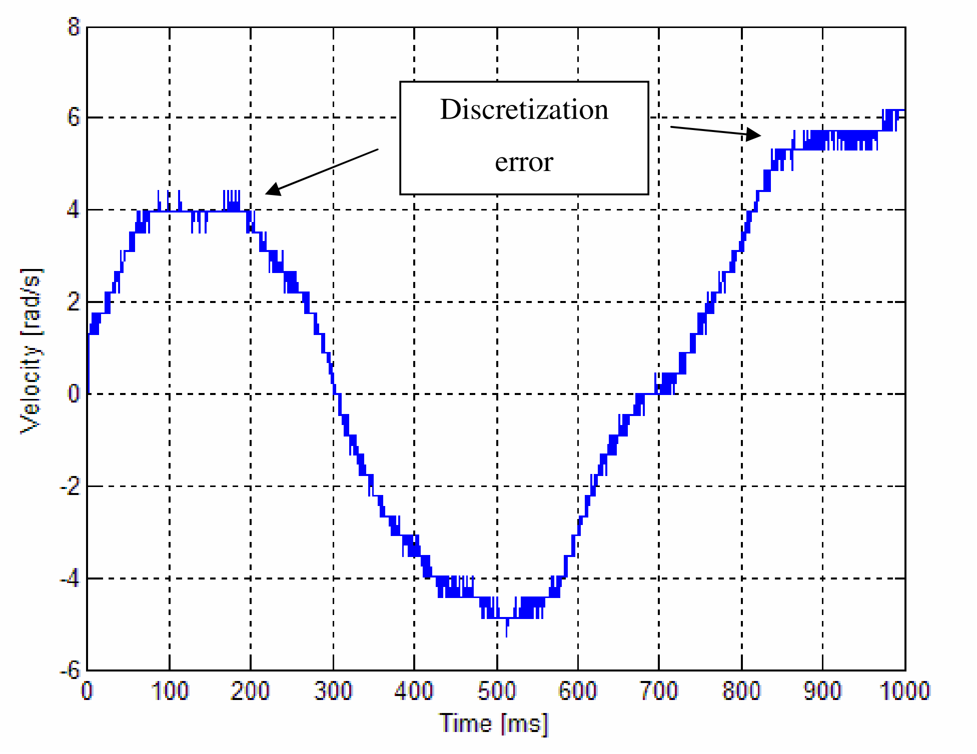

Figure 6.2 Effect of discretization on velocity estimation in low velocity region

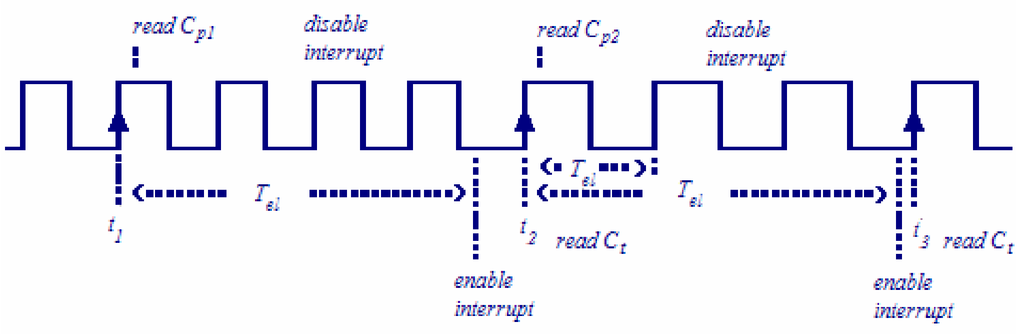

Figure 6.3 CET Method

6.2.1 Adaptive Velocity Estimation

Another way of improving velocity estimation is using a variable time step. Looking at the poison data an adaptive algorithm can decide when to calculate the velocity estimation. In Chapter 5 an adaptive algorithm is presented in Figure 5.1. This method is implemented using the Haptic Box, and the results are compared to the monitor velocity, which is obtained from the Scancon encoder that has 5000 pulse/turn at A nad B channels, in Figure 6.4. The algorithm parameters are set as: sampling time $T = 0.001s$, number of counts per turn $N = 2000$, relative accuracy $r_j = 5\%$ and the time limit for velocity detection $m = 0.05$ (50 ms).

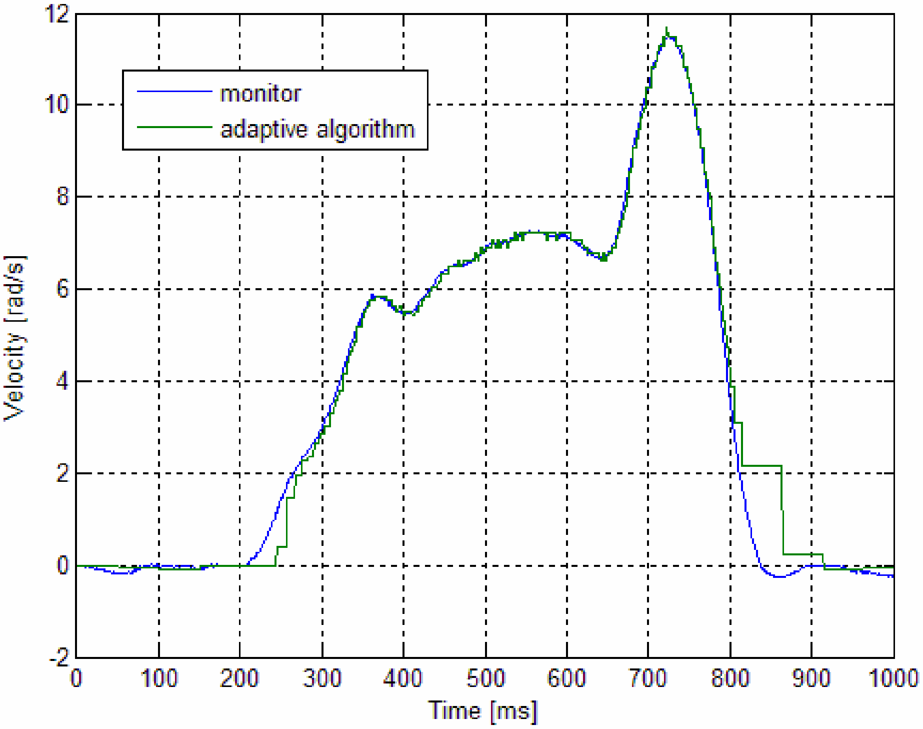

Figure 6.4 Velocity estimation with adaptive algorithm

Figure 6.4 shows that the algorithm works better at higher speeds. In low speed regions (~230 - 800 ms) the algorithm is forced to calculate a velocity value as the maximum allowable time limit is reached. With a relative accuracy $r_j = 2\%$, as the accuracy increases more steps back are required, and so more delays are introduced.

6.2.2 Velocity Estimation with Kalman Filters

It is pointed in Chapter 5 that Kalman Filtering is a good estimation method from noisy data. In this study, a Kalman Filter with Constant Velocity model is used to estimate velocity and the system is assumed to have zero-mean white Gaussian noises. In this method the system matrix is a 2x2 matrix as

$$\phi = \begin{bmatrix} 1 & T \\ 0 & 1 \end{bmatrix} \tag{6.1}$$

and according to Eq.5.15 and Eq.6.1 predicted state values for position and velocity become

$$\hat{x}^-_{i+1} = \hat{x}_i + T\hat{\dot{x}}_i \tag{6.2}$$

$$\hat{\dot{x}}^-_{i+1} = \hat{\dot{x}}_i \tag{6.3}$$

After prediction of P matrix as in Eq.5.20, Kalman gain matrix K is obtained as in Eq.5.19 and correction of predicted states is done as in Eq.5.17 such that

$$\hat{x}_{i+1} = \hat{x}^-_{i+1} + K_{i+1}\left(y_{i+1} - \hat{x}^-_{i+1}\right) \tag{6.4}$$

$$\hat{\dot{x}}_{i+1} = \hat{\dot{x}}^-_{i+1} + K_{i+1}\left(\dot{y}_{i+1} - \hat{\dot{x}}^-_{i+1}\right) \tag{6.5}$$

assuming that the velocity is measured. If velocity is not measured than the measurement matrix H will have a zero at the right-bottom corner and this will cancel the effect of Kalman gain and the estimated value will be equal to the predicted (previous) value in Eq.6.5.

A Kalman Filter with constant velocity estimation is modeled in Simulink® and it is run on the target pc in real time. The Kalman algorithm code is embedded into Simulink® model (Appendix A). Figure 6.5 shows the experiment results. In the experiment the matrices Q and R are selected as

$$Q = \begin{bmatrix} 0.1 & 0 \\ 0 & 0.1 \end{bmatrix} \qquad\qquad R = \begin{bmatrix} 0.01 & 0 \\ 0 & 0.1 \end{bmatrix}$$

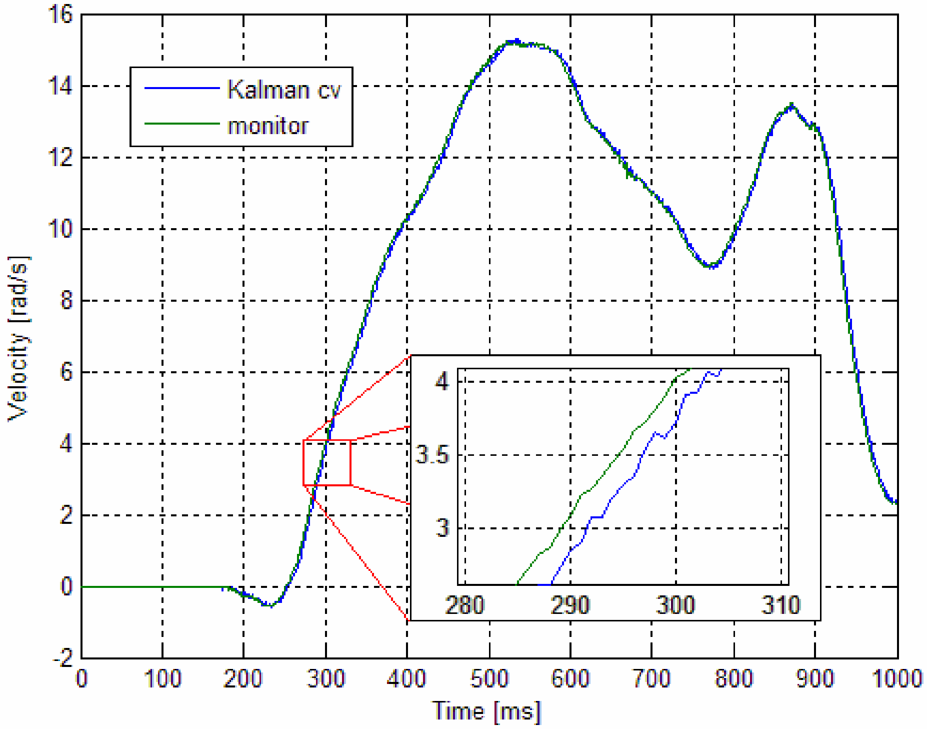

Figure 6.5 Velocity Estimation with Kalman Filter – Constant Velocity model

Q is the system noise matrix and R is matrix that represents the measurement variances. These matrices are obtained experimentally. It is seen in the experiments that the changes in system noise matrix Q does not effect the estimation too much but measurement variance matrix R does a lot. When small values are selected for r_{11} and r_{22} then the filter responds fast but some oscillations begin to appear and when they are selected larger the filter follows the monitor velocity by some shift proportional to greatness of the R matrix elements but with a smoother profile. Thus, an optimum pair for matrix R is tired to be selected. One can recognize that r_{22} is greater than r_{11} . The reason of this is that the encoder gives good position measurement. However, velocity measurement is obtained by numerical differentiation and it has greater error. The figure shows that with the selected parameters the filter gives good results at it is seen in the magnified segment that the filter has an acceptable time delay (~4 ms).

Actually, most of the haptic applications do not use inertial forces in applications. Most generally, users touch some surfaces having stiffness and damping characteristics. However, in this study inertial forces are also aimed and thus acceleration measurement or estimation is required. For this purpose, general approach is to use a numerical differentiation after a good velocity profile is obtained. In the methods that use the numerical differentiation to estimate velocity, the second differentiation increases the errors more and generally acceleration estimation becomes impossible. Thus, using Kalman Filters for acceleration estimation becomes more suitable. To estimate acceleration a constant acceleration model is used similar to constant velocity model. The state transition matrix for this approach is

$$\phi = \begin{bmatrix} 1 & T & T^2/2 \\ 0 & 1 & T \\ 0 & 0 & 1 \end{bmatrix} \tag{6.6}$$

in this case the predicted states can be written as

$$\hat{x}_{i+1}^{-} = \hat{x}_i + T\hat{\dot{x}}_i + \left(T^2/2\right)\hat{\ddot{x}}_i \tag{6.7}$$

$$\hat{\dot{x}}_{i+1}^{-} = \hat{\dot{x}}_i + T\hat{\ddot{x}}_i \tag{6.8}$$

$$\hat{\ddot{x}}_{i+1}^{-} = \hat{\ddot{x}}_i \tag{6.9}$$

and the corrections are made after prediction of P and calculation of K as in Eq.6.4 and Eq.6.5 for position and velocity, and for acceleration it is made as

$$\hat{\hat{x}}_{i+1} = \hat{\hat{x}}^{-}_{i+1} + K_{i+1}\left(\ddot{y}_{i+1} - \hat{\hat{x}}^{-}_{i+1}\right) \tag{6.10}$$

The code is similar to the one for constant velocity model as given in Appendix A but with some differences. The matrix ϕ given in Eq.6.6 and H , P , Q and R matrices become a 3x3 square matrix and measurement and state matrices Y and X become 3x1 matrices and state order rises to 3.

In the experiment the acceleration measurement is also given to the filter obtained by the second derivative of the velocity numerically. However, 20 steps back is traced to make it smoother. Q and R matrices are selected as

$$Q = \begin{bmatrix} 0.1 & 0 & 0 \\ 0 & 0.1 & 0 \\ 0 & 0 & 0.1 \end{bmatrix} \qquad R = \begin{bmatrix} 0.01 & 0 & 0 \\ 0 & 0.1 & 0 \\ 0 & 0 & 1 \end{bmatrix}$$

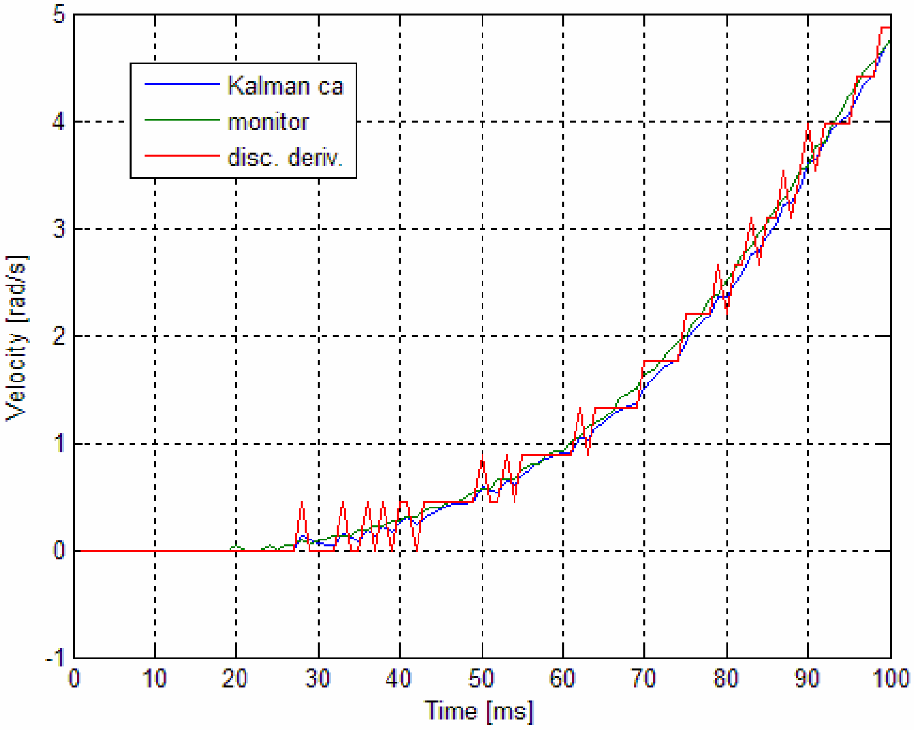

Figure 6.6 Velocity Est. – Kalman Filter Const. Acc. – Low Velocity Region

The velocity estimation with inclusion of acceleration measurement can be seen in Figure 6.6 and Figure 6.7. For both low and high velocity regions the Kalman Filter gives close results to the monitor velocity and it is clear that it is superior to the discrete derivation estimator. With current matrix estimations for Q and R the filter seems to perform well. The filter has a negligible lag (~2ms for low & high velocity regions) compared to monitor signal.

Acceleration estimation is a more complex work. Using the just previous velocity measurement data for differentiation increases the errors resulting in increased oscillations. Thus some steps back are traced to have a smoother acceleration profile. This profile is used as the measurement data given to the Kalman filter. The result is compared to the acceleration monitor signal (from Scancon encoder) in Figure 6.8. The filter gives good estimation results with a little greater delay (~5 ms) than the one for velocity estimation.

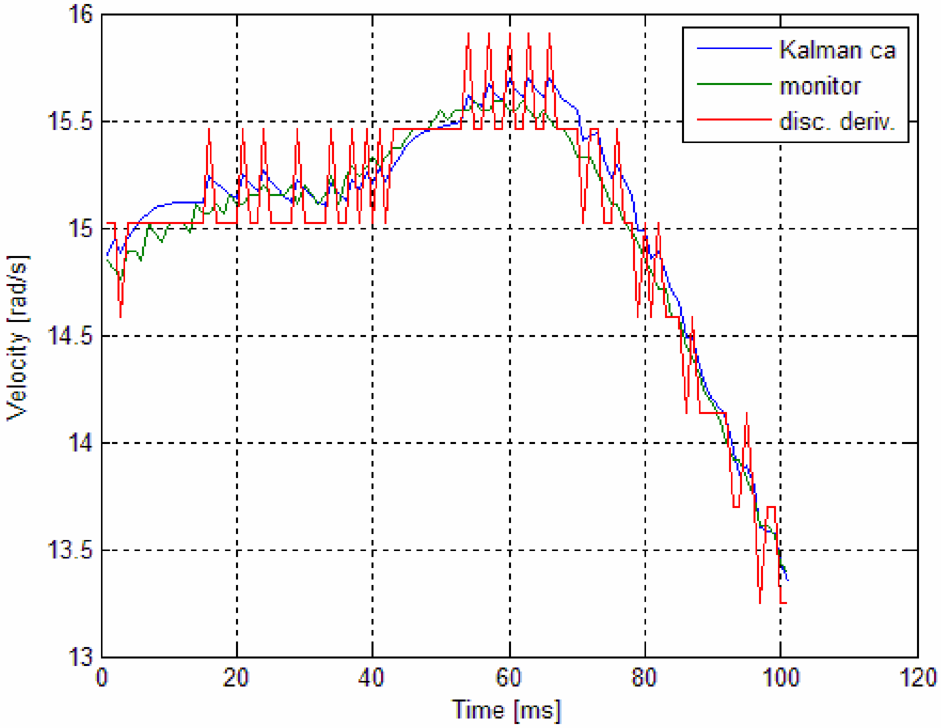

Figure 6.7 Velocity Est. – Kalman Filter Const. Acc. – High Velocity Region

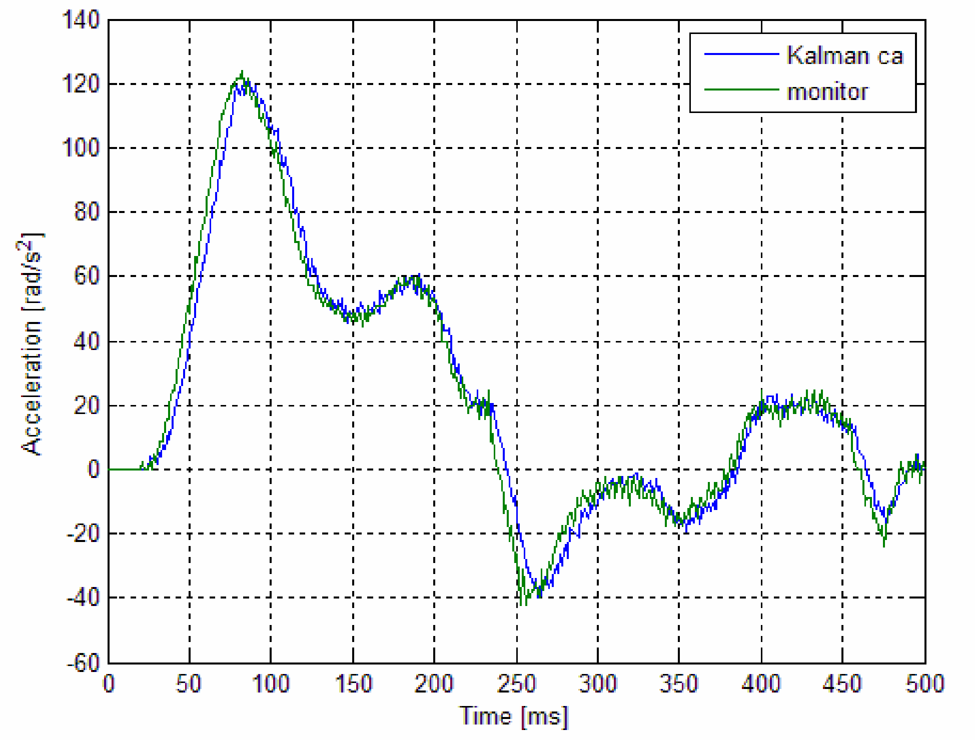

Figure 6.8 Acceleration estimation with Kalman Filter – Constant Acc. Model

6.3 Control System Applications

In this section velocity/acceleration estimation and haptic control implementations are presented. The applications demonstrate the control algorithms mentioned in Chapter 4, Virtual Reality for visual perception and effects of estimations of velocity and acceleration on the force feeling.

For output confirmation and different control applications, a force transducer is attached to the back side of the knob of the Haptic Box. The relation between output voltage and the input torque is not given in the specifications of the transducer and it is found experimentally as show in Figure 6.9. A torque arm is fixed to the front side of the transducer and from a 10cm distance several weights are applied. The relation between torque and voltage is shown in the figure. For getting a constant K_t converting the output voltage to the corresponding torque value, a line is fit to the max & min values of the measurements as seen in the figure and its slope is calculated. This assumption is done depending on the linear transition seen in the figure. The voltage-torque constant is calculated as

$$K_t = 1.027[Nm/V]$$

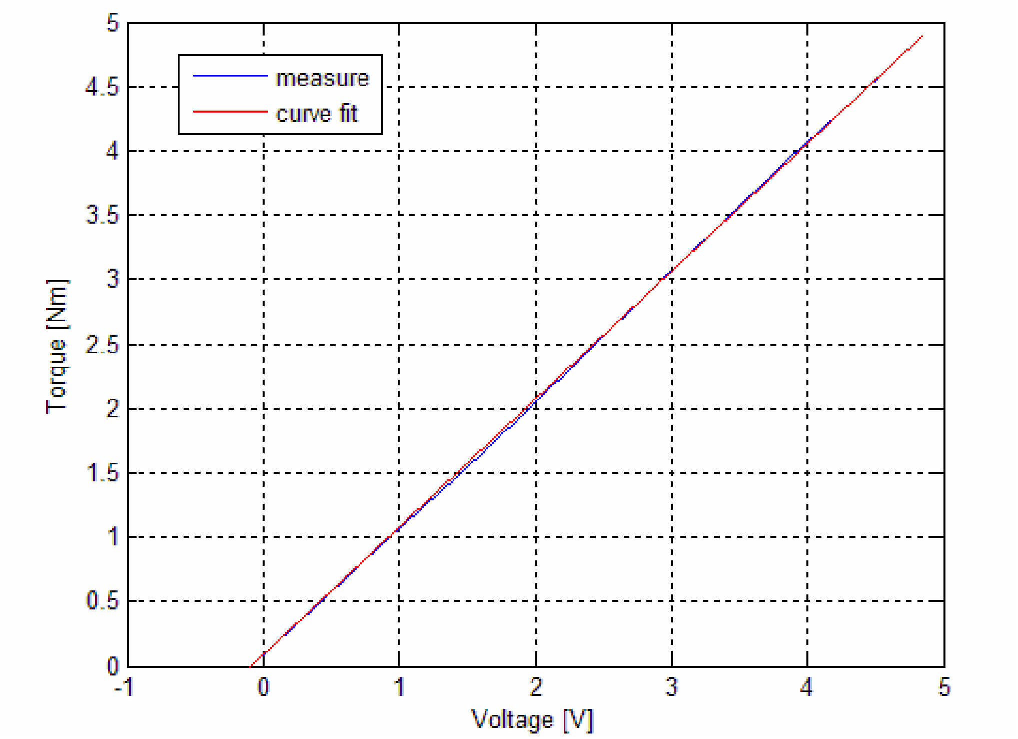

Figure 6.9 Transducer output voltage & torque input relation

Another component that has to be experimented for obtaining a constant parameter was the Copley 413CE servo amplifier. It is configured to torque mode so for a given voltage it applies a corresponding current to the DC brush motor. However the relation between reference voltage and current output was not known. Thus, firstly the motor is replaced by a 5W 33R resistor and current flowing through it measured for different voltages. Second, the motor is replaced by the resistor and its shaft is held stationary. It is seen in the experiments that the relation was linear as shown in

Figure 6.10 (test results with motor). A line is fit to the max & min values and the slope of the curve, that is the constant K_{av} is calculated as

$$K_{av} = -0.6385[A/V]$$

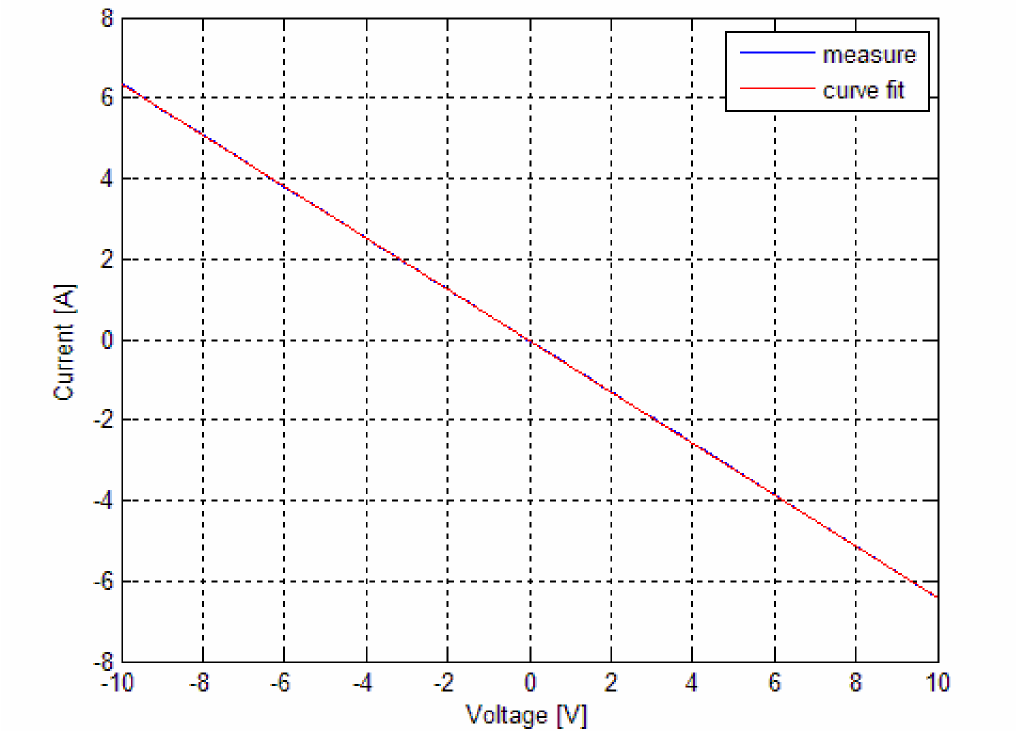

Figure 6.10 Copley 413CE reference voltage & output current relation

After the constants K_t and K_{av} are obtained, a variable reference voltage is given to the amplifier and the corresponding torque is compared by the measured one. It was seen the profiles show the same characteristics but reference torque leads measured torque in both negative and positive torque values in means of torque magnitude. This showed that the calculated measurement constant K_t was greater than it had to be. This comment is done depending on the fact that the test for Copley 413CE was much more reliable than the test for transducer calibration. The measurement constant is lowered to

$K_t = 1.0[Nm/V]$

and the two curves were nearly coincided as shown in Figure 6.11. The aim of the following experiments are not measuring true values of applied forces but measuring the effectiveness of the interface. Fast transitions at high torque values cause an amount of delay (~20ms) or error because of the inertia added to the system by the transducer and its attachments. The transducer gives a noisy voltage output at transitions and it has to be filtered. Thus, a Kalman filter is also used here to smoothen the transducer output as shown in the figure with the red color. The code is similar to the one given in Appendix A and parameters were set as

$Q = 0.0005$, $\quad R = .1$, $\quad H = 1$

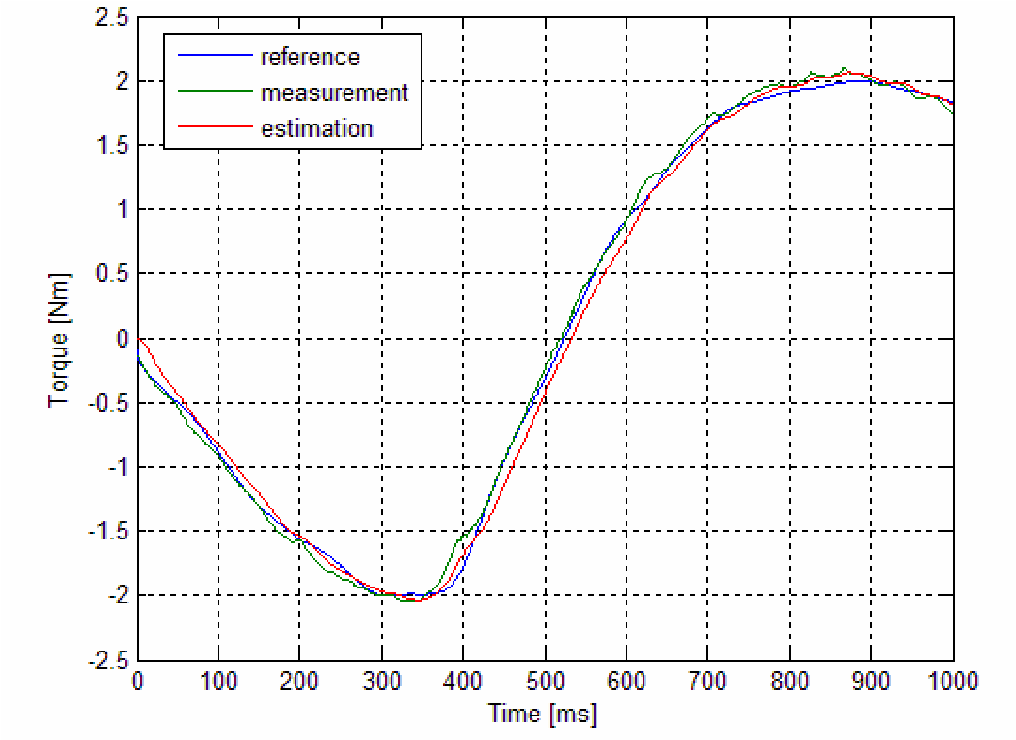

Figure 6.11 Reference, measured and estimated torques

6.4.1 Open Loop Impedance Control

As the reflection of the reference force to the user is confirmed, control algorithms can be experimented. Open loop impedance control is the most generally used and simple control scheme. Beginning with it makes it easier to understand other methods. In this control type, simply the motion of the Haptic Box knob is acquired and through the virtual environment a reference force is calculated to be reflected to the user. For this experiment a virtual disk is modeled that has inertia and it was connected to the ground by a spring and a damper pair. The Simulink® model of the interface is showed in Figure 6.12 and block details are given in Appendix E.

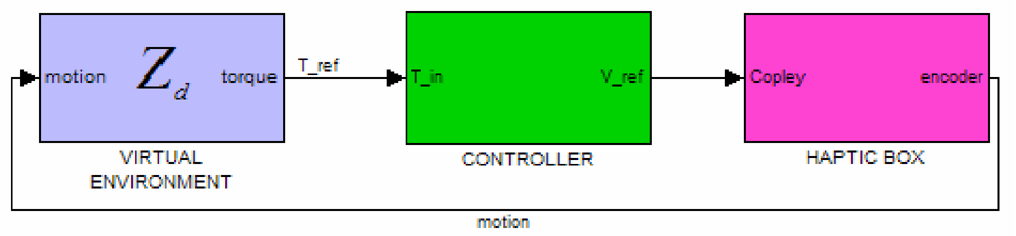

Figure 6.12 Simulink model of open loop impedance control

As stated before in these experiments the effects of Kalman Filter is also important and it is also mentioned. In the experiments with open-loop impedance control it was seen that after certain inertia and damping force limits, the system became unstable. Actually, when the parameters for inertia and damping set high and than the simulation started the knob starts to oscillate. At low speeds velocity estimation error is much higher. When the knob is stationary at initial position velocity and acceleration are zero and no corresponding torque is applied to the knob. However, when the user just touches to the knob a small motion with larger error compared to high speed error occurs. This error magnifies by inertia and damping gains. This starts an oscillation and system behavior becomes unstable. Thus, several experiments are done to determine those parameters. The transducer is detached from the Haptic Box to reduce unmodeled dynamics that affects inertia gain limit too much. Sampling period is set to $T = 0.001s$ for the experiments. The power supply characteristics are not certain. However it is determined that a torque value of $\pm 3Nm$ on the knob can be generated by the motor.

The Virtual Environment is a model with stiffness, damping and inertia and the reference force is calculated as

$$\tau_{ref} = I\hat{\ddot{\theta}} + b\hat{\dot{\theta}} + k\hat{\theta} \qquad (6.11)$$

Where $\hat{\ddot{\theta}}, \hat{\dot{\theta}}, \hat{\theta}$ are estimated angular acceleration, velocity and position values coming from the Kalman Filter. They are multiplied by the corresponding constants and added to each other to calculate the reference torque. In the experiments it is seen that the stiffness gain k does not have a limit value affecting stabilization. Also, it is seen that oscillations begin at about $b = 1.5[Nm * s / rad]$ damping coefficient and $i = 0.0045[Nm * s\text{^}2 / rad]$ inertia. This value corresponds to the inertia of an aluminum disk with $1cm$ thickness and $20.3cm$ diameter.

6.4.2 Impedance Control with Force-feedback

Impedance control with force feed-back is done employing the torque transducer actively in the interface as shown in the Figure 6.13. The measured torque is compared by the reference torque and torque error is given to the force control block as an input. A proportional control law is used to control the force.

For reference torque calculation Eq.6.11 is used again. The output of the filter gives a very smooth voltage output. P control law is used in the force control block and it was set as $K_p = -0.2$. By this method the maximum damping coefficient that can be reflected satisfying stability was $b = 2[Nm * s / rad]$ and the inertia was $i = 0.005[Nm * s\text{^}2 / rad]$. This value corresponds to the inertia of an aluminum disk with $1cm$ thickness and $20.84cm$ diameter.

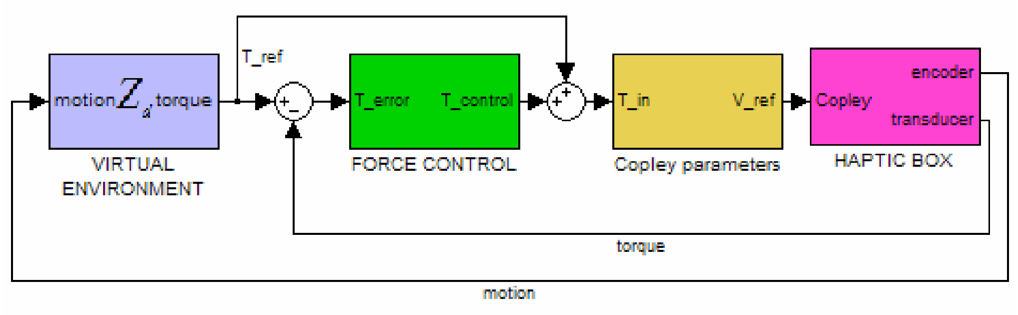

Figure 6.13 Impedance control with force-feed back

6.4.3 Admittance Control

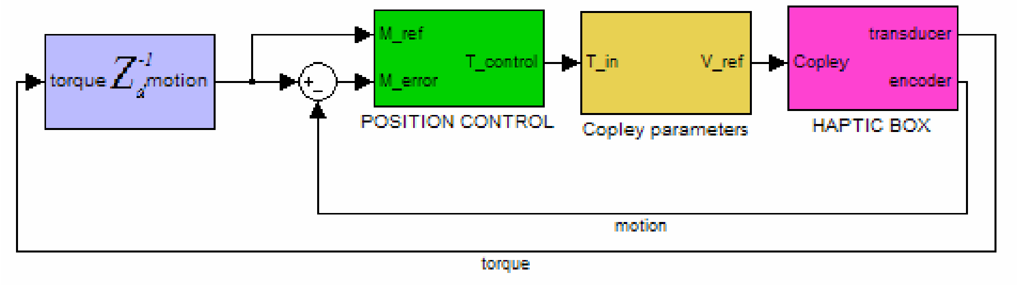

Figure 6.14 Admittance Control

In admittance control the force is supplied to the virtual environment and motion is taken out through the desired admittance as shown in Figure 6.14. The reference motion is calculated using the Eq.6.11. As in the admittance display mode the input is force and the output is motion the equation must be reversed. Thus, Laplace transform of the equation was taken assuming zero initial conditions and Eq.6.12 is obtained.

$$\theta(s) = \frac{1}{Is^2 + bs + k}\tau(s) \tag{6.12}$$

Once the measured torque is given to Eq.6.12 the knob position is obtained. After that a position controller can be employed to control device position. In the experiments with admittance control a spring model as a virtual environment was simulated and it was seen that the interface works well. However, the experiments for damping and inertia reflection did not perform well as the system was unstable.

6.4 Case Study

In haptic interfaces the control loop is closed by the virtual environment. The virtual environment in the haptic interface is the place where the reference control input is generated. The reference input is calculated according to the virtual environment properties, and it is given to the control unit in the form of force or motion according to the type of the display mode as described in Chapter 4.

For representing virtual environments, different methods can be used. A 3D environment for representing the virtual environment would be the best way to make it realistic. Thus, several 3D modeling languages are used in such applications. OpenGL® and DirectX® are most popular platforms for developing those environments and VRML (Virtual Reality Modeling Language) is another language to model interactive virtual environments. As the general application platform for system implementation is decided to be MATLAB® and Simulink®, the preferred language for developing virtual environments is VRML, as Simulink® uses this language to simulate virtual models in its Virtual Reality Toolbox®.

The virtual environment of the haptic interface is modeled so that it contains mass, damper and spring. The Virtual Reality Toolbox® of Simulink® is used to display and simulate the virtual environment. Virtual Reality Toolbox® accepts the virtual environments modeled using VRML language. Thus, the environment is modeled using a CAD program and it is saved as a VRML file. There is a program coming with MATLAB® named *vrbuil2* which can also be used to model the virtual environments. In this study it is used to modify the VRML file created by the CAD program previously. After modeling of virtual environment is complete, Virtual Reality Toolbox® is used to add it to the interface. Blocks of this toolbox can access the objects in the modeled virtual environment. Their position, orientation, scale, etc., can be modified in real-time according to the rules defined by the Simulink® model. This is the method used in this study to visualize the virtual environments as shown in Figure 6.15.

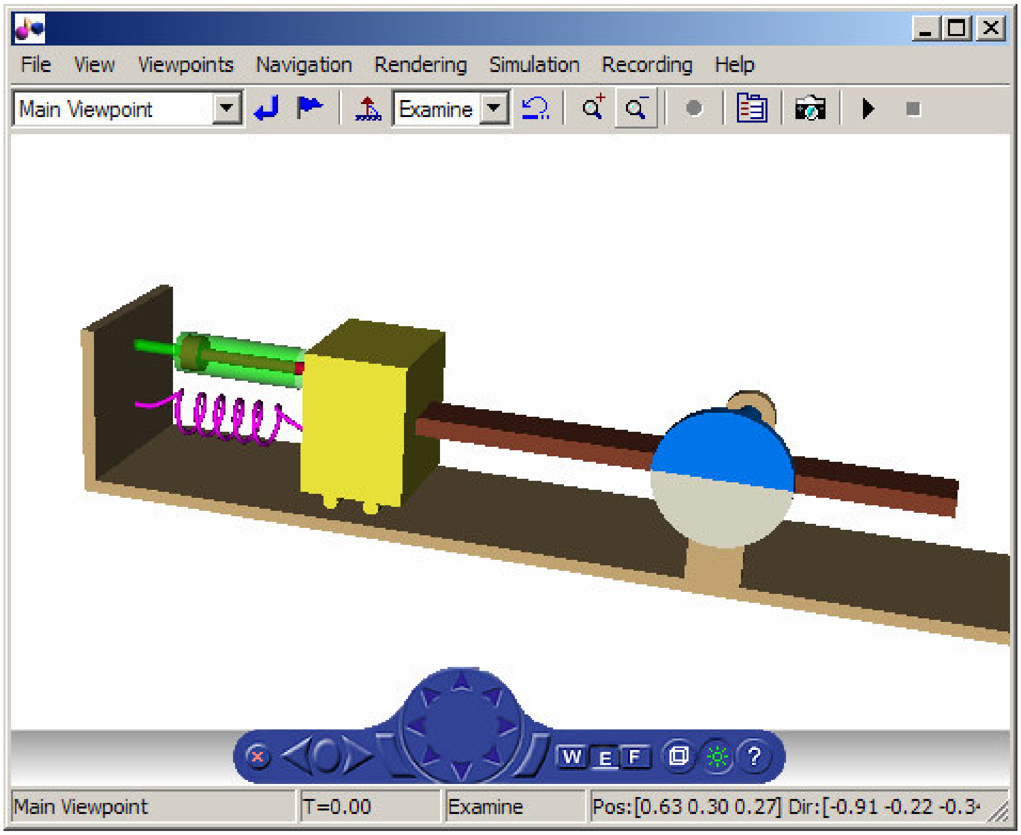

Main Viewpoint

Examine

Main Viewpoint T=0.00 Examine Pos:[0.63 0.30 0.27] Dir:[-0.91 -0.22 -0.3

Figure 6.15 Simulated Virtual Environment

As the Haptic Box is a 1DOF haptic device the virtual environment is also modeled as a 1DOF mechanism as shown in Figure 6.15. The knob with blue-white color is the part the user interacts with via the Haptic Box knob. As the user rotates the knob the knob motion is converted to a linear motion, by a rack and pinion mechanism, which is identical with the motion of the mass which is yellow colored. To the left side of the mass a spring and damper couple is attached to apply stiffness and damping effects to the mass and so the user. The virtual knob does not have dynamic properties so it does not add inertial forces to the system. The open loop impedance control algorithm is used to control the interface.

CHAPTER 7

CONCLUSION

7.1 Conclusions

In this study Haptic Devices are presented and their control strategies are explained. In the way trough the control applications importance of precise motion measurement/estimation is emphasized. General velocity estimation algorithms are examined and Kalman Filters is found to be the best. As stated in the related chapter acceleration estimation from an incremental encoder is not examined too much in the literature. And, acceleration estimation using the Kalman Filter is made and found to perform well. Control strategies are tried experimentally by employing the motion estimators modeled previously. It is gathered from the experiments that the feeling of touch is not affected by the motion estimator, that is to say the estimator does not unstabilize the system.

The control schemes are experimented and satisfactory results are taken from the interface. Especially inertia feeling with *open loop impedance* and *impedance control with force feed-back* algorithms were very good. Stiffness and damping feeling was very sensible. The inclusion of force feed-back into the control strategy increases the capability of the interface as the maximum values for inertia and damping were increased.

Tests for admittance control algorithm was also done and unsatisfactory results are taken from the system. The reason was depending on the modeling errors. From these results it can not be concluded that admittance control strategy is not a suitable algorithm.

7.2 Future Work

The interface works well but admittance control algorithm can be studied more and implementation with this algorithm can be done. The Haptic Box is a 1 DOF haptic device and can only simulate 1 DOF virtual/remote environments. For more flexibility a new haptic device with more freedoms can be constructed. As the degrees of freedom increases the control strategy becomes more complicated. For this new device new control strategies can be experimented and new algorithms can be developed.

REFERENCES

[1] Marc Ueberle, Martin Buss, “Design, Control, and Evaluation of a new 6DOF Haptic Device”, Proceedings of the 2002 IEEE/RSJ Intl. Conference on Intelligent Robots and Systems, pp. 2949-2954, EPFL, Lausanne, Switzerland, October 2002.

[2] Ronald H.Brown, Susan C.Schneider, and Michael G.Mulligan, “Analysis of Algorithms for Velocity Estimation from Discrete Position versus Time Data”, IEEE Transactions in Industrial Electronics, Vol.39, No.1, February 1992

[3] J.N. Lygouras, “Accurate Velocity Evaluation Using Adaptive Sampling Intervals”, Microprocessors and Microsystems 24, 2000, pp. 269-275

[4] G. Liu, “On Velocity Estimation Using Position Measurements”, Proceedings of the American Control Conference, Anchoage, AK May 8-10, 2002, pp. 1115-1120

[5] Robert D. Lorenz, Keith Van Patten, “High resolution velocity estimation for all digital, AC servo drives”, IEEE, 1988.

[6] Se-Han Lee, Ty A.Lasky, and Steven A.Velinsky, “Improved Velocity Estimation for Low-Speed and Transient Regimes Using Low-Resolution Encodes”, IEEE,ASME Transactions on Mechatronics, Vol.9, No.3, September 2004

[7] R.E. Kalman, “ A new approach to linear filtering and prediction problems”, Transactions of the ASME-Journal of Basic Engineering, 82(Series D):35-45, 1960

[8] G.C. Dean, “An introduction to Kalman filters”, Measurement + Control, Volume 19, March 1986, pp:69-73

[9] Heui-Wook Kim, Seung-Ki, “A new motor speed estimator using Kalman filter in low-speed range”, IEEE Transactions on Industrial Electronics, Vol. 43, No 4, August 1996

[10] Ge Yang, “A practical introduction to Kalman filtering”, Technology and Algorithms Seminar, Department of Cell Biology, TSRI, July 22, 2004

[11] Soo Jeon, Masayoshi Tomizuka, “Benefits of acceleration measurement in velocity estimation and motion control”, Control Engineering Practice 15, 2007, pp:325-332

[12] Jesse D. Hwang, Michael D. Williams, Günter Niemeyer, “Toward Event-Based Haptics: Rendering Contact Using Open-Loop Force Pulses”, Proceedings of the 12th International Symposium on Haptic Interfaces for Virtual Environment and Teleoperator Systems, HAPTICS’04.

[13] SensAble Technologies, Phantom Haptic Devices, http://www.sensable.com/haptic-phantom-premium-6dof.htm, last access July 2007.

[14] Immersion Corporation, CyberGraspExoskeleton, http://www.immersion.com/3d/products/cyber_grasp.php, Immersion Corp., last access july 2007

[15] Force Dimension Company, Omega, http://www.forcedimension.com, last access july 2007

[16] H. Maass, H.K. Cakmak, U.G. Kuehnapfel, C. Trantakis, G. Strauss, “Providing more possibilities for haptic devices in surgery simulation”, International Congress Series 1281, 2005, pp.725-729

[17] Toshio Tsuji, Yusaka Takeda, Yoshiyki Tanaka, “Analysis of mechanical impedance in human arm movement using virtual tennis system”, Biol. Cybern.91, 2004, pp.295-305

[18] Zhan Gao and Ian Gibson, “Haptic B-spline Surface Sculpting with a Shaped Tool of Implicit Surface”, Computer-Aided Design & Applications, Vol.2, Nos. 1-4, 2005, pp263-272.

[19] W.Baxter, V.Scheib, M.Lin, and D.Manocha, “DAB: Interactive Haptic Painting with 3D Virtual Brushes”, In Proceedings of ACM SIGGRAPH 01, August 2001, pp.461-468.

[20] Angelika Peer, Bartlomiej Stanczyk, and Martin Buss, “Haptic Telemanipulation with Dissimilar Kinematics”, IEEE/RSJ International Conference on Intelligent Robots and Systems,2005, pp 2483-2488.

[21] Michigan Engineering - University of Michigan, The New Haptic Box, http://sitemaker.umich.edu/haptixbox/home, last access 2007.

[22] Craig R. Carignan, Kevin R. Cleary, “Closed-loop force control for haptic simulation of virtual environments”, Haptics-s Vol.1 No.2, February 23, 2000.

[23] Siena Robotics and Systems Lab - University of Siena, Control of Kinesthetic Haptic Interfaces, http://www.dii.unisi.it/~sirslab/teaching/RoboticaL2/download/UeberleBu04-ControlKinestheticHapticInterfaces.pdf, 23 March 2005, last access July 2007.

[24] R. Volpe, “Real and artificial forces in the control of manipulators: Theory and experiments”, Ph.D. dissertation, Robotics Institute, Department of Physics, Carnegie Mellon University, Pittsburg PA, USA,1990.

[25] Heon Park, JangMyung Lee, “Adaptive impedance control of a haptic interface”, Mechatronics 14, 2004, pp.237-253.

[26] Stephen M.Philips and Michael S.Branicky, “Velocity Estimation Using Quantized Measurements”, Proceedings of the 42nd IEEE Conference on Decision and Control, Maui, Hawaii USA, December 2003, pp. 4847-4852

[27] Marco A.Arteage, “Robot Control and Parameter Estimation with only Joint Position Measurements”, Automatica 39, 2003, pp. 67-73

[28] Pierre R.Bélanger, “Estimation of Angular Velocity and Acceleration from Shaft Encoder Measurements”, Proceedings of the 1992 IEE International Conference of Robotics and Automation, Nice, France, May 1992

[29] Richard Bonert, “Design of a High Performance Digital Tachometer with a Microcontroller”, IEEE Transactions on Instrumentation and Measurement, Vol.38, No.6, December 1989

APPENDIX A

KALMAN FILTER CODE FOR CONSTANT VELOCITY MODEL

```
function [p_e, x_e] = HBkalman_cont_vel(measurement, p_prev,x_prev)

% by Suleyman Bideci
% Haptic Box study
% Kalman Filtering
%measurement --> 2x1 for const vel - 3x1 for const acc
%p_prev      --> 2x2 for const vel - 3x3 for const acc
%x_prev      --> 2x1 for const vel - 3x1 for const acc

%system matrices
T = 0.001; %sampling period
A = [1 T ; 0 1]; %system matrix
H = [1 0;                      %measurement matrix
     0 1];
y = [measurement(1);             %measurement input
     measurement(2)];

%manipulate P and x previous matrices
x_prev_est = [x_prev(1);
              x_prev(2)];
p_prev_est = [p_prev(1) p_prev(2);
              p_prev(3) p_prev(4)];

q11 = 0.1;
q22 = 0.1;
Q_est = [q11^2 0; 0 q22^2];
r11 = 0.01;
r22 = 0.1;
R_est = [r11 0; 0 r22];

state_order = 2;

%KALMAN
[p_pred, x_pred] = KF_prediction(x_prev_est, A, p_prev_est, Q_est);
[p_est, x_est, Kalman_gain]   = KF_correction(H, R_est, x_pred, 
p_pred, y, state_order);
%-------------------------------------------------------
```

```
%outputs
x_e = [x_est(1) x_est(2)];
p_e = [p_est(1,1) p_est(1,2) p_est(2,1) p_est(2,2)];

%kalman loops
function [p_prediction, x_prediction] =
KF_prediction(x_prev_estimation, A, p_prev_estimation, Q)
x_prediction = A * x_prev_estimation;
p_prediction = A * p_prev_estimation * A' + Q;
%end function

function [p_estimation, x_estimation, Kalman_gain] = KF_correction(H,
R, x_prediction, p_prediction, mea, state_order)
Kalman_gain = p_prediction * H' * inv(H * p_prediction * H' + R);
x_estimation = x_prediction + Kalman_gain * (mea - H * x_prediction);
p_estimation = (eye(state_order) - Kalman_gain * H) * p_prediction;
%end function
```

APPENDIX B

HAPTIC BOX COMPONENTS AND EXPERIMENTAL MATERIALS

Specifications of electromechanical and mechanical components used in construction of the Haptic Box are given in this section.

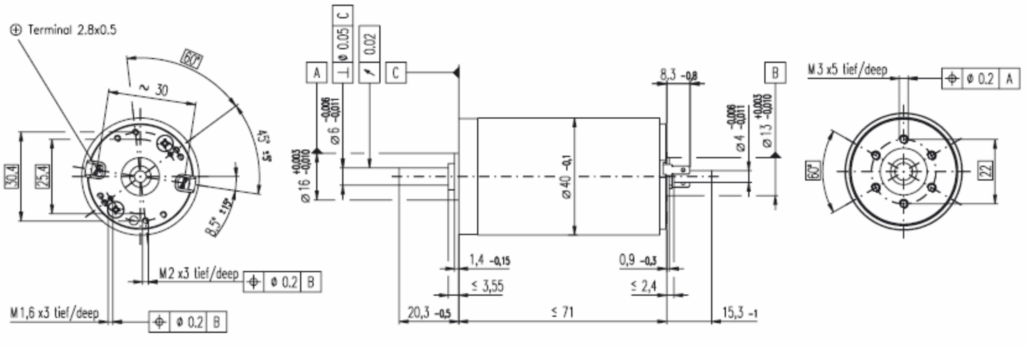

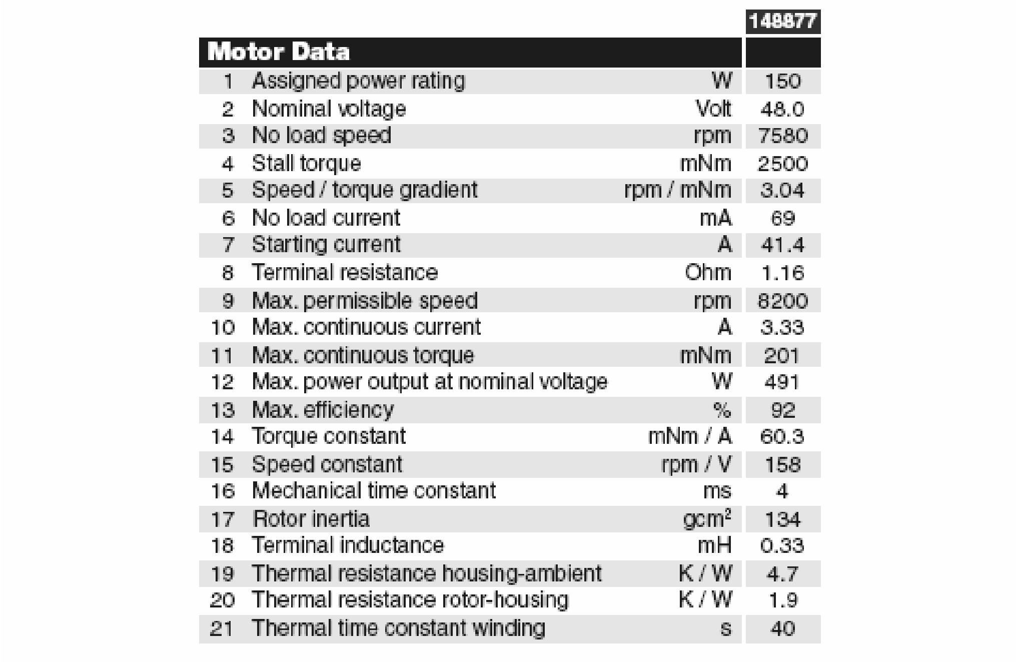

Motor Data			148877
1	Assigned power rating	W	150
2	Nominal voltage	Volt	48.0
3	No load speed	rpm	7580
4	Stall torque	mNm	2500
5	Speed / torque gradient	rpm / mNm	3.04
6	No load current	mA	69
7	Starting current	A	41.4
8	Terminal resistance	Ohm	1.16
9	Max. permissible speed	rpm	8200
10	Max. continuous current	A	3.33
11	Max. continuous torque	mNm	201
12	Max. power output at nominal voltage	W	491
13	Max. efficiency	%	92
14	Torque constant	mNm / A	60.3
15	Speed constant	rpm / V	158
16	Mechanical time constant	ms	4
17	Rotor inertia	gcm^2	134
18	Terminal inductance	mH	0.33
19	Thermal resistance housing-ambient	K / W	4.7
20	Thermal resistance rotor-housing	K / W	1.9
21	Thermal time constant winding	s	40

Figure B.1 Maxon RE40 DC Brushes Motor Specifications

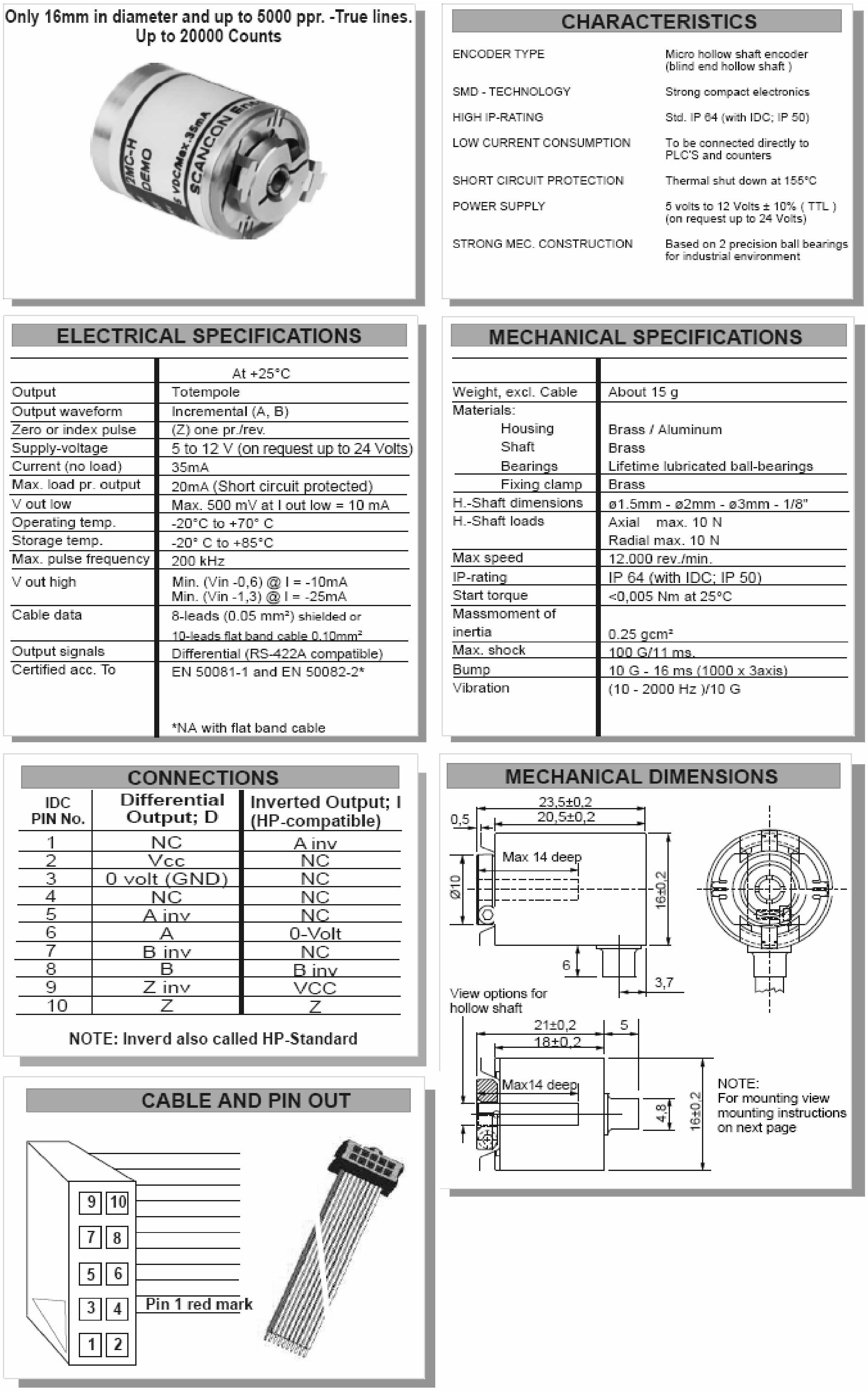

Only 16mm in diameter and up to 5000 ppr. -True lines. Up to 20000 Counts

MC-H
DEMO
5 VDC/Max.35mA
SCANCON

CHARACTERISTICS

ENCODER TYPE	Micro hollow shaft encoder (blind end hollow shaft)
SMD - TECHNOLOGY	Strong compact electronics
HIGH IP-RATING	Std. IP 64 (with IDC; IP 50)
LOW CURRENT CONSUMPTION	To be connected directly to PLC'S and counters
SHORT CIRCUIT PROTECTION	Thermal shut down at 155°C
POWER SUPPLY	5 volts to 12 Volts ± 10% (TTL) (on request up to 24 Volts)
STRONG MEC. CONSTRUCTION	Based on 2 precision ball bearings for industrial environment

ELECTRICAL SPECIFICATIONS

	At +25°C
Output	Totempole
Output waveform	Incremental (A, B)
Zero or index pulse	(Z) one pr./rev.
Supply-voltage	5 to 12 V (on request up to 24 Volts)
Current (no load)	35mA
Max. load pr. output	20mA (Short circuit protected)
V out low	Max. 500 mV at I out low = 10 mA
Operating temp.	-20°C to +70° C
Storage temp.	-20° C to +85°C
Max. pulse frequency	200 kHz
V out high	Min. (Vin -0,6) @ I = -10mA Min. (Vin -1,3) @ I = -25mA
Cable data	8-leads (0.05 mm²) shielded or 10-leads flat band cable 0.10mm²
Output signals	Differential (RS-422A compatible)
Certified acc. To	EN 50081-1 and EN 50082-2*

*NA with flat band cable

MECHANICAL SPECIFICATIONS

Weight, excl. Cable	About 15 g
Materials:	
Housing	Brass / Aluminum
Shaft	Brass
Bearings	Lifetime lubricated ball-bearings
Fixing clamp	Brass
H.-Shaft dimensions	ø1.5mm - ø2mm - ø3mm - 1/8"
H.-Shaft loads	Axial max. 10 N Radial max. 10 N
Max speed	12.000 rev./min.
IP-rating	IP 64 (with IDC; IP 50)
Start torque	<0,005 Nm at 25°C
Massmoment of inertia	0.25 gcm²
Max. shock	100 G/11 ms.
Bump	10 G - 16 ms (1000 x 3axis)
Vibration	(10 - 2000 Hz)/10 G

CONNECTIONS

IDC PIN No.	Differential Output; D	Inverted Output; I (HP-compatible)
1	NC	A inv
2	Vcc	NC
3	0 volt (GND)	NC
4	NC	NC
5	A inv	NC
6	A	0-Volt
7	B inv	NC
8	B	B inv
9	Z inv	VCC
10	Z	Z

NOTE: Inverd also called HP-Standard

MECHANICAL DIMENSIONS

View options for hollow shaft

NOTE: For mounting view mounting instructions on next page

CABLE AND PIN OUT

Figure B.2 Scancon Encoder Specifications

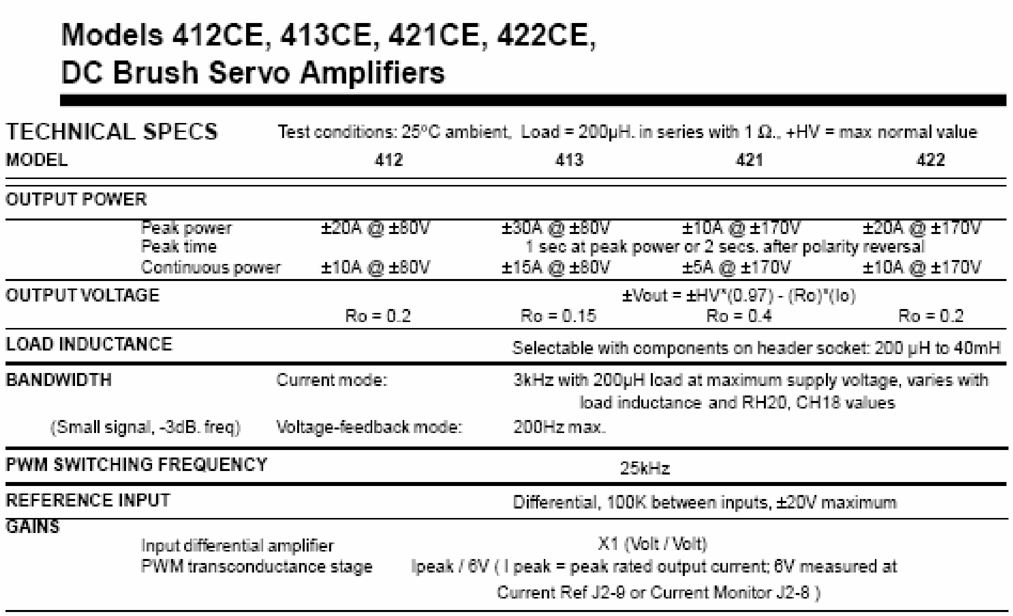

Models 412CE, 413CE, 421CE, 422CE,
DC Brush Servo Amplifiers

TECHNICAL SPECS Test conditions: 25°C ambient, Load = 200μH. in series with 1 Ω., +HV = max normal value

MODEL		412	413	421	422
OUTPUT POWER					
	Peak power	±20A @ ±80V	±30A @ ±80V	±10A @ ±170V	±20A @ ±170V
	Peak time	1 sec at peak power or 2 secs. after polarity reversal			
	Continuous power	±10A @ ±80V	±15A @ ±80V	±5A @ ±170V	±10A @ ±170V
OUTPUT VOLTAGE		±Vout = ±HV*(0.97) - (Ro)*(Io)			
		Ro = 0.2	Ro = 0.15	Ro = 0.4	Ro = 0.2
LOAD INDUCTANCE		Selectable with components on header socket: 200 μH to 40mH			
BANDWIDTH	Current mode:	3kHz with 200μH load at maximum supply voltage, varies with load inductance and RH20, CH18 values			
(Small signal, -3dB. freq)	Voltage-feedback mode:	200Hz max.			
PWM SWITCHING FREQUENCY		25kHz			
REFERENCE INPUT		Differential, 100K between inputs, ±20V maximum			
GAINS					
	Input differential amplifier	X1 (Volt / Volt)			
	PWM transconductance stage	Ipeak / 6V (I peak = peak rated output current; 6V measured at Current Ref J2-9 or Current Monitor J2-8)			

Figure B.3 Copley 413CE Servo Amplifier

HEDS5540 Optical Encoder

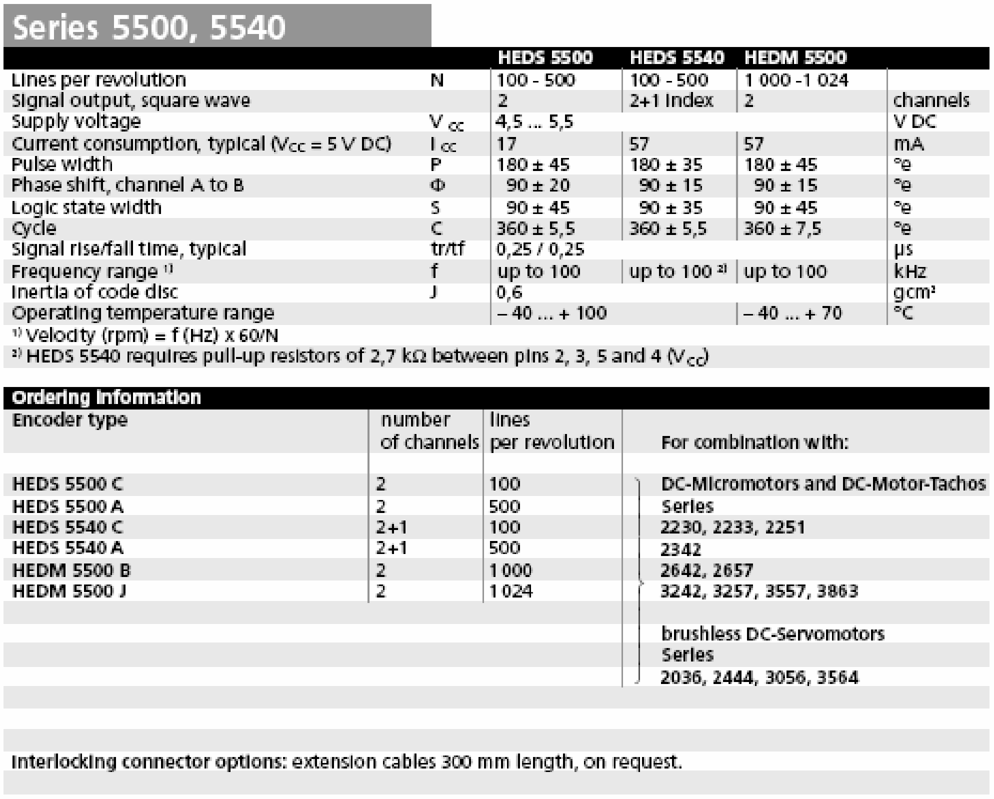

Series 5500, 5540

		HEDS 5500	HEDS 5540	HEDM 5500	
Lines per revolution	N	100 - 500	100 - 500	1 000 -1 024	
Signal output, square wave		2	2+1 Index	2	channels
Supply voltage	V_{CC}	4,5 ... 5,5			V DC
Current consumption, typical (V_{CC} = 5 V DC)	I_{CC}	17	57	57	mA
Pulse width	P	180 ± 45	180 ± 35	180 ± 45	°e
Phase shift, channel A to B	Φ	90 ± 20	90 ± 15	90 ± 15	°e
Logic state width	S	90 ± 45	90 ± 35	90 ± 45	°e
Cycle	C	360 ± 5,5	360 ± 5,5	360 ± 7,5	°e
Signal rise/fall time, typical	tr/tf	0,25 / 0,25			μs
Frequency range [1]	f	up to 100	up to 100 [2]	up to 100	kHz
Inertia of code disc	J	0,6			gcm^2
Operating temperature range		– 40 ... + 100		– 40 ... + 70	°C

[1] Velocity (rpm) = f (Hz) x 60/N

[2] HEDS 5540 requires pull-up resistors of 2,7 kΩ between pins 2, 3, 5 and 4 (V_{CC})

Ordering Information

Encoder type	number of channels	lines per revolution	For combination with:
HEDS 5500 C	2	100	DC-Micromotors and DC-Motor-Tachos
HEDS 5500 A	2	500	Series
HEDS 5540 C	2+1	100	2230, 2233, 2251
HEDS 5540 A	2+1	500	2342
HEDM 5500 B	2	1 000	2642, 2657
HEDM 5500 J	2	1 024	3242, 3257, 3557, 3863
			brushless DC-Servomotors
			Series
			2036, 2444, 3056, 3564

Interlocking connector options: extension cables 300 mm length, on request.

Figure B.4 HEDS 5540A Encoder

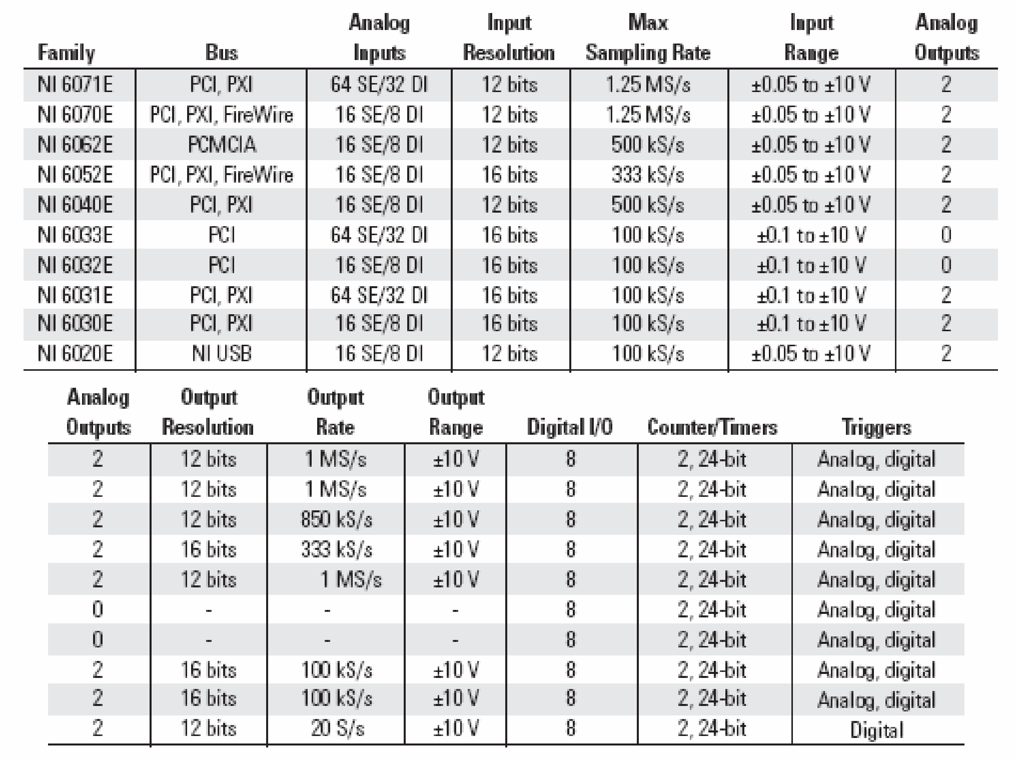

Family	Bus	Analog Inputs	Input Resolution	Max Sampling Rate	Input Range	Analog Outputs
NI 6071E	PCI, PXI	64 SE/32 DI	12 bits	1.25 MS/s	±0.05 to ±10 V	2
NI 6070E	PCI, PXI, FireWire	16 SE/8 DI	12 bits	1.25 MS/s	±0.05 to ±10 V	2
NI 6062E	PCMCIA	16 SE/8 DI	12 bits	500 kS/s	±0.05 to ±10 V	2
NI 6052E	PCI, PXI, FireWire	16 SE/8 DI	16 bits	333 kS/s	±0.05 to ±10 V	2
NI 6040E	PCI, PXI	16 SE/8 DI	12 bits	500 kS/s	±0.05 to ±10 V	2
NI 6033E	PCI	64 SE/32 DI	16 bits	100 kS/s	±0.1 to ±10 V	0
NI 6032E	PCI	16 SE/8 DI	16 bits	100 kS/s	±0.1 to ±10 V	0
NI 6031E	PCI, PXI	64 SE/32 DI	16 bits	100 kS/s	±0.1 to ±10 V	2
NI 6030E	PCI, PXI	16 SE/8 DI	16 bits	100 kS/s	±0.1 to ±10 V	2
NI 6020E	NI USB	16 SE/8 DI	12 bits	100 kS/s	±0.05 to ±10 V	2

Analog Outputs	Output Resolution	Output Rate	Output Range	Digital I/O	Counter/Timers	Triggers
2	12 bits	1 MS/s	±10 V	8	2, 24-bit	Analog, digital
2	12 bits	1 MS/s	±10 V	8	2, 24-bit	Analog, digital
2	12 bits	850 kS/s	±10 V	8	2, 24-bit	Analog, digital
2	16 bits	333 kS/s	±10 V	8	2, 24-bit	Analog, digital
2	12 bits	1 MS/s	±10 V	8	2, 24-bit	Analog, digital
0	-	-	-	8	2, 24-bit	Analog, digital
0	-	-	-	8	2, 24-bit	Analog, digital
2	16 bits	100 kS/s	±10 V	8	2, 24-bit	Analog, digital
2	16 bits	100 kS/s	±10 V	8	2, 24-bit	Analog, digital
2	12 bits	20 S/s	±10 V	8	2, 24-bit	Digital

Figure B.5 NI PCI6052E Multifunction DAQ

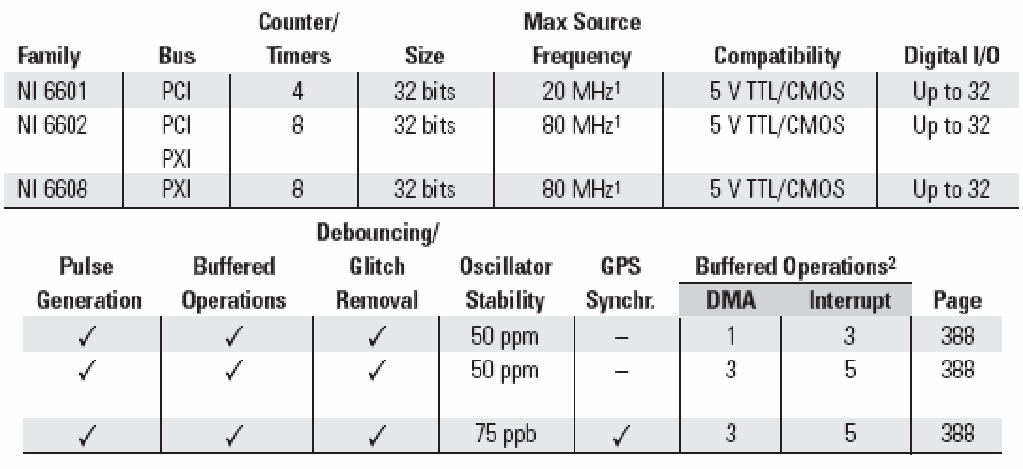

Family	Bus	Counter/ Timers	Size	Max Source Frequency	Compatibility	Digital I/O
NI 6601	PCI	4	32 bits	20 MHz[1]	5 V TTL/CMOS	Up to 32
NI 6602	PCI PXI	8	32 bits	80 MHz[1]	5 V TTL/CMOS	Up to 32
NI 6608	PXI	8	32 bits	80 MHz[1]	5 V TTL/CMOS	Up to 32

Pulse Generation	Buffered Operations	Debouncing/ Glitch Removal	Oscillator Stability	GPS Synchr.	Buffered Operations[2]		Page
					DMA	Interrupt	
✓	✓	✓	50 ppm	–	1	3	388
✓	✓	✓	50 ppm	–	3	5	388
✓	✓	✓	75 ppb	✓	3	5	388

Figure B.6 NI PCI6602 Counter/Timer DAQ

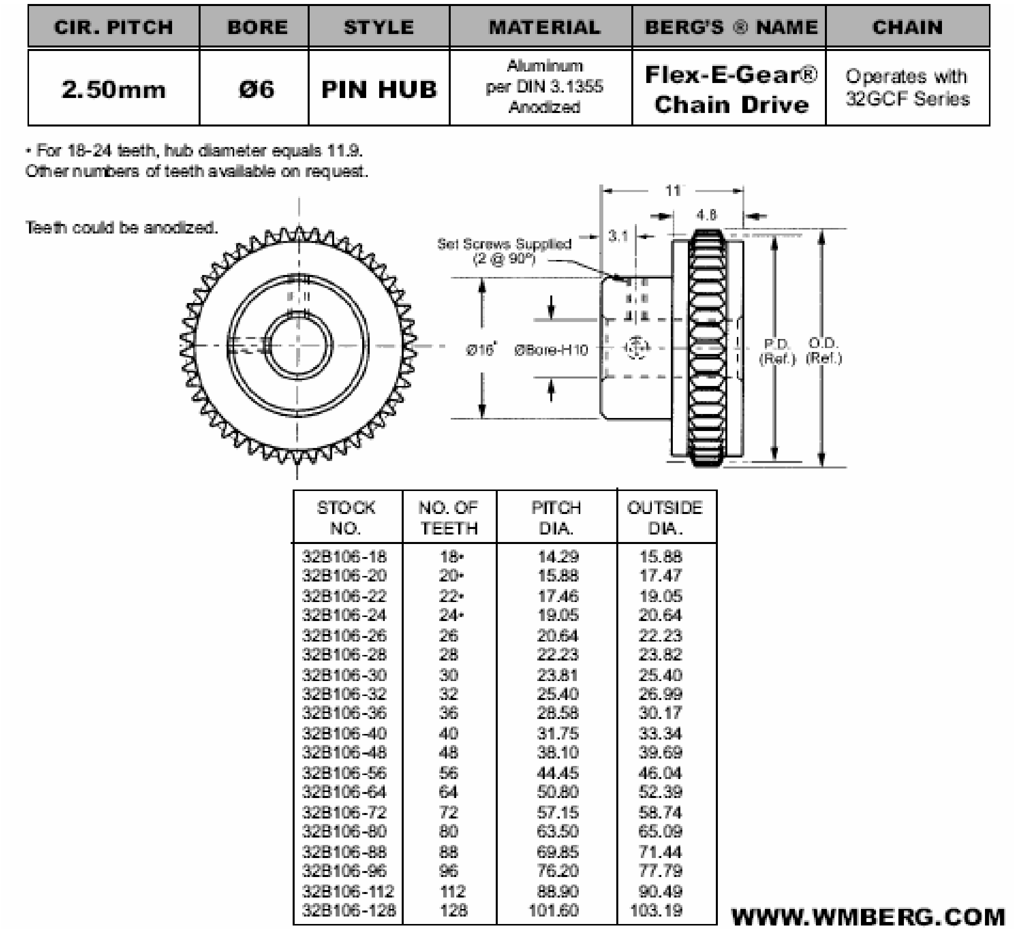

CIR. PITCH	BORE	STYLE	MATERIAL	BERG'S ® NAME	CHAIN
2.50mm	Ø6	PIN HUB	Aluminum per DIN 3.1355 Anodized	Flex-E-Gear® Chain Drive	Operates with 32GCF Series

• For 18-24 teeth, hub diameter equals 11.9.
Other numbers of teeth available on request.

Teeth could be anodized.

STOCK NO.	NO. OF TEETH	PITCH DIA.	OUTSIDE DIA.
32B106-18	18•	14.29	15.88
32B106-20	20•	15.88	17.47
32B106-22	22•	17.46	19.05
32B106-24	24•	19.05	20.64
32B106-26	26	20.64	22.23
32B106-28	28	22.23	23.82
32B106-30	30	23.81	25.40
32B106-32	32	25.40	26.99
32B106-36	36	28.58	30.17
32B106-40	40	31.75	33.34
32B106-48	48	38.10	39.69
32B106-56	56	44.45	46.04
32B106-64	64	50.80	52.39
32B106-72	72	57.15	58.74
32B106-80	80	63.50	65.09
32B106-88	88	69.85	71.44
32B106-96	96	76.20	77.79
32B106-112	112	88.90	90.49
32B106-128	128	101.60	103.19

WWW.WMBERG.COM

Figure B.7 W.M.Berg Sprocket Gear

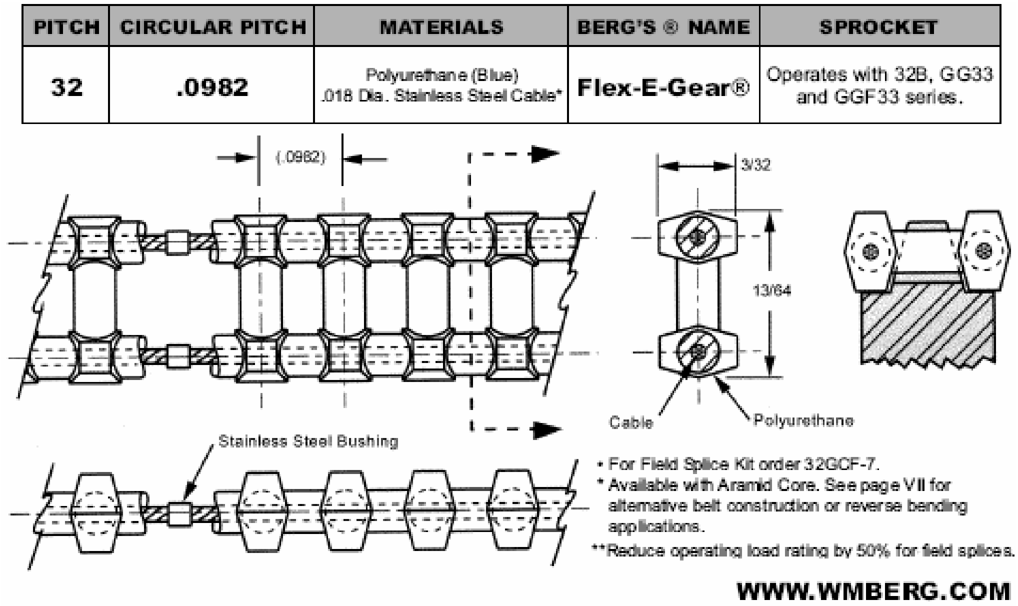

PITCH	CIRCULAR PITCH	MATERIALS	BERG'S ® NAME	SPROCKET
32	.0982	Polyurethane (Blue) .018 Dia. Stainless Steel Cable*	Flex-E-Gear®	Operates with 32B, GG33 and GGF33 series.

• For Field Splice Kit order 32GCF-7.
* Available with Aramid Core. See page VII for alternative belt construction or reverse bending applications.
**Reduce operating load rating by 50% for field splices.

WWW.WMBERG.COM

Figure B.8 W.M.Berg Polyurethane/Steel Cable Chain

APPENDIX C

HAPTIC INTERFACE ELECTRICAL CONNECTIONS

The electrical connections inside the Haptic Box and between Target computer and the Haptic Box are presented in this section.

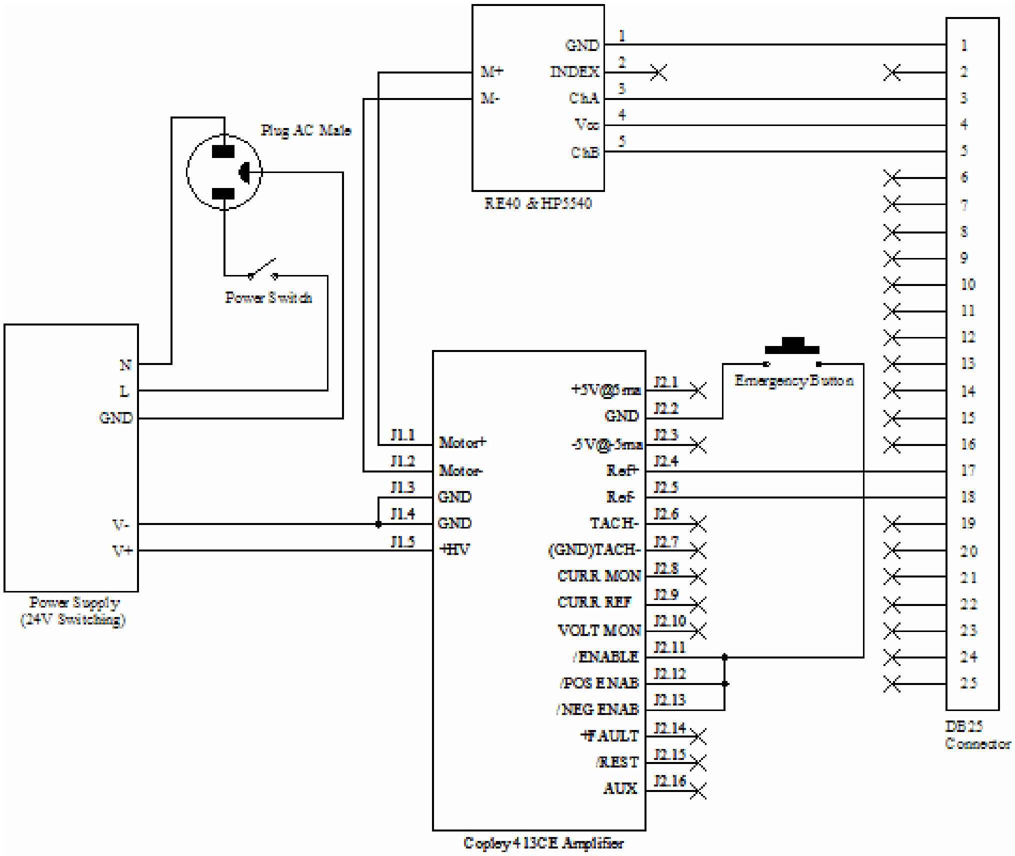

Figure C.1 Electrical connections inside the Haptic Box

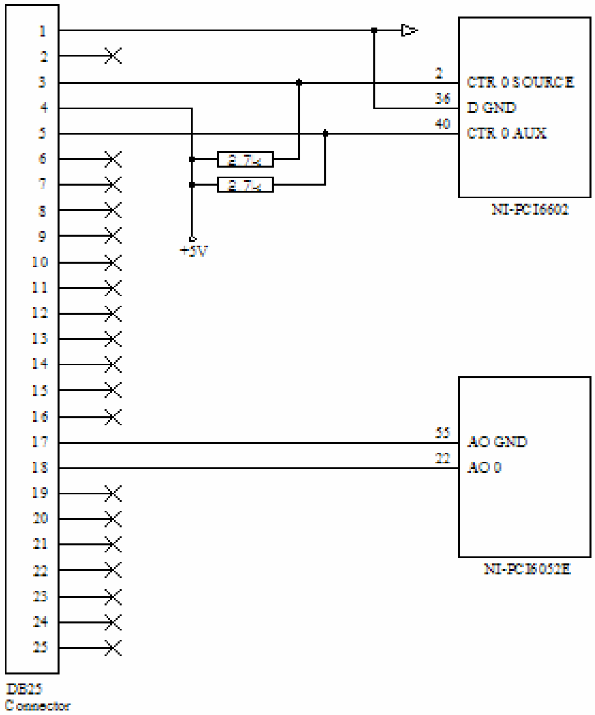

Figure C.2 Electrical connections between Haptic Box and Target Computer

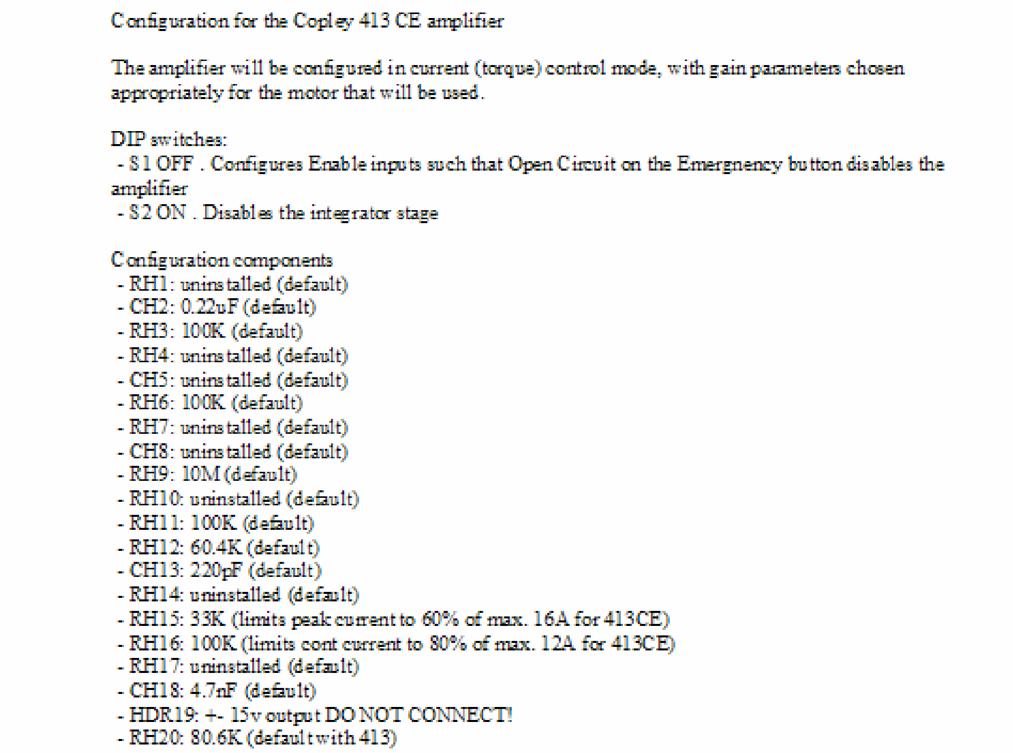

Configuration for the Copley 413 CE amplifier

The amplifier will be configured in current (torque) control mode, with gain parameters chosen appropriately for the motor that will be used.

DIP switches:
- S1 OFF . Configures Enable inputs such that Open Circuit on the Emergnency button disables the amplifier
- S2 ON . Disables the integrator stage

Configuration components
- RH1: uninstalled (default)
- CH2: 0.22uF (default)
- RH3: 100K (default)
- RH4: uninstalled (default)
- CH5: uninstalled (default)
- RH6: 100K (default)
- RH7: uninstalled (default)
- CH8: uninstalled (default)
- RH9: 10M (default)
- RH10: uninstalled (default)
- RH11: 100K (default)
- RH12: 60.4K (default)
- CH13: 220pF (default)
- RH14: uninstalled (default)
- RH15: 33K (limits peak current to 60% of max. 16A for 413CE)
- RH16: 100K (limits cont current to 80% of max. 12A for 413CE)
- RH17: uninstalled (default)
- CH18: 4.7nF (default)
- HDR19: +- 15v output DO NOT CONNECT!
- RH20: 80.6K (default with 413)

Figure C.3 Configuration for Copley 413CE Servo Amplifier

APPENDIX D

HAPTIC BOX TECHNICAL DRAWINGS

Technical drawings of the components forming the Haptic Box are presented in this section.

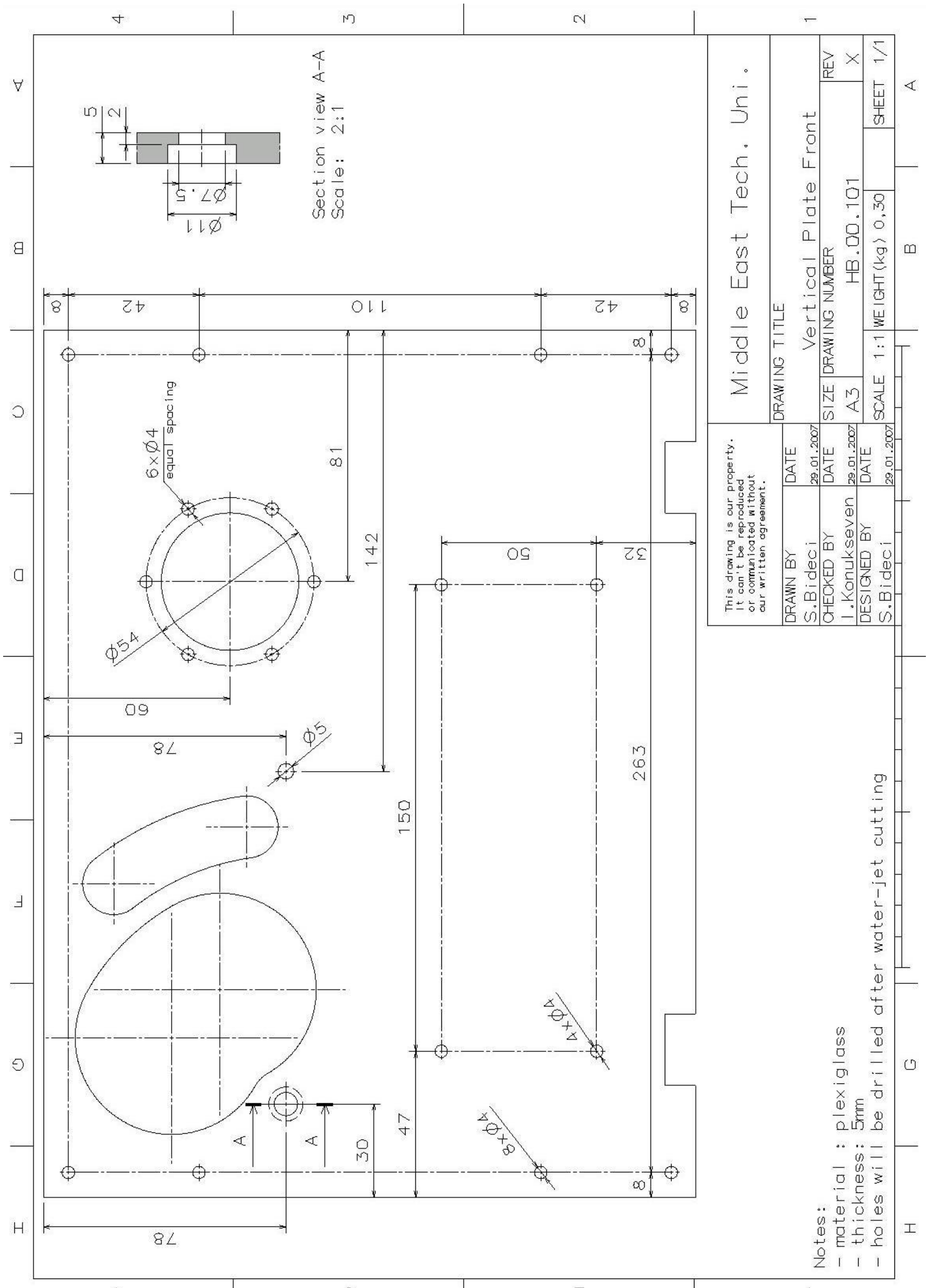

Figure D.1 Vertical Plate Front

]

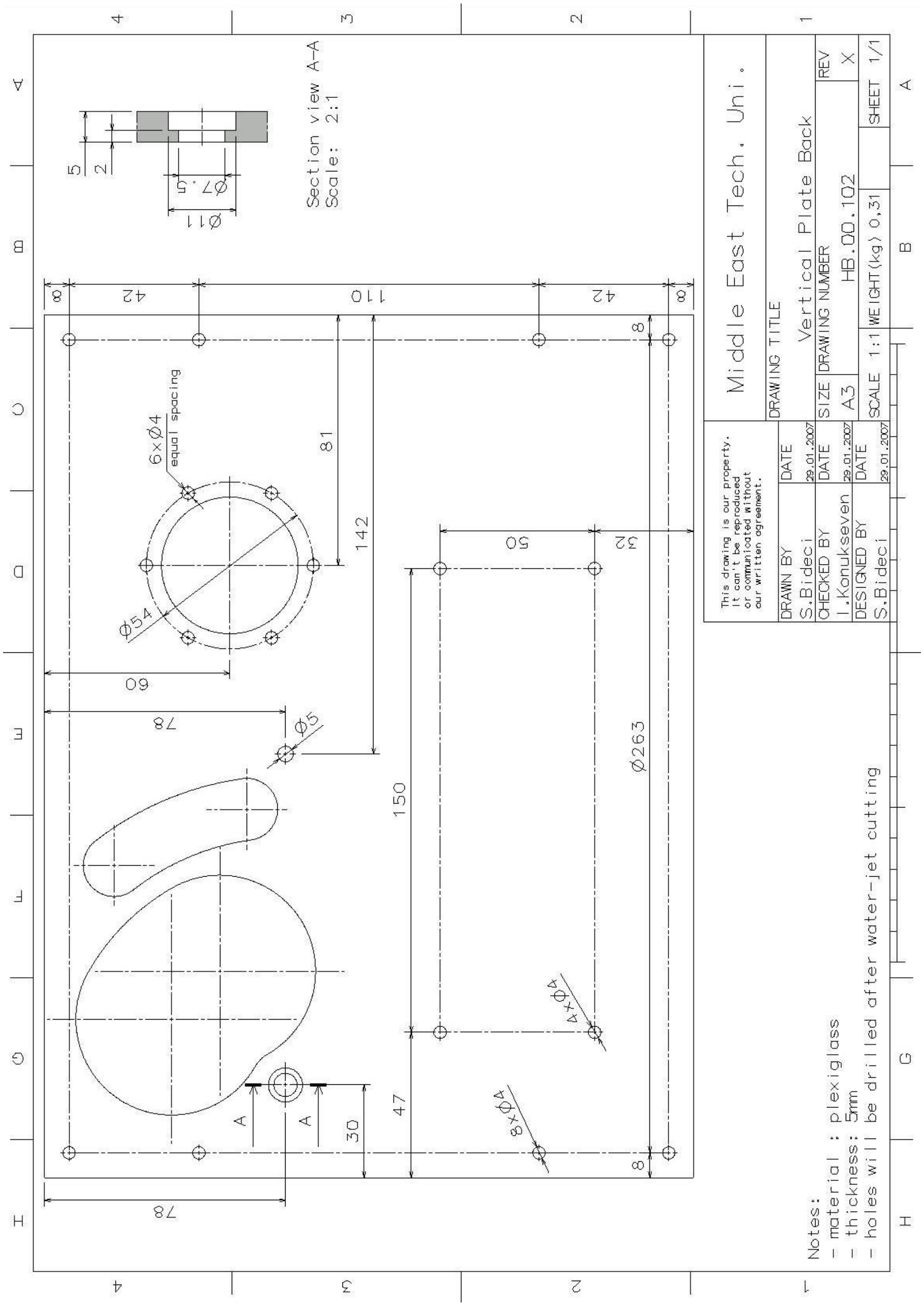

Figure D.2 Vertical Plate Back

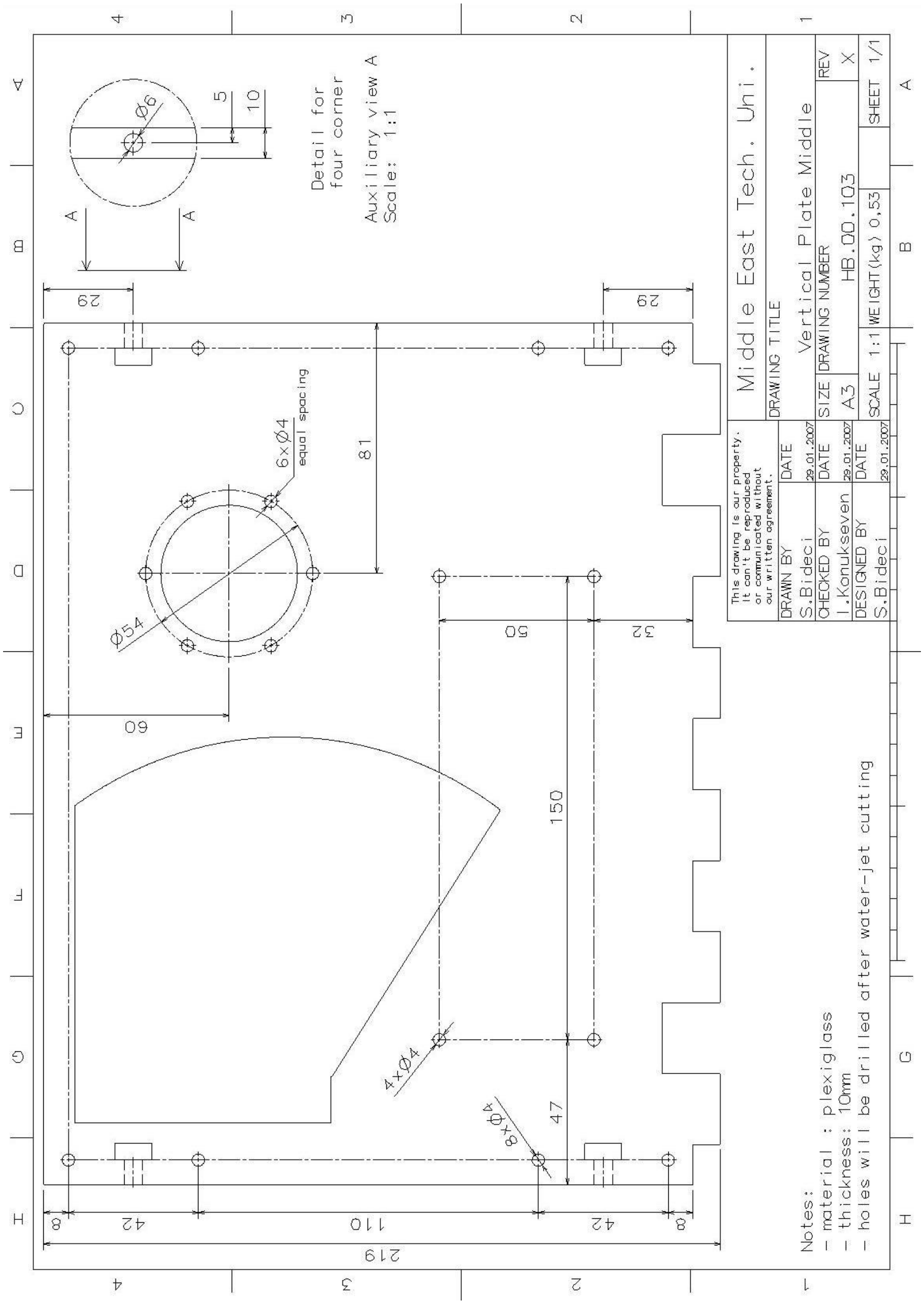

Figure D.3 Vertical Plate Middle

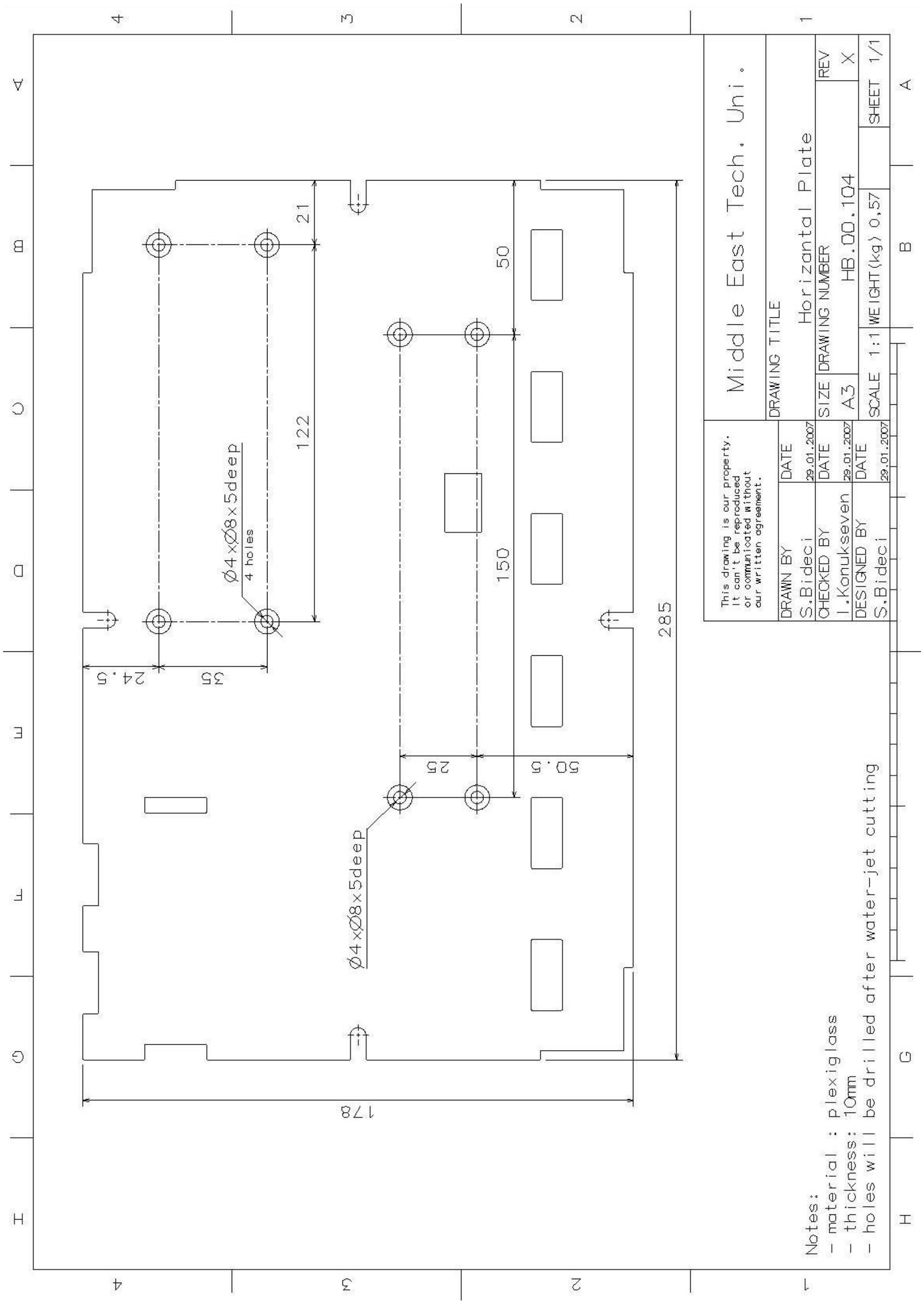

Figure D.4 Horizontal Plate

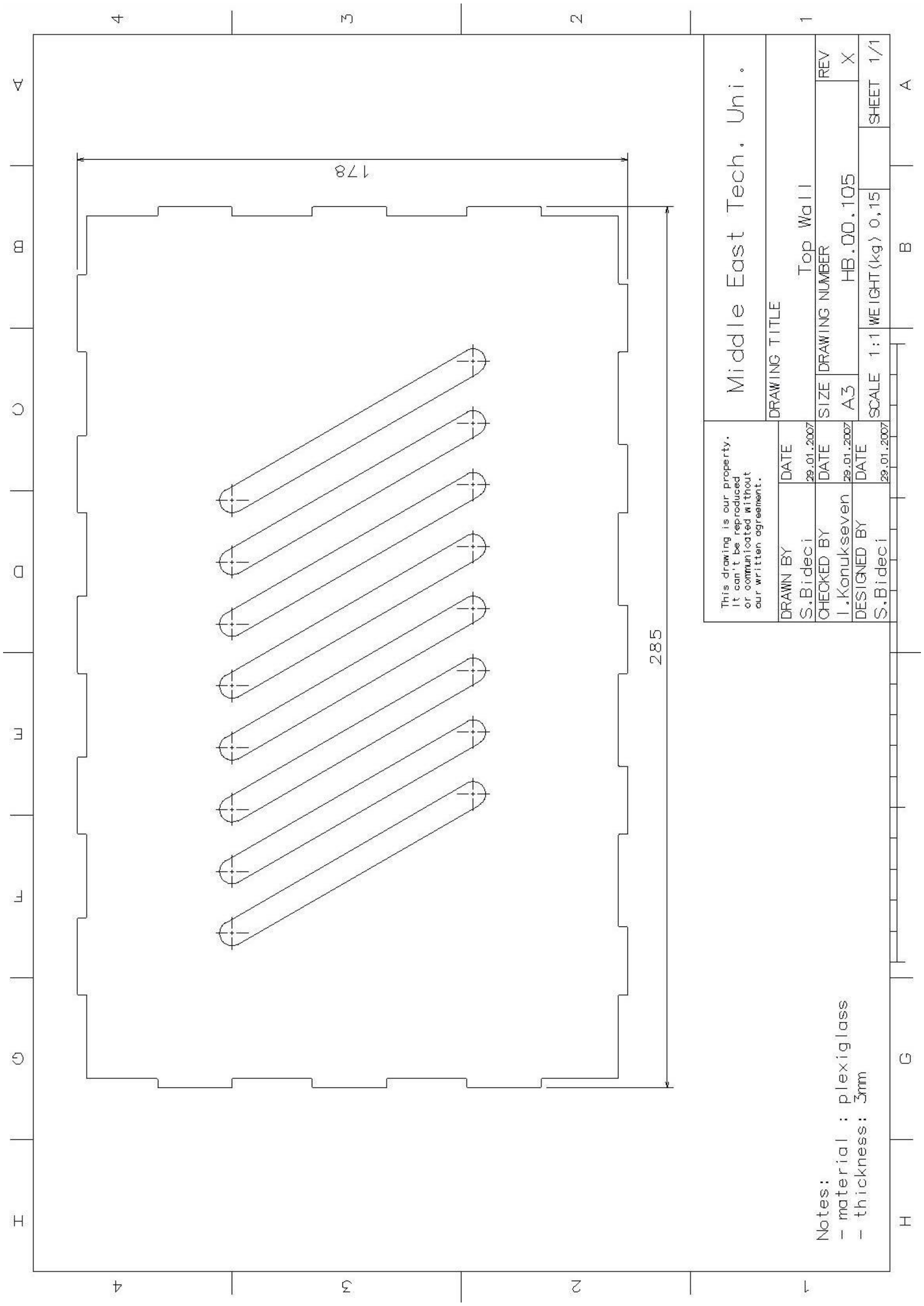

Figure D.5 Top Wall

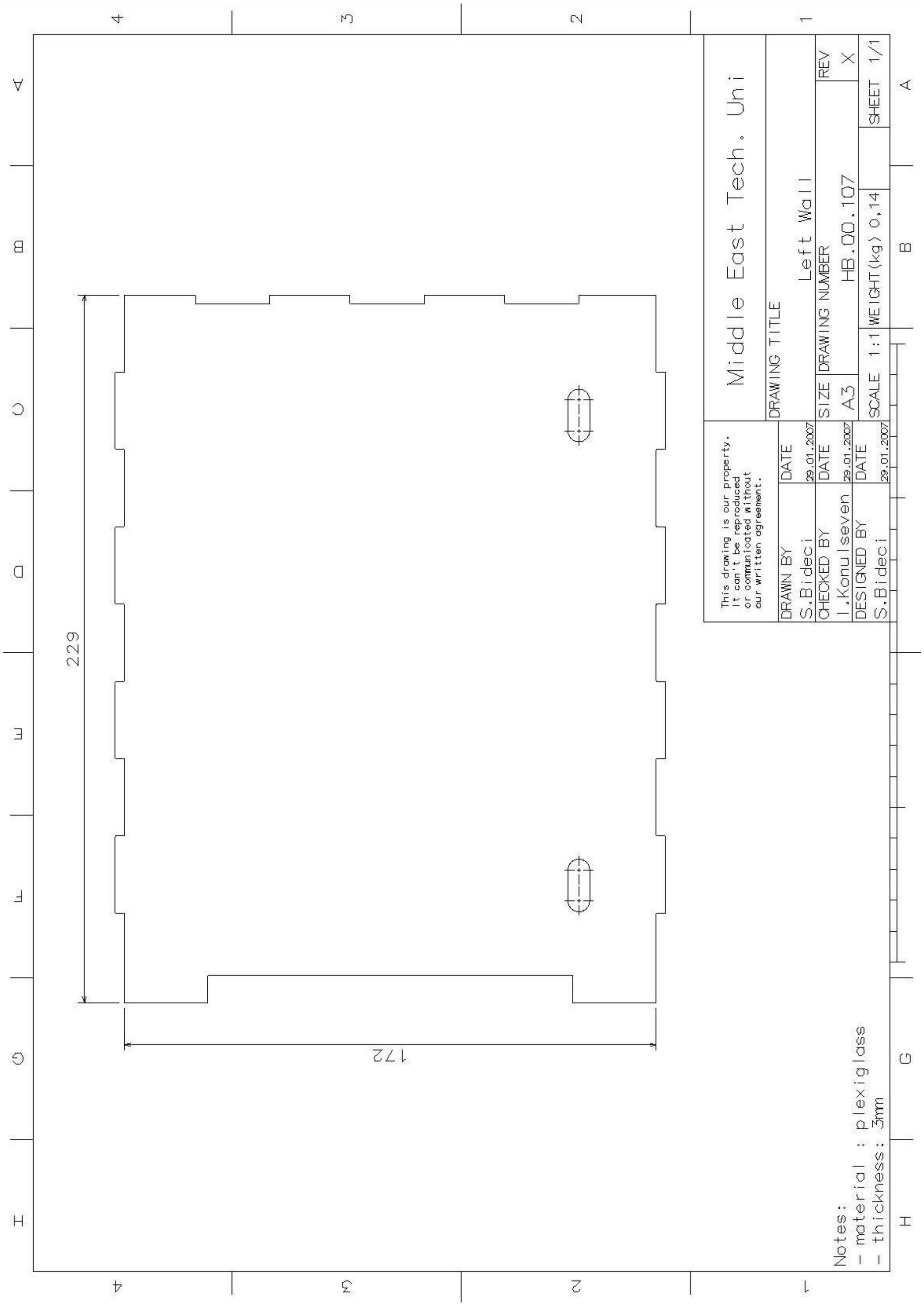

Figure D.6 Left Wall

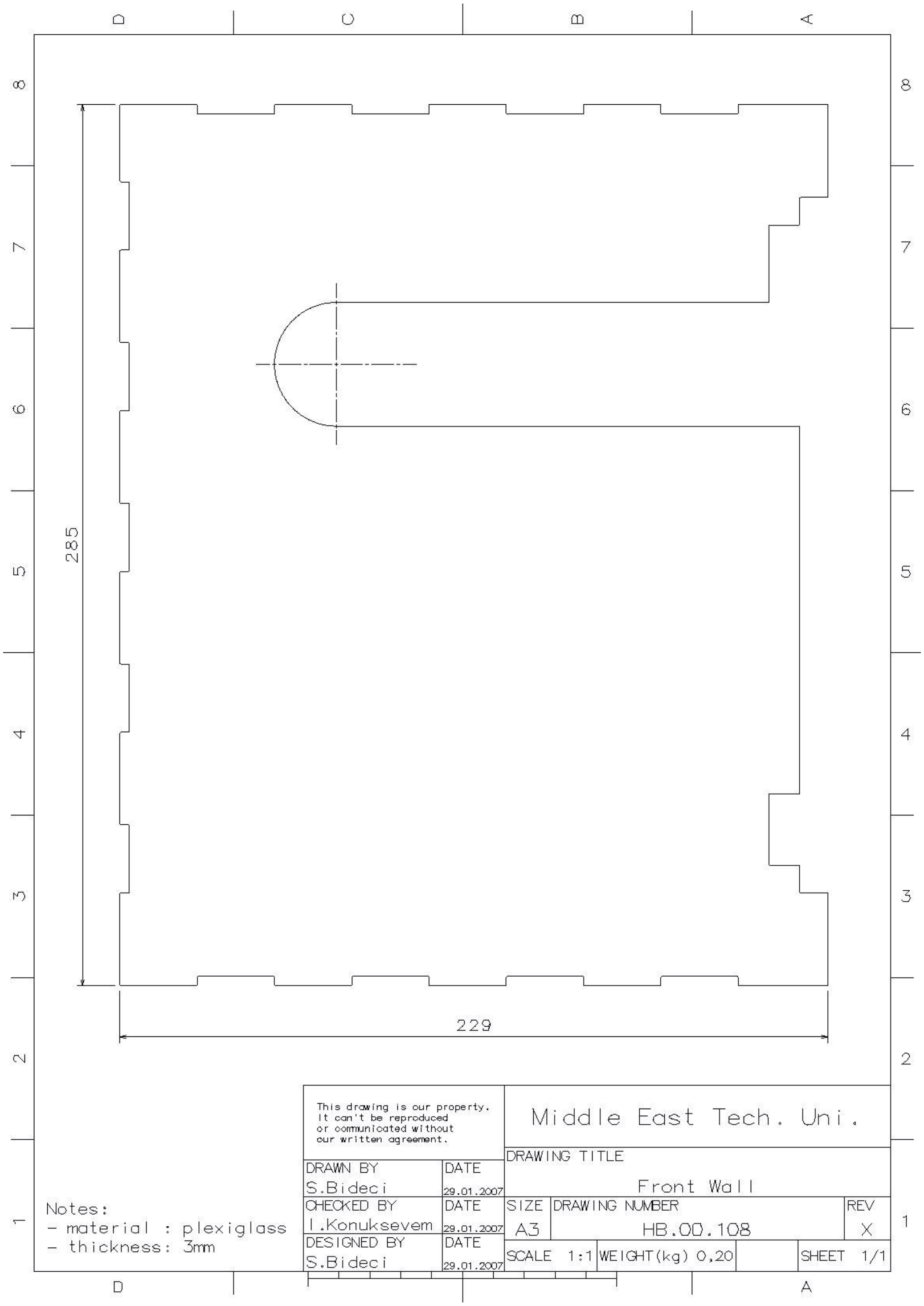

Notes:
- material : plexiglass
- thickness: 3mm

This drawing is our property. It can't be reproduced or communicated without our written agreement.

Middle East Tech. Uni.

DRAWN BY S.Bideci	DATE 29.01.2007	DRAWING TITLE Front Wall			
CHECKED BY I.Konuksevem	DATE 29.01.2007	SIZE A3	DRAWING NUMBER HB.00.108		REV X
DESIGNED BY S.Bideci	DATE 29.01.2007	SCALE 1:1	WEIGHT(kg) 0,20		SHEET 1/1

Figure D.7 Front Wall

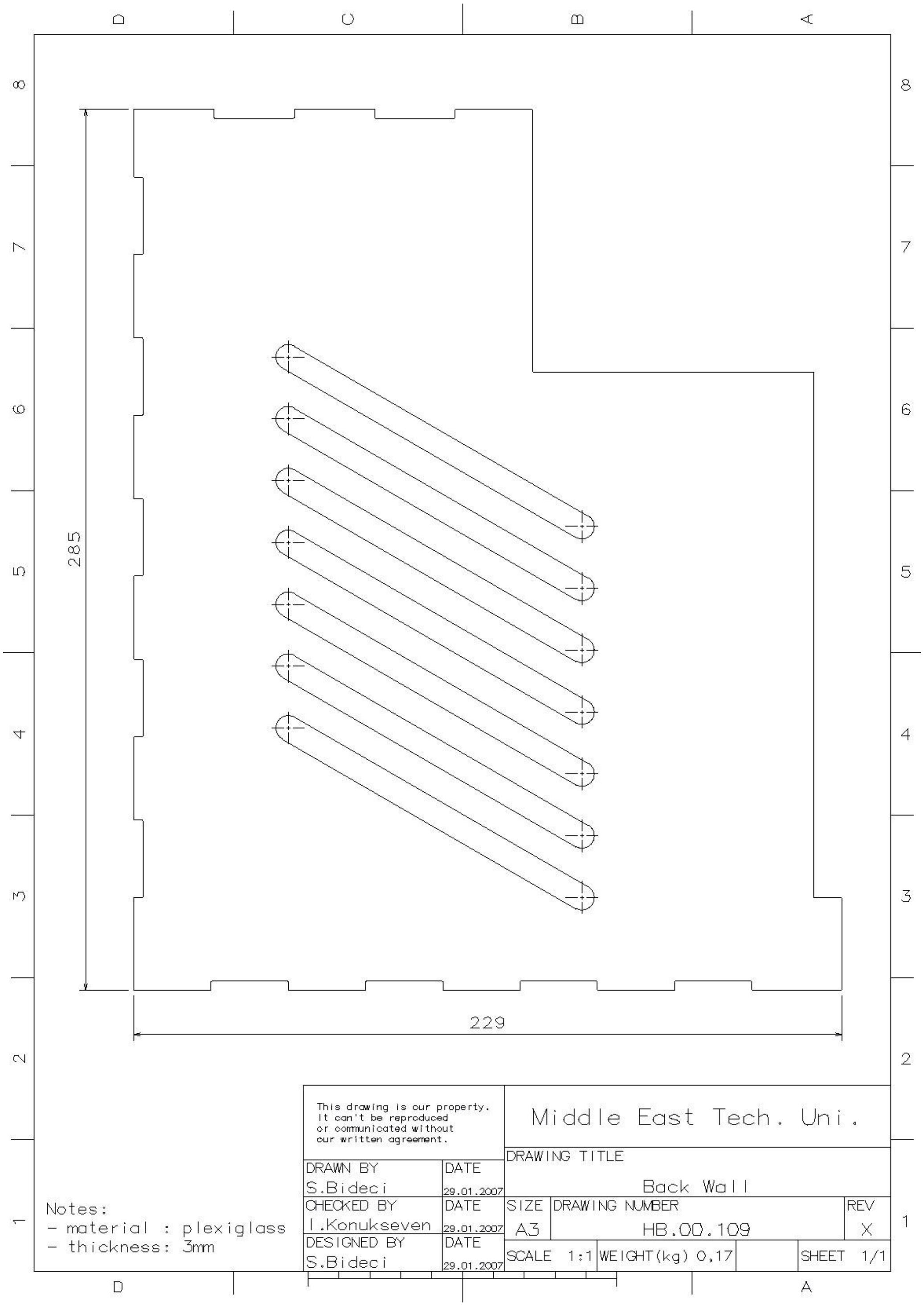

Figure D.8 Back Wall

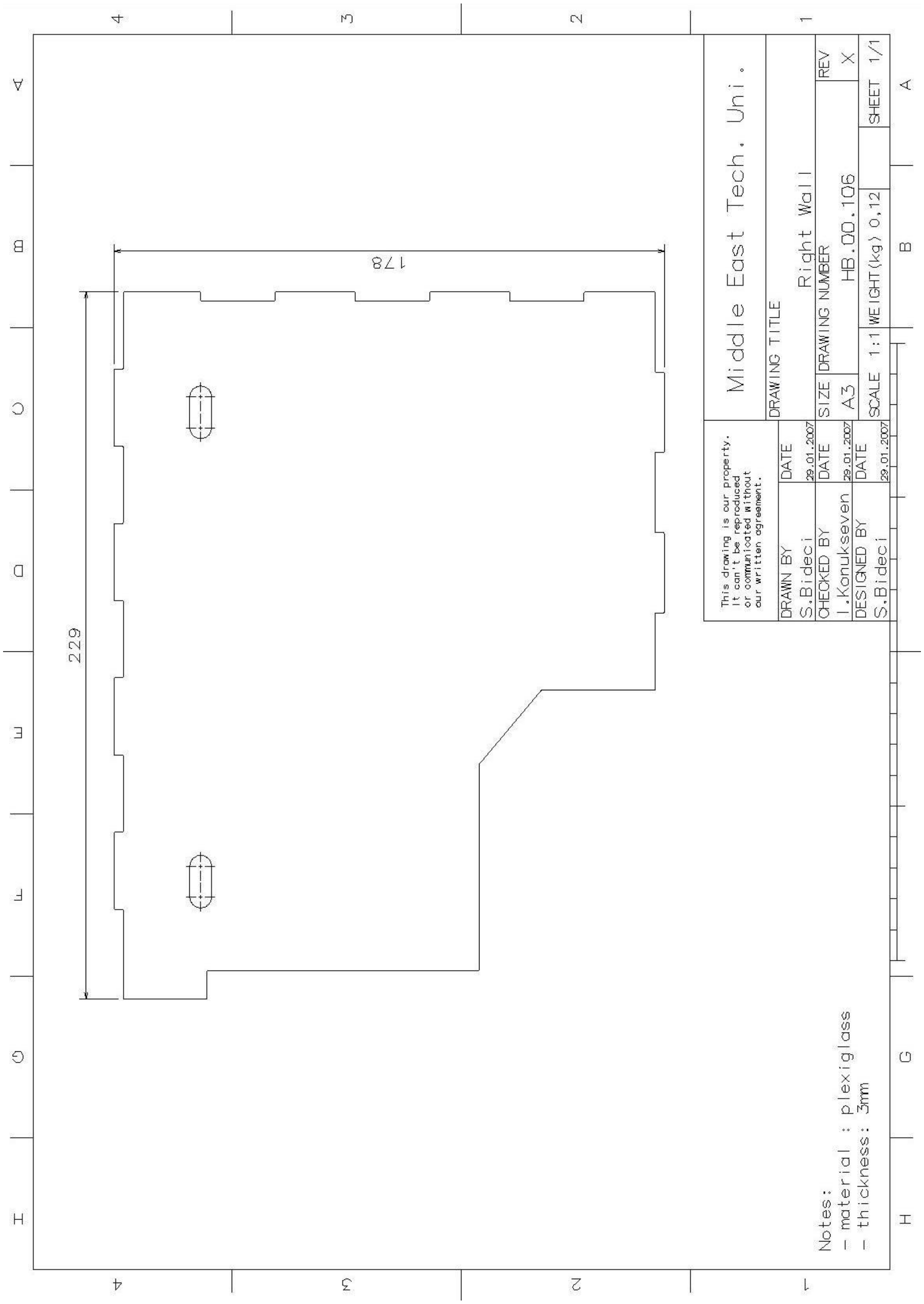

Figure D.9 Right Wall

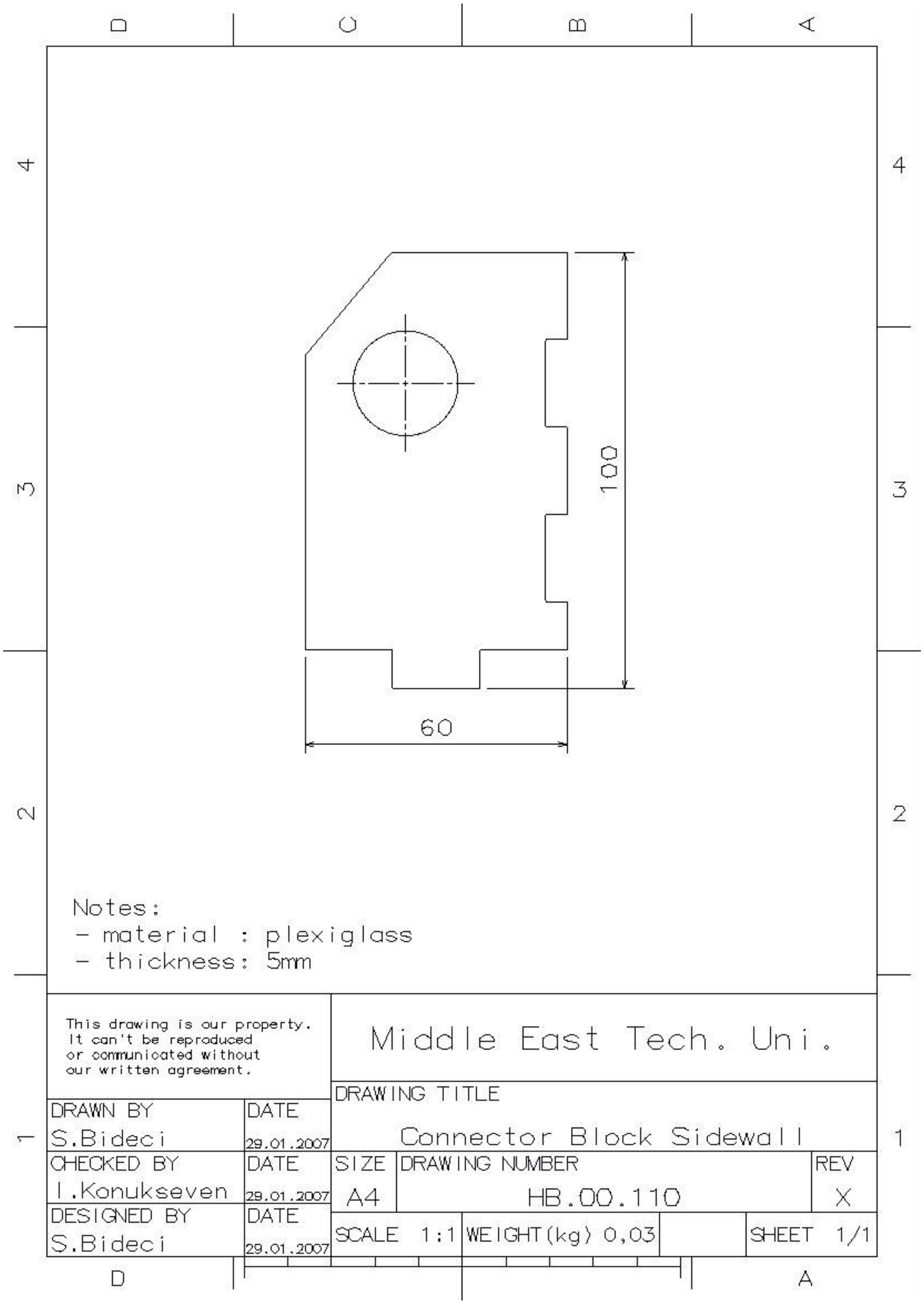

Notes:
- material : plexiglass
- thickness: 5mm

This drawing is our property. It can't be reproduced or communicated without our written agreement.		Middle East Tech. Uni.			
DRAWN BY S.Bideci	DATE 29.01.2007	DRAWING TITLE Connector Block Sidewall			
CHECKED BY I.Konukseven	DATE 29.01.2007	SIZE A4	DRAWING NUMBER HB.00.110		REV X
DESIGNED BY S.Bideci	DATE 29.01.2007	SCALE 1:1	WEIGHT(kg) 0,03		SHEET 1/1

Figure D.10 Connector Block Sidewall

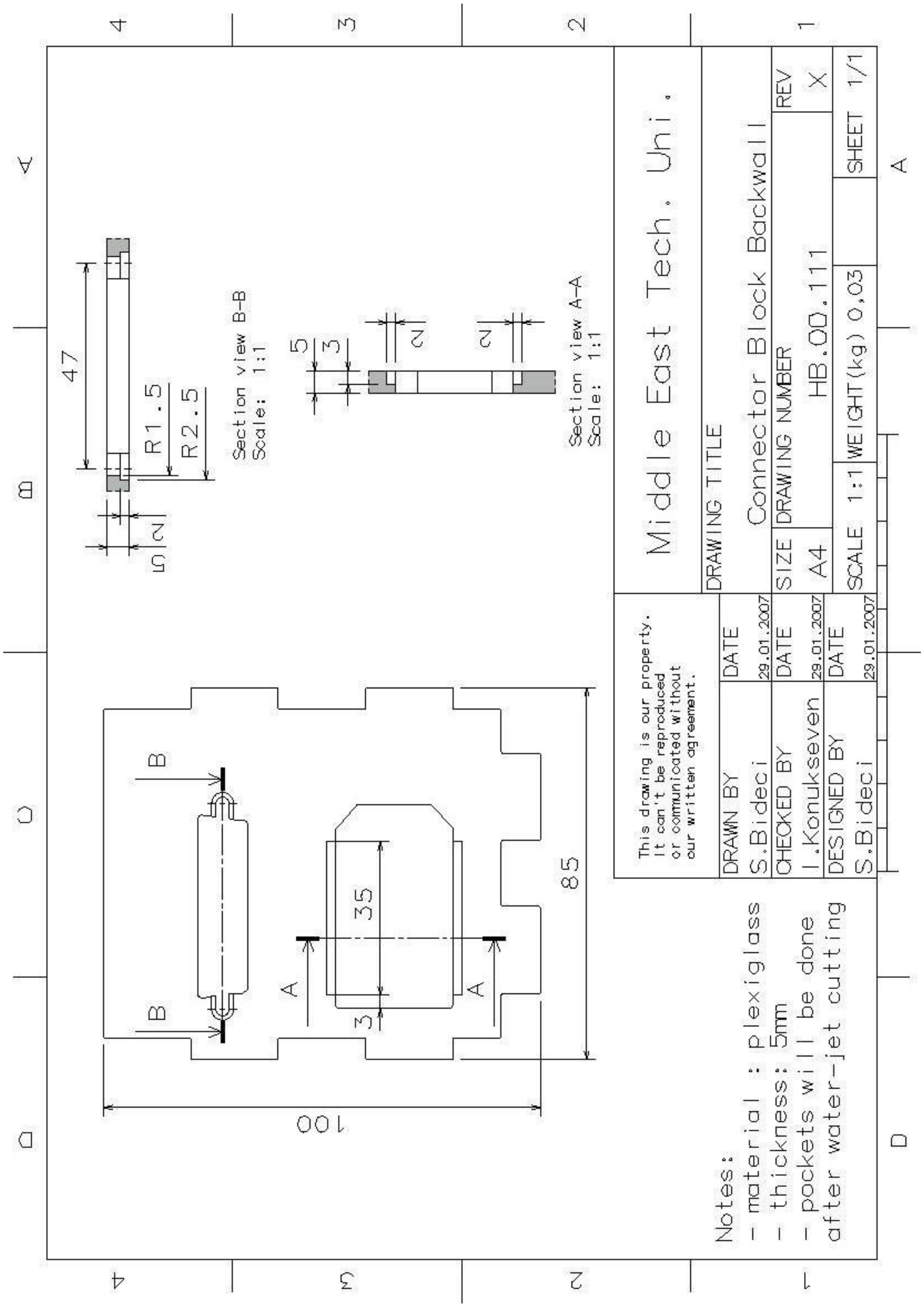

Figure D.11 Connector Block Backwall

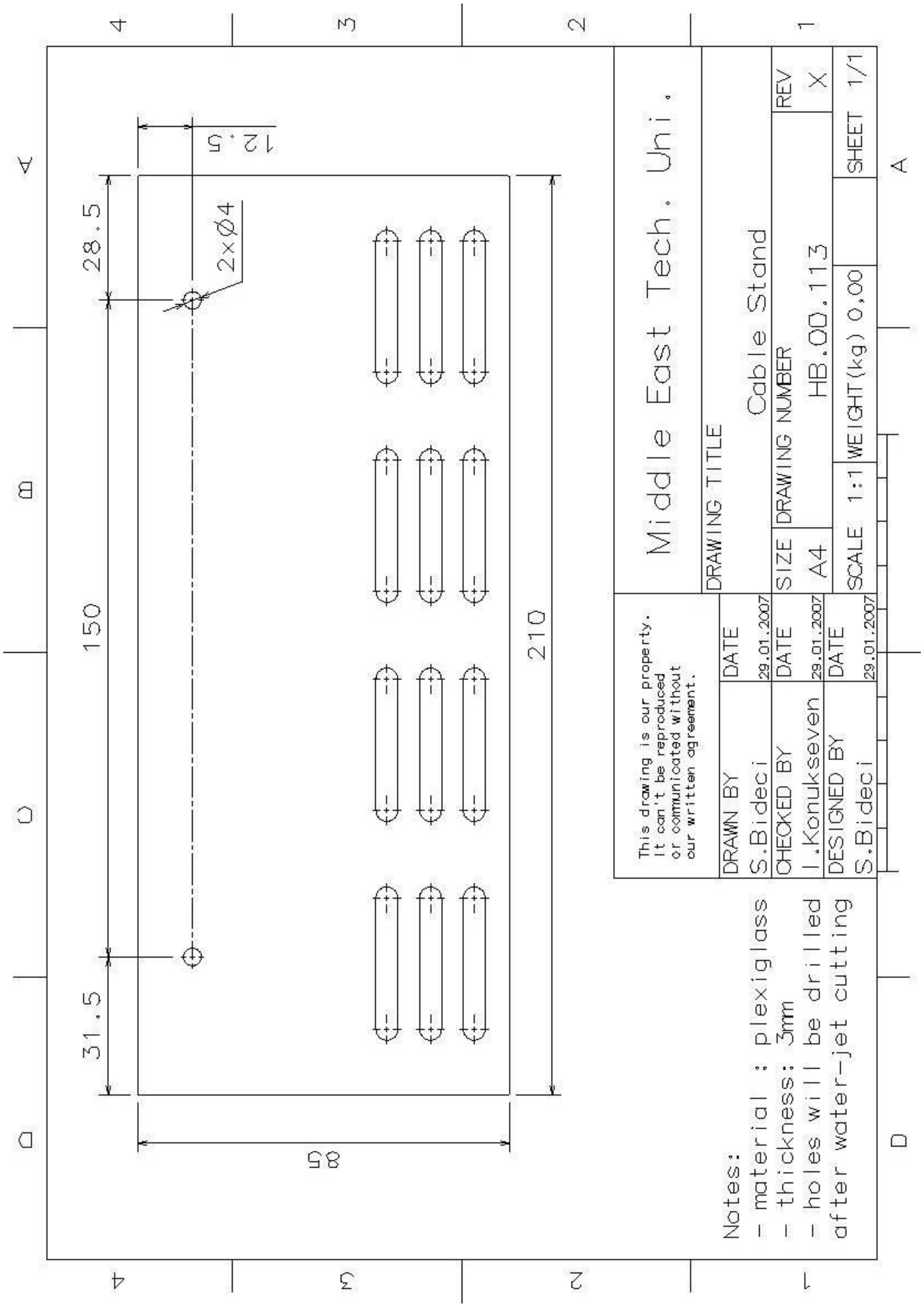

Figure D.12 Cable Stand

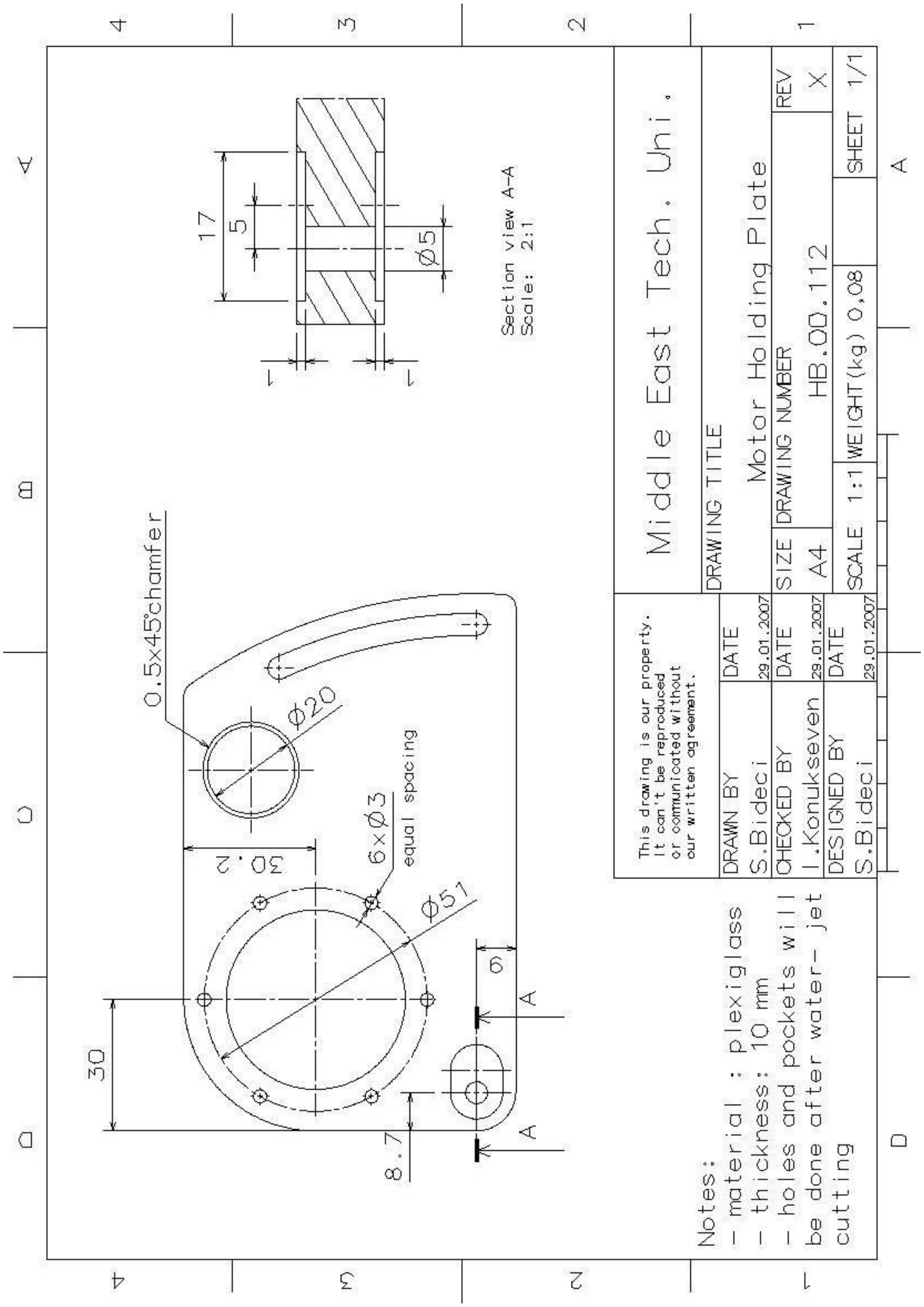

Figure D.13 Motor Holding Plate

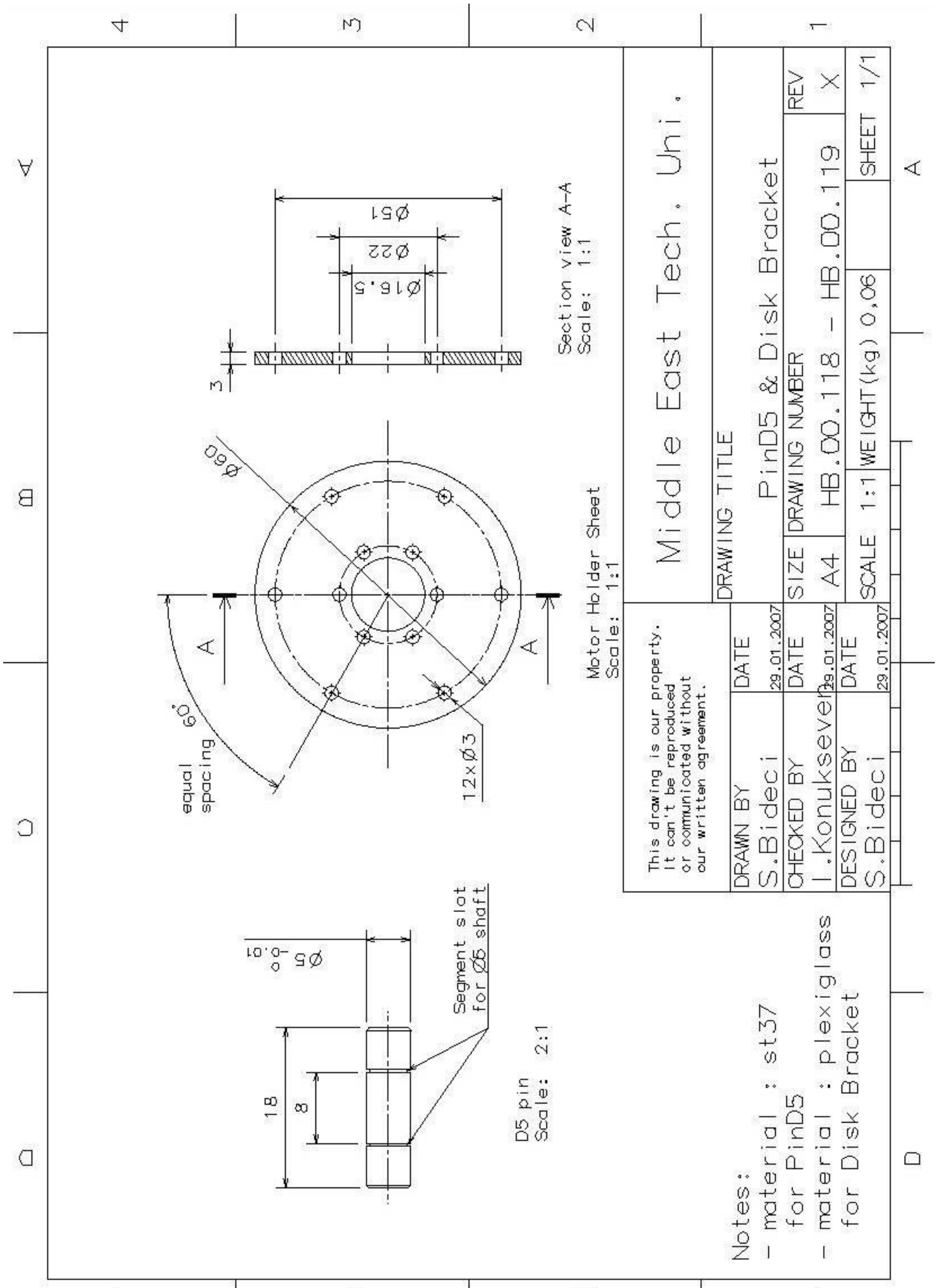

Figure D.14 PinD5 & Disk Bracket

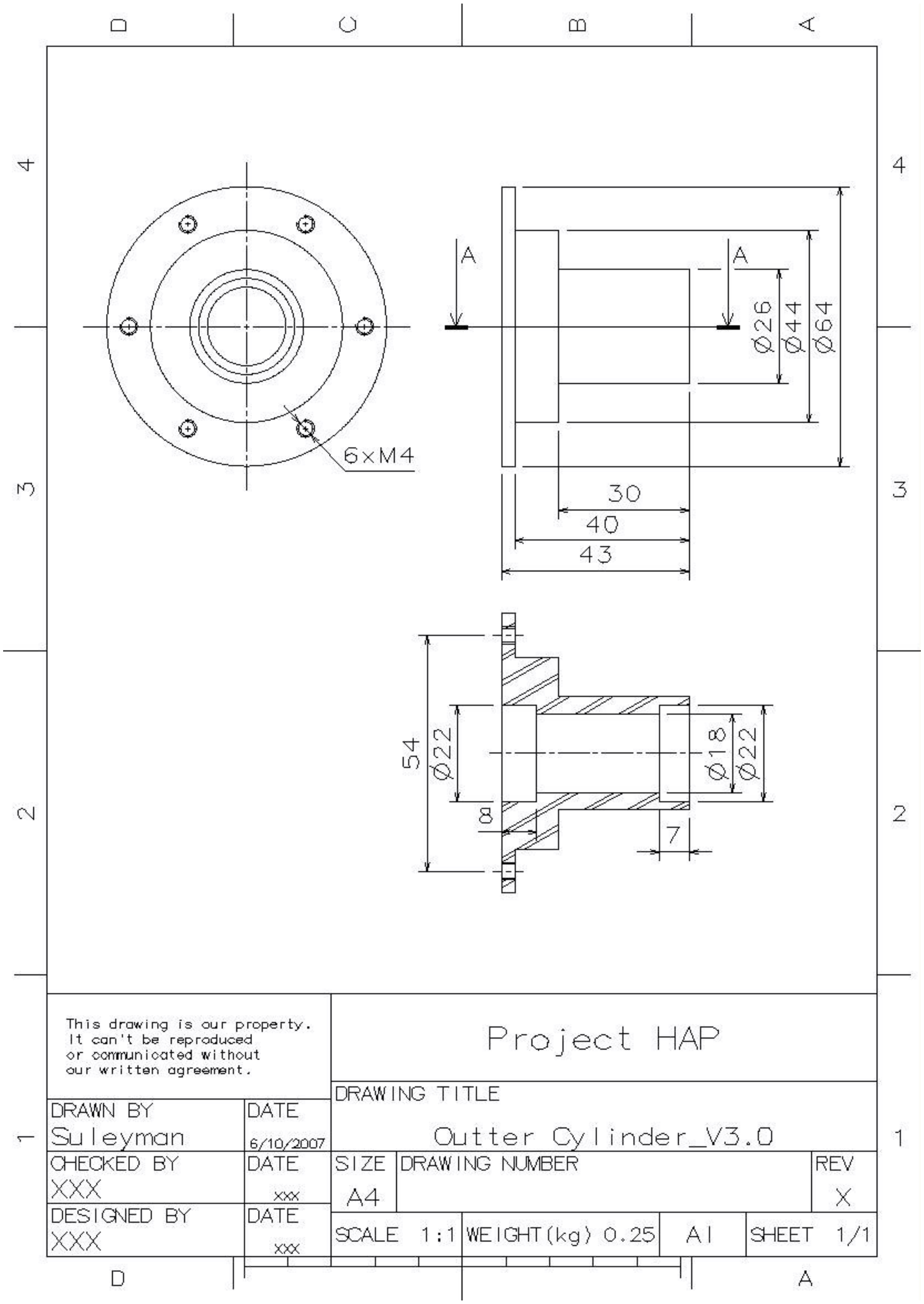

Figure D.15 Outer Cylinder

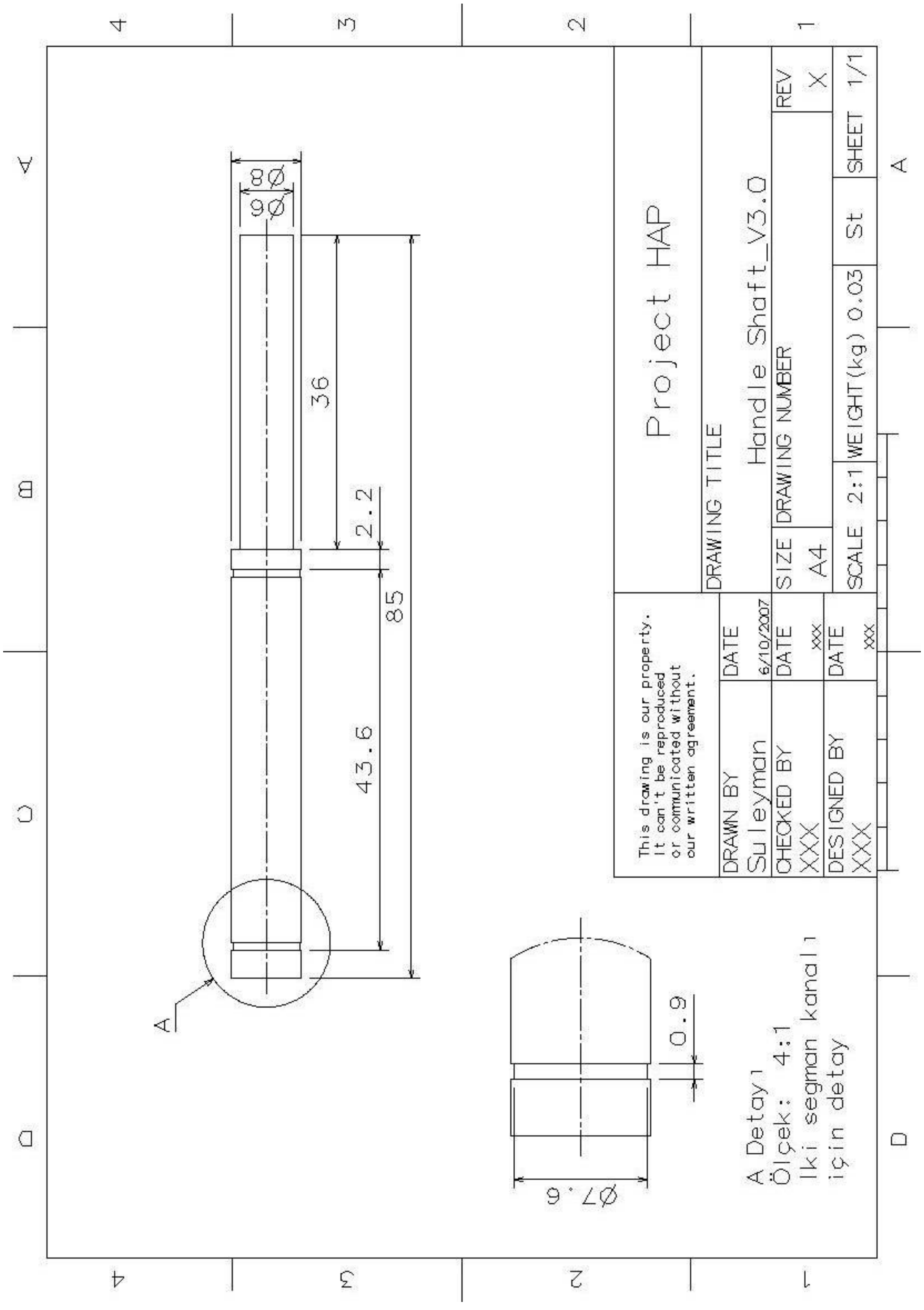

Figure D.16 Handle Shaft V3.0

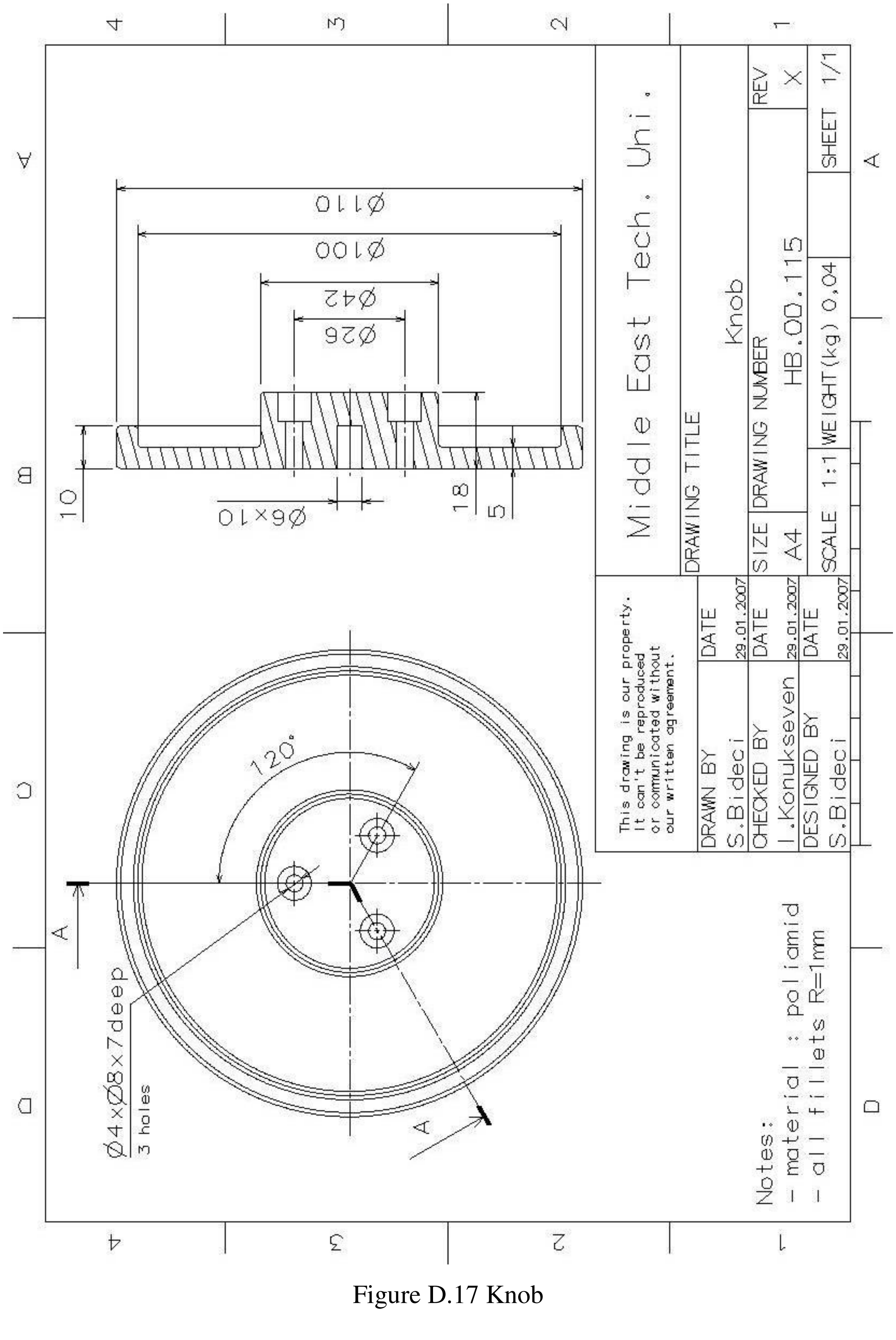

Figure D.17 Knob

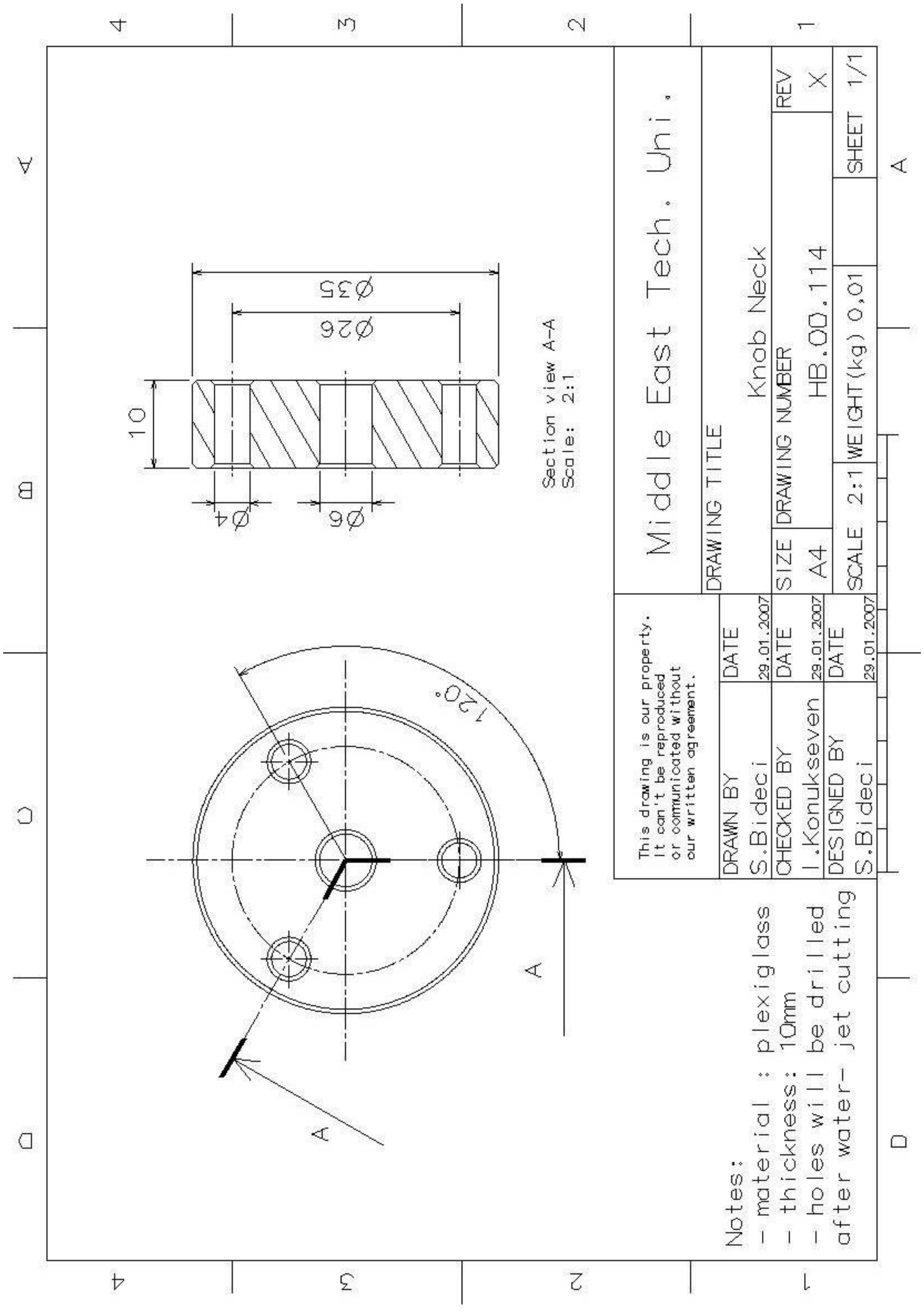

Figure D.18 Knob Neck

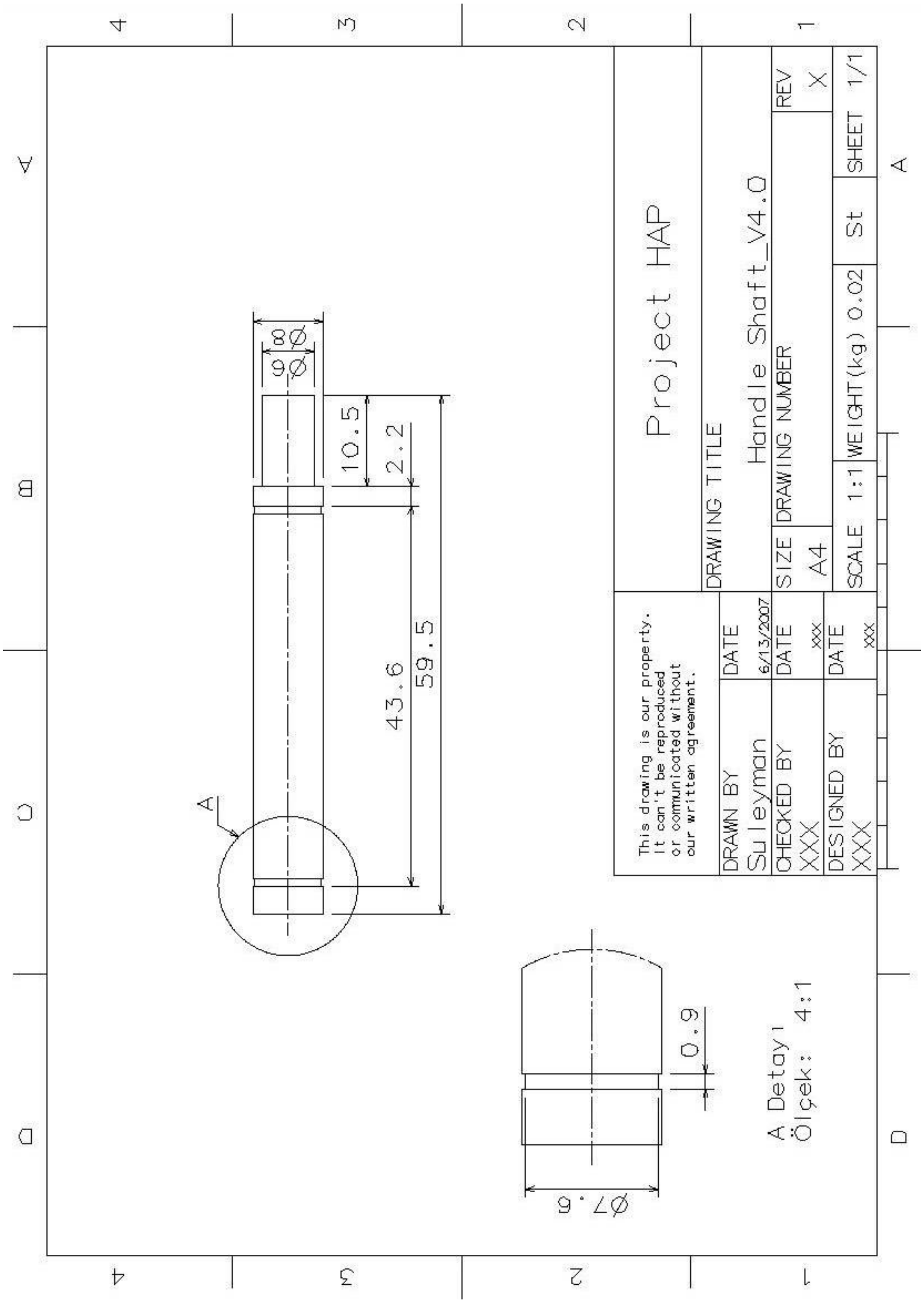

Project HAP

This drawing is our property. It can't be reproduced or communicated without our written agreement.

DRAWN BY Suleyman DATE 6/13/2007

CHECKED BY XXX DATE xxx

DESIGNED BY XXX DATE xxx

DRAWING TITLE Handle Shaft_V4.0

SIZE A4 DRAWING NUMBER REV X

SCALE 1:1 WEIGHT(kg) 0.02 St SHEET 1/1

Figure D.19 Handle Shaft V4.0

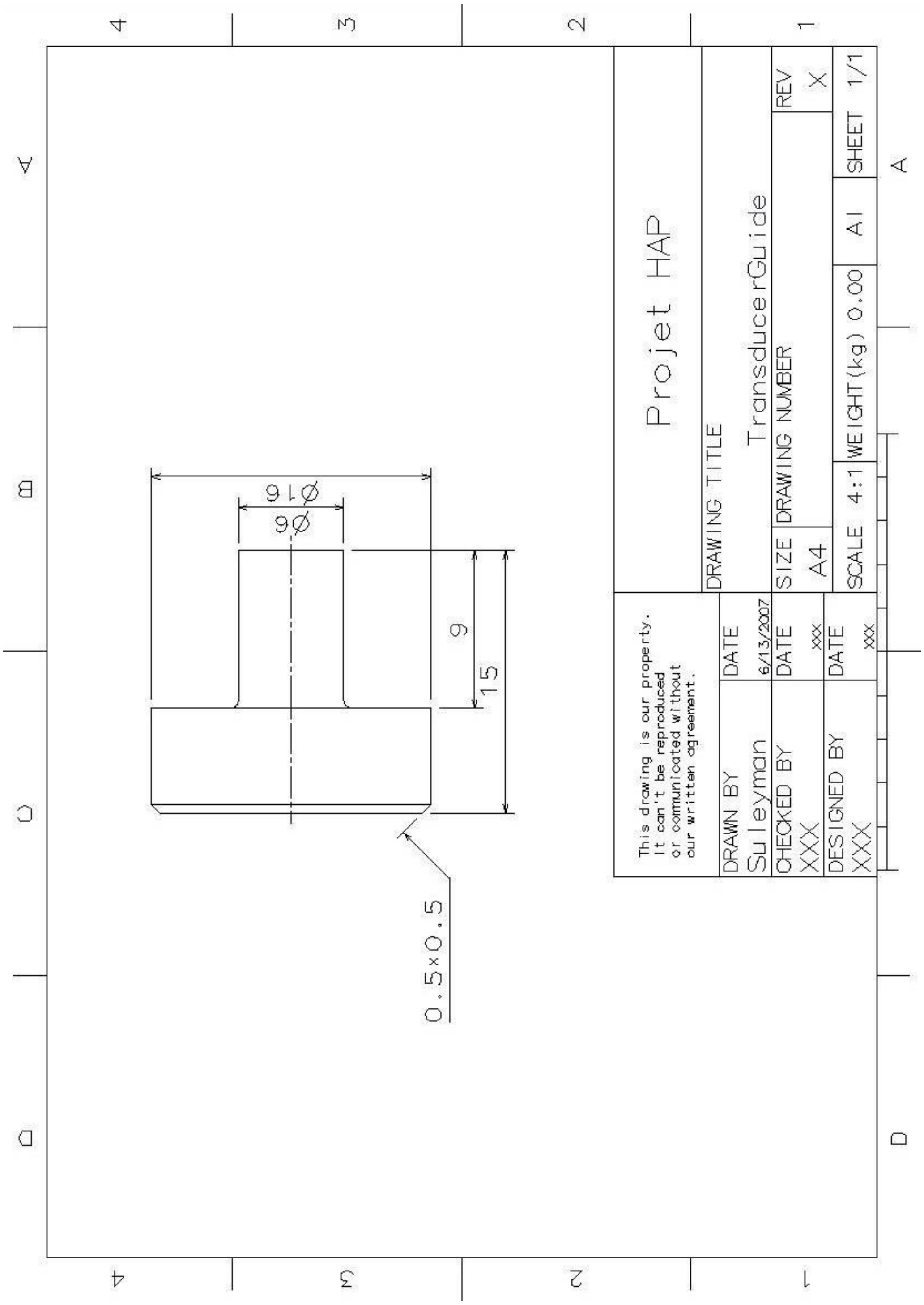

Figure D.20 Transducer Guide

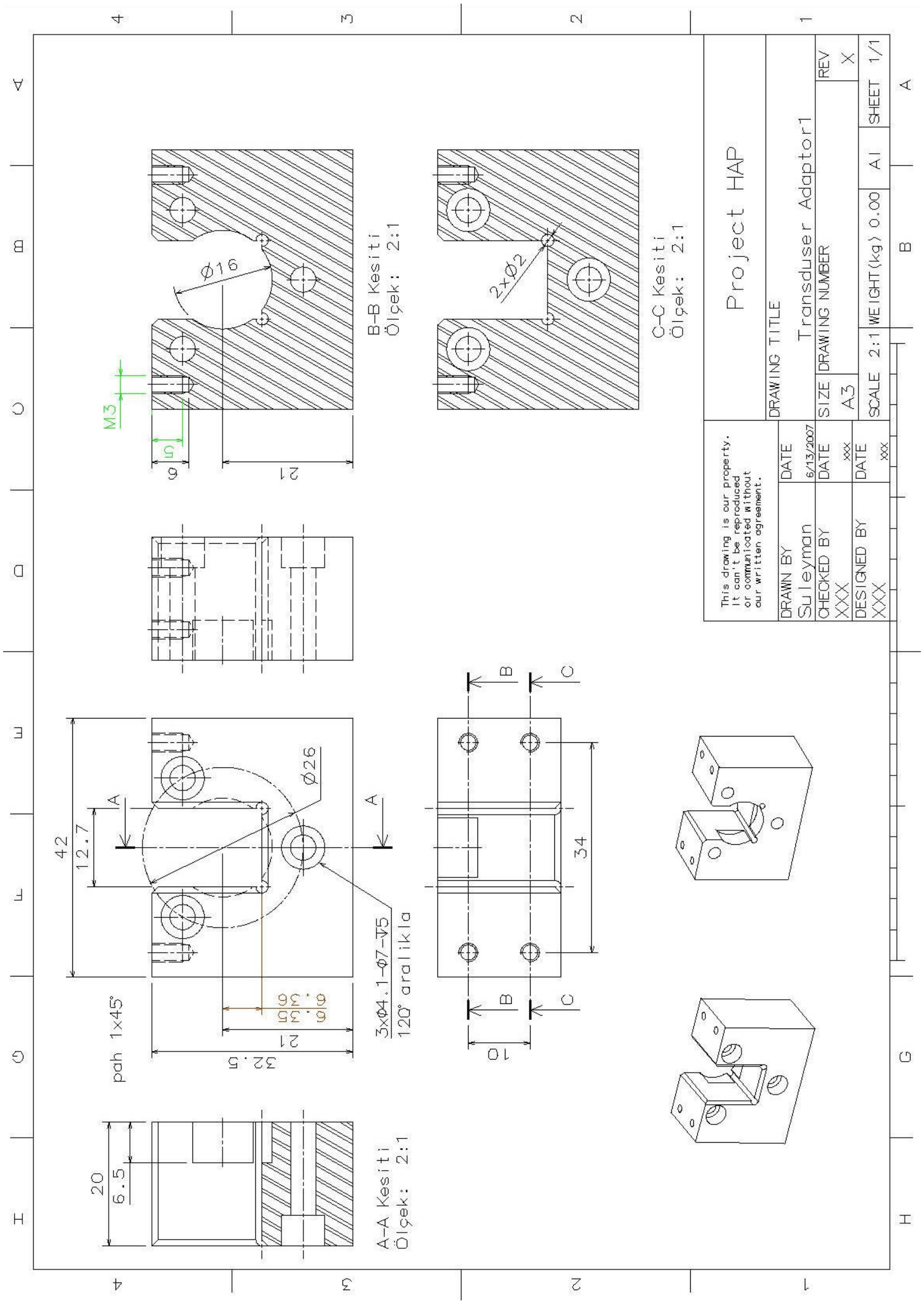

Figure D.21 Transducer Adaptor 1

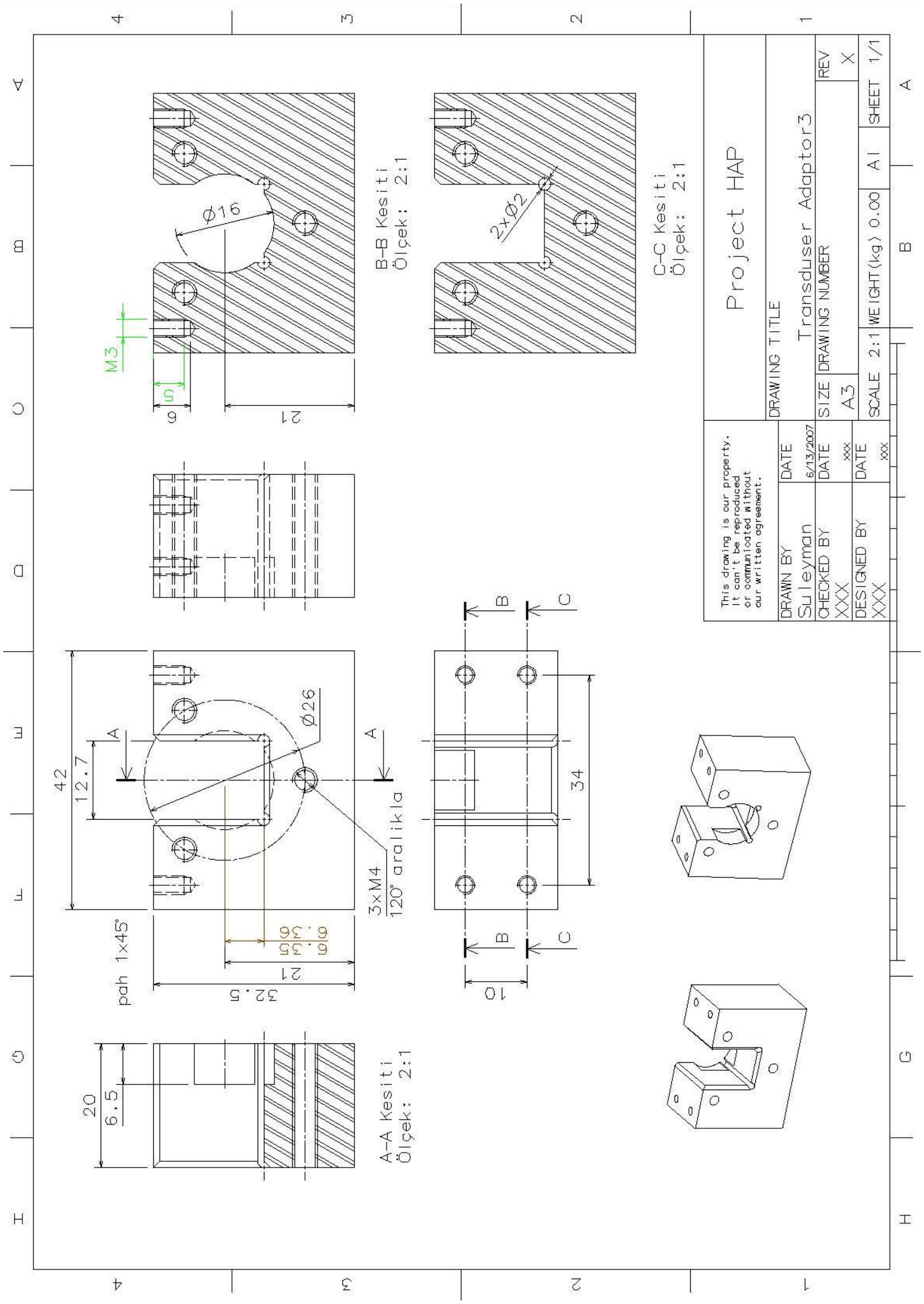

Figure D.22 Transducer Adaptor 3

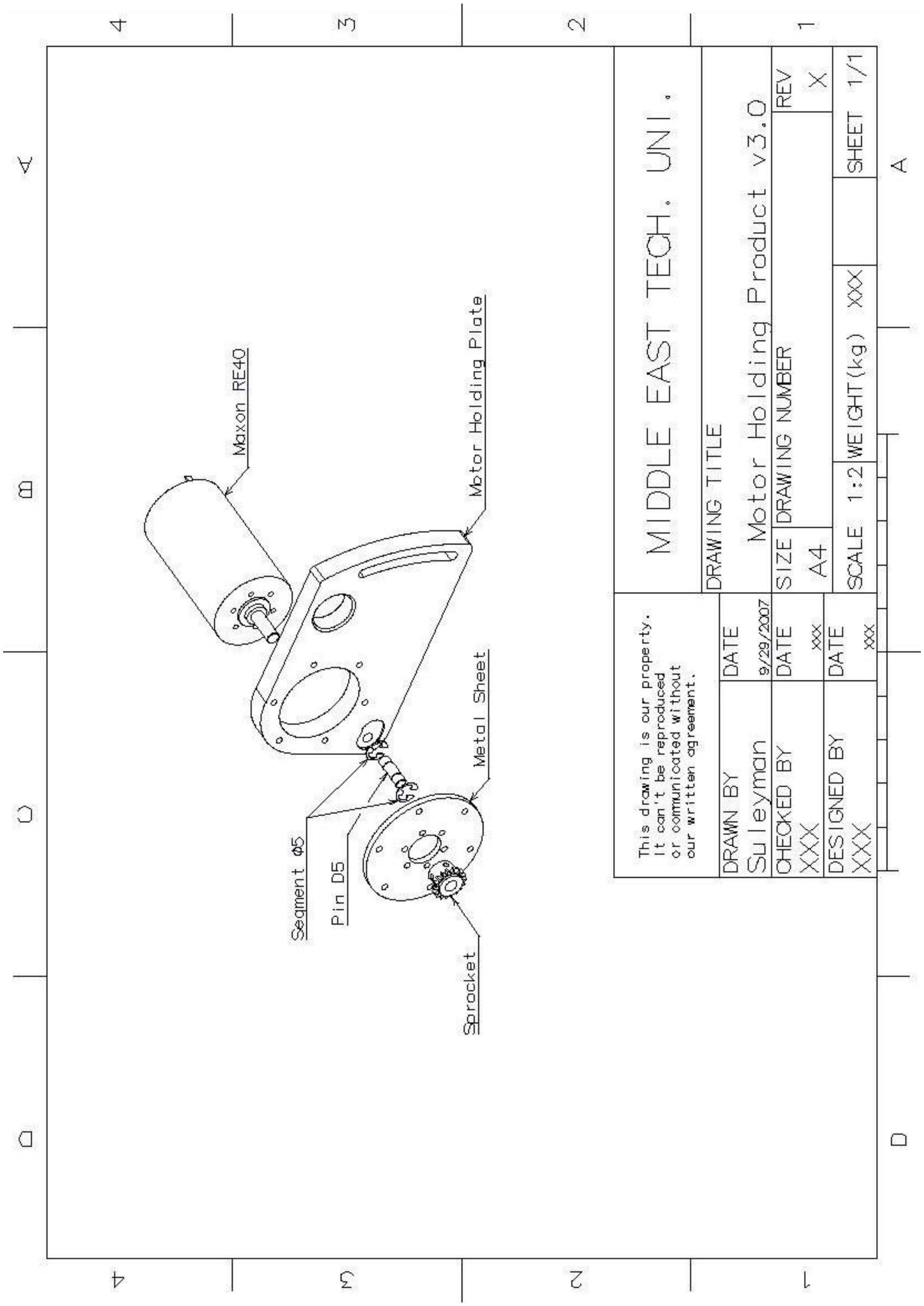

Figure D.23 Motor Holding Product V3.0

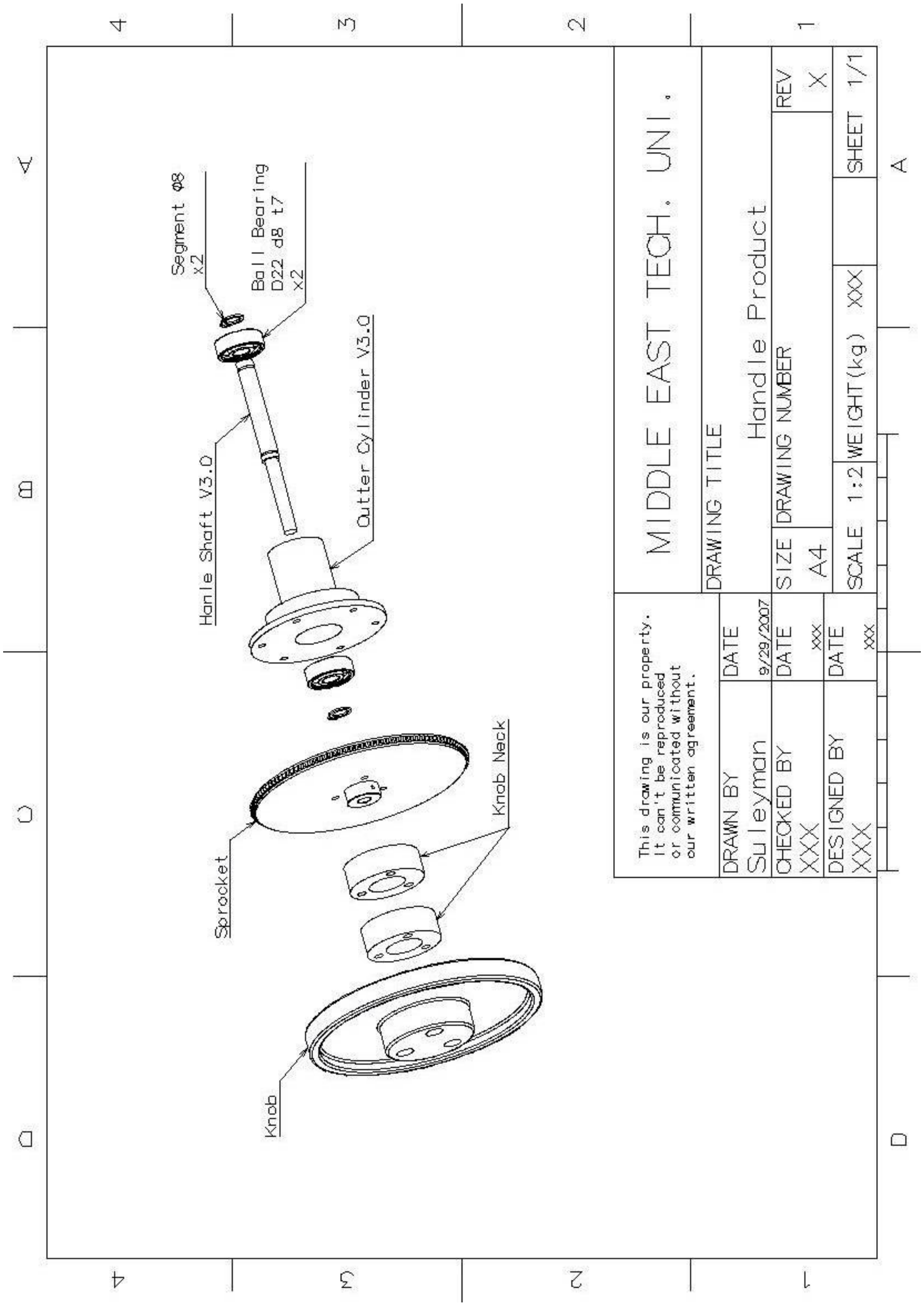

Figure D.24 Handle Product V3.0

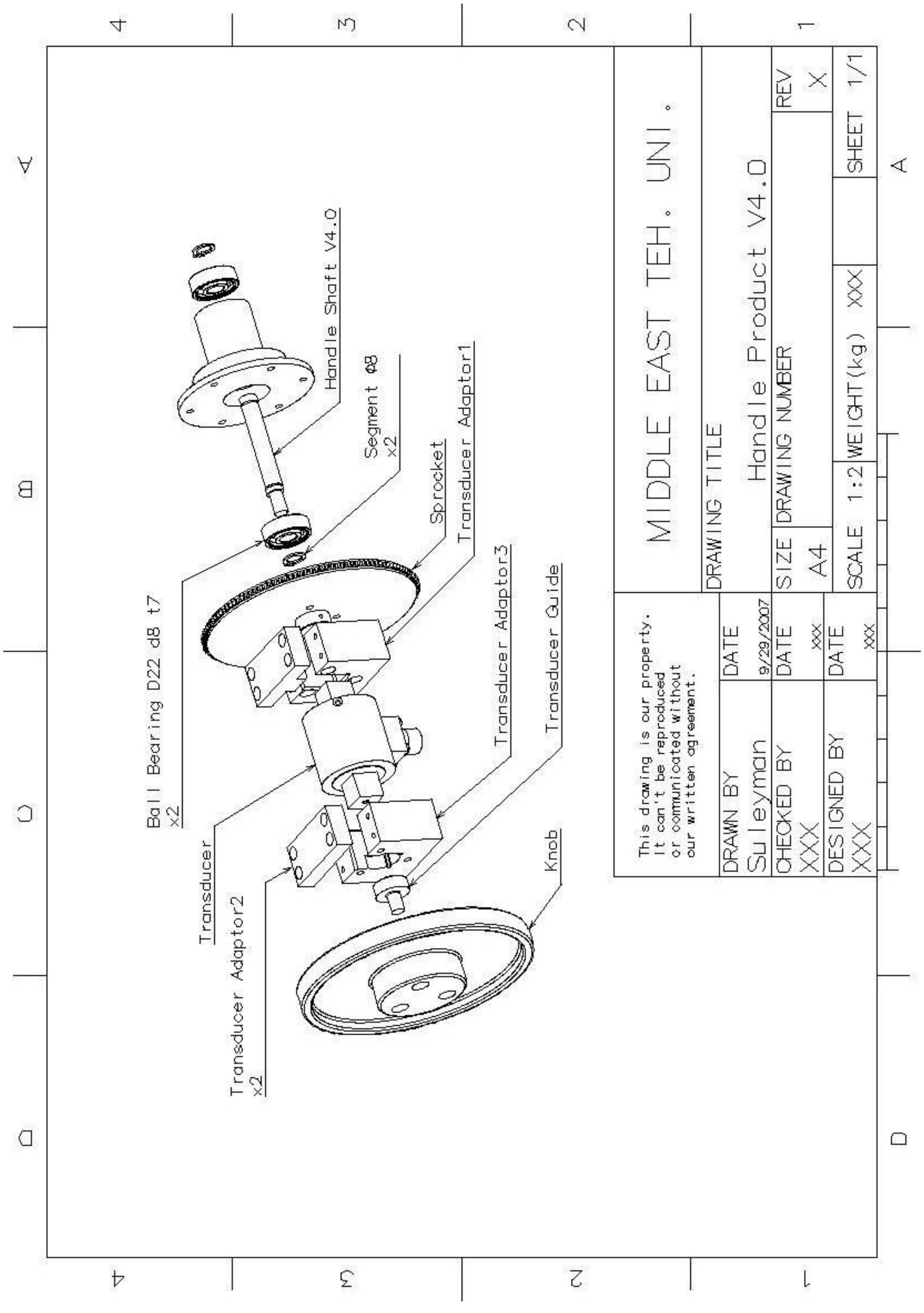

Figure D.25 Handle Product V4.0

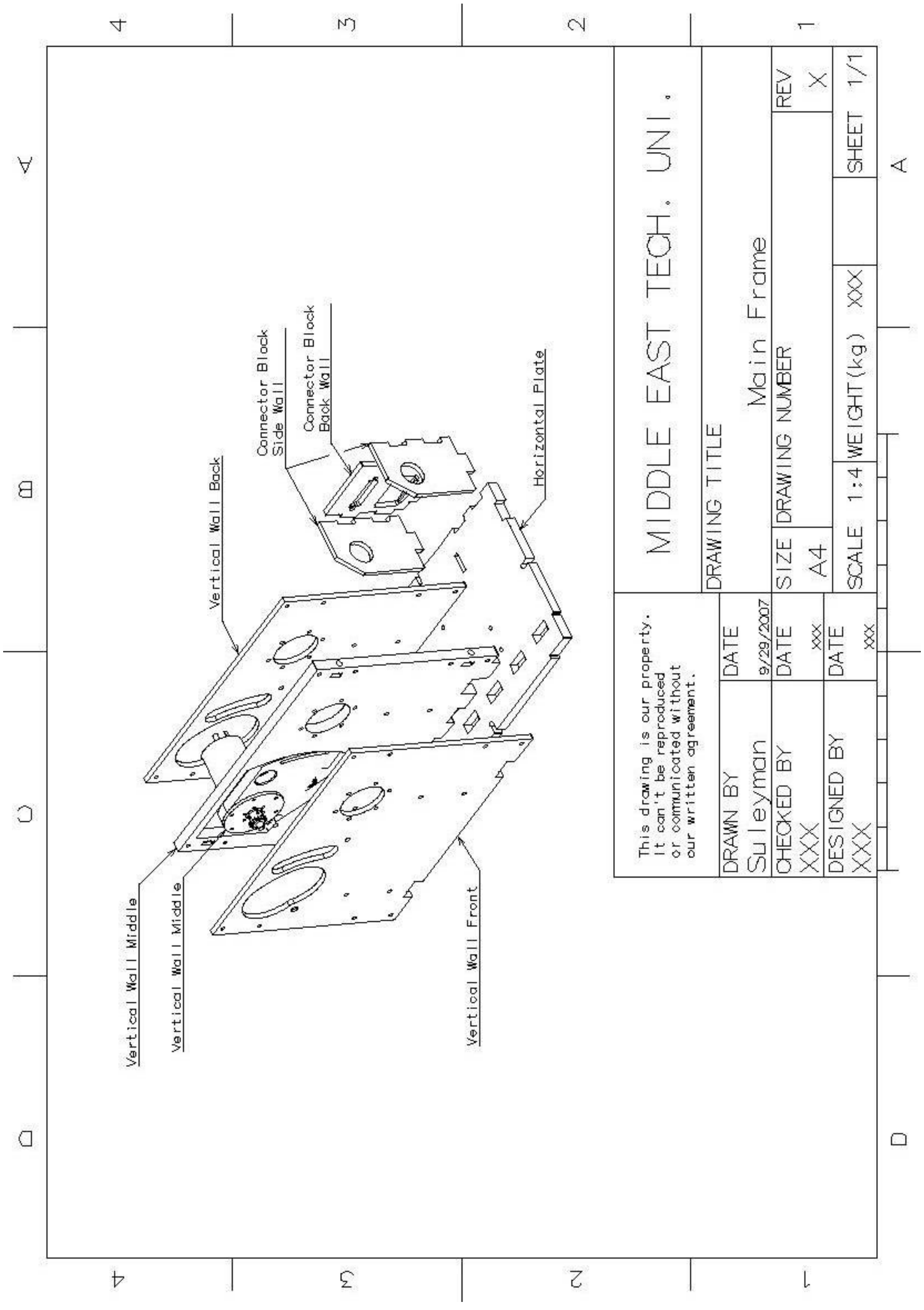

Figure D.26 Main Frame

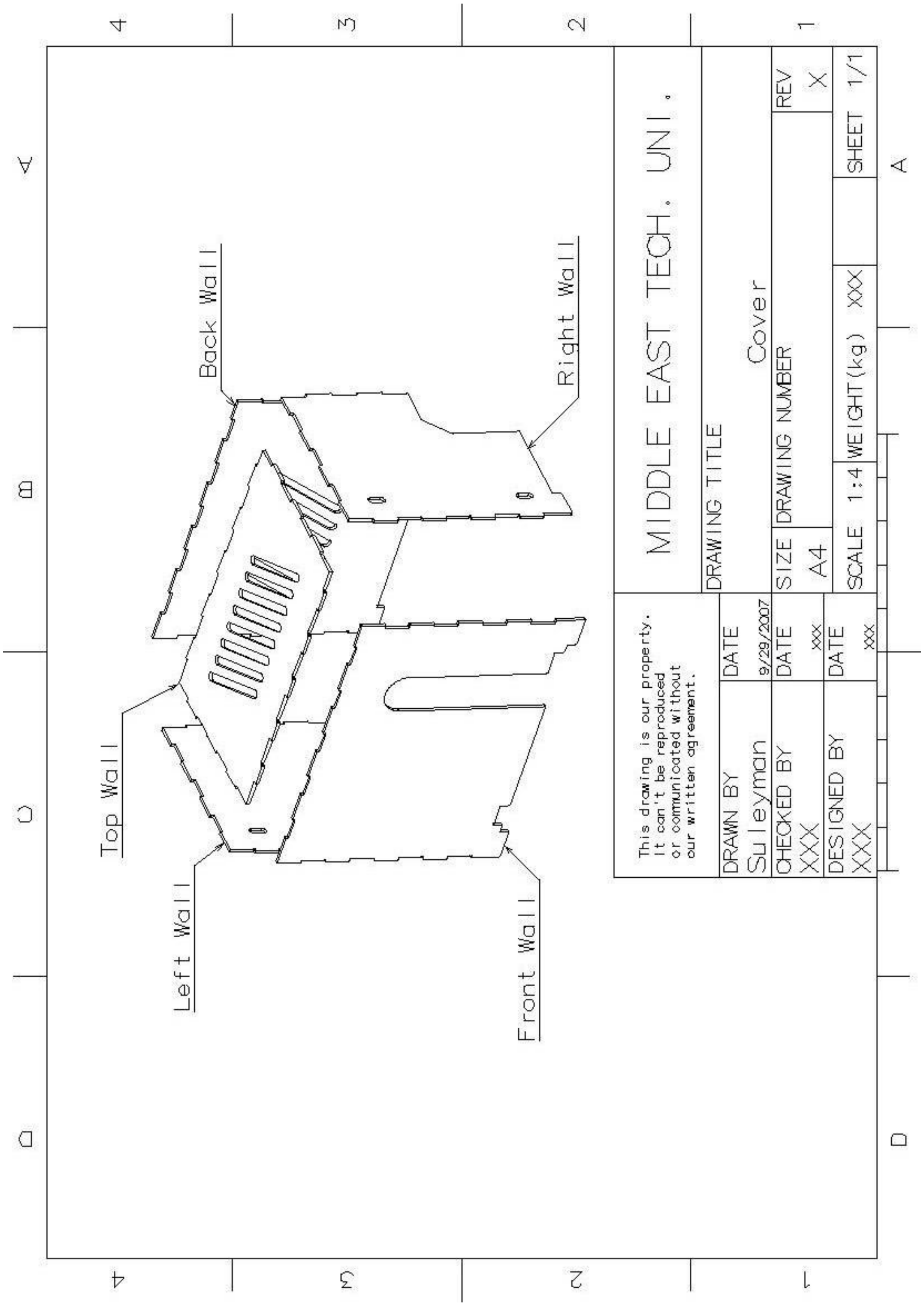

Figure D.27 Cover

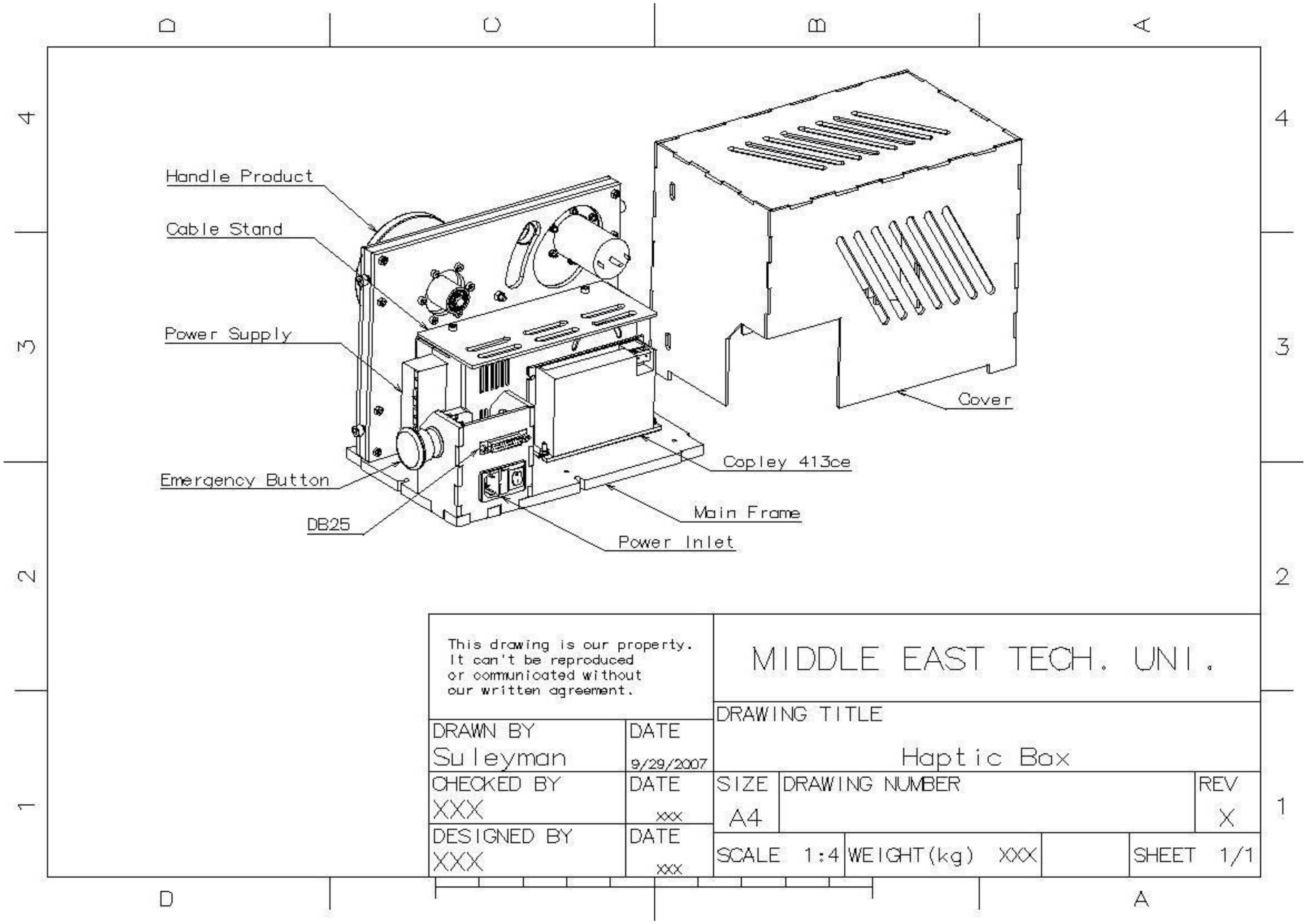

Figure D.28 Haptic Box

APPENDIX E

SIMULINK BLOCK DETAILS USED IN EXPERIMENTS

General control diagrams of the control methods are give in the respective sections. In this section, details of those blocks are given.

E.1 Open Loop Impedance Control

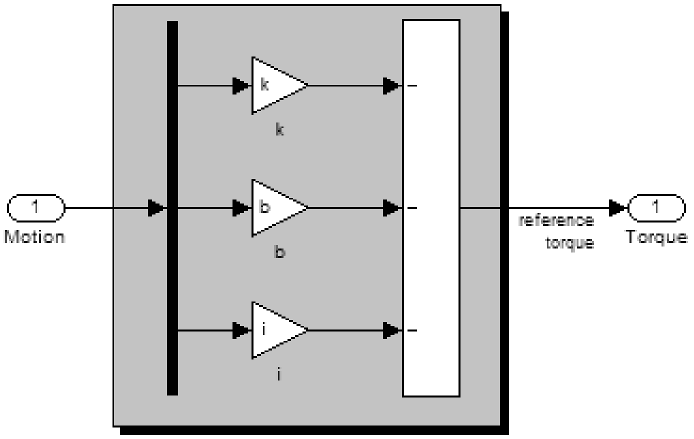

Figure E.1 Virtual Environment Model Block

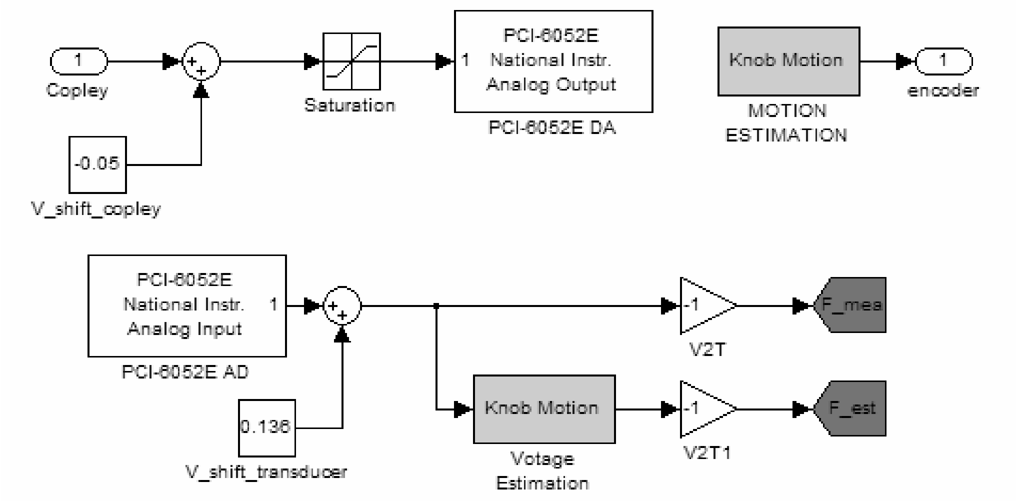

Figure E.2 Haptic Box Block

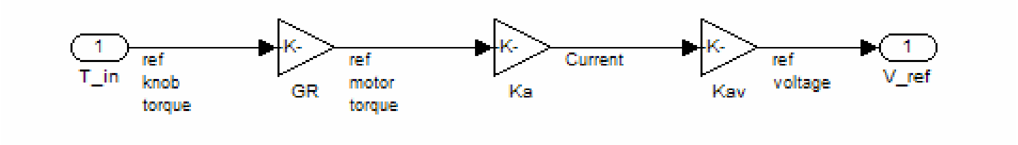

Figure E.3 Controller Block

E.2 Impedance Control with Force Feed-back

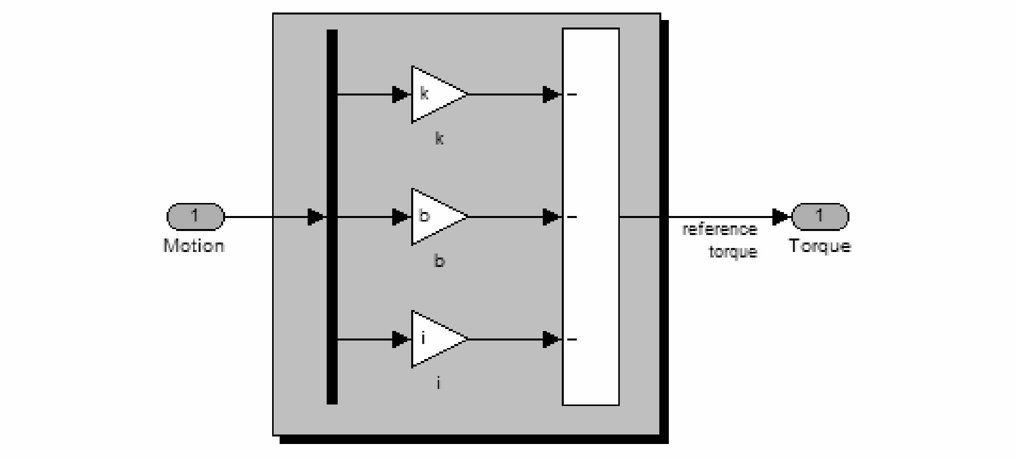

Figure E.4 Virtual Environment Block

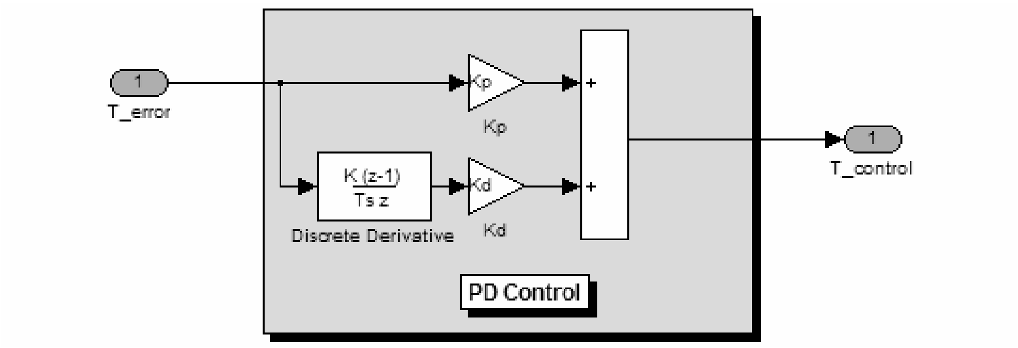

Figure E.5 Controller Block

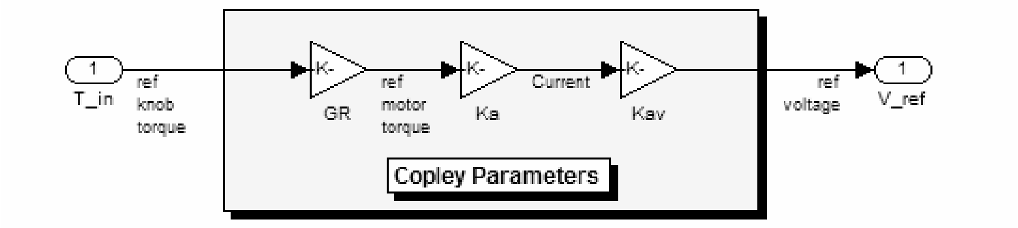

Figure E.6 Copley Parameters Block

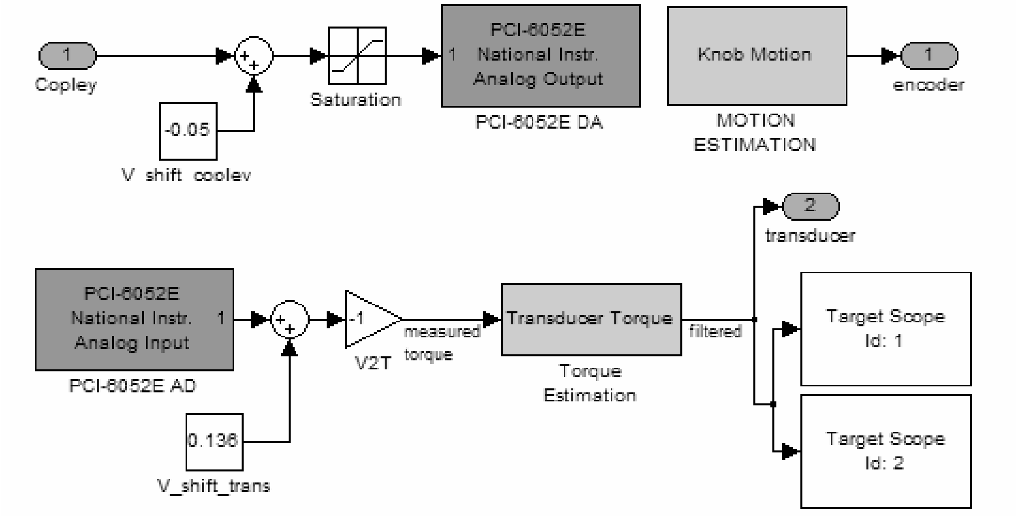

Figure E.7 Haptic Box Block

E.3 Admittance Control

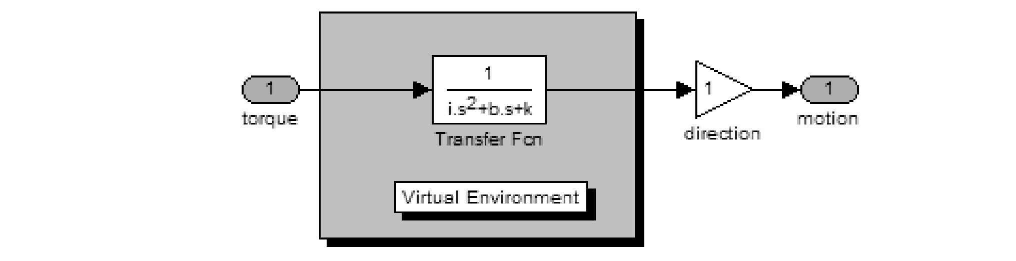

Figure E.8 Virtual Environment Block

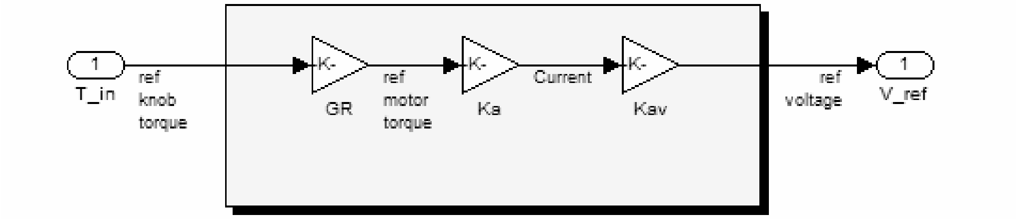

Figure E.9 Copley Parameters Block

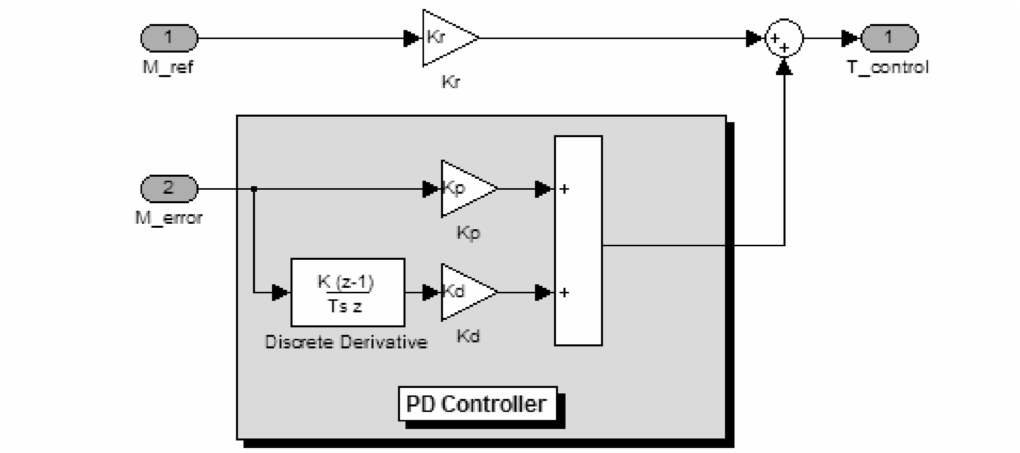

Figure E.10 Controller Block

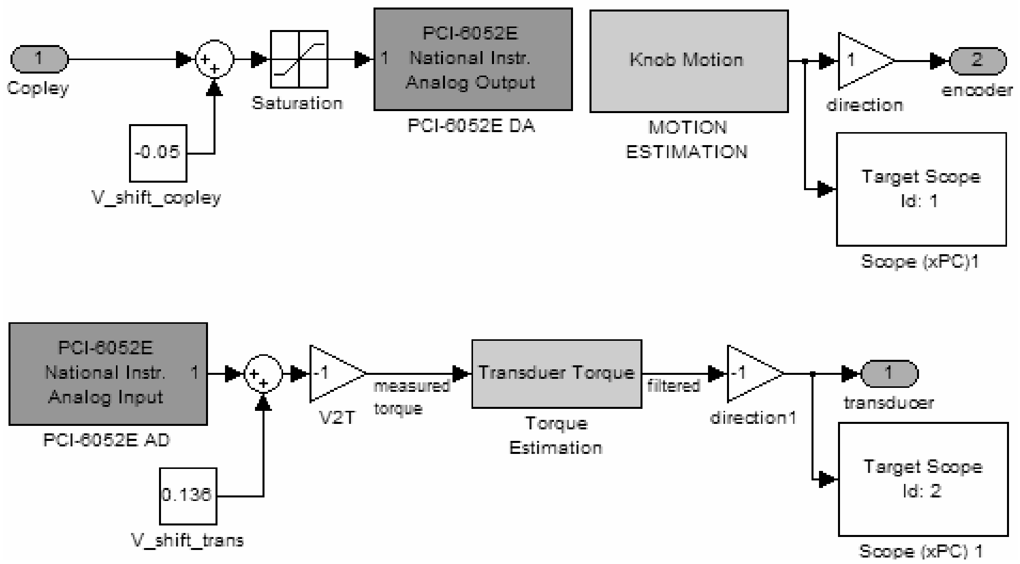

Figure E.11 Haptic Box Block